Translating 3D Gel Dosimetry Research into Clinical Routine Use in Radiotherapy

Jacqueline Elizabeth Poxon

Submitted in partial fulfilment of the requirements
of the Degree of Doctor of Philosophy

Barts Cancer Institute

Barts and The London School of Medicine and Dentistry

Queen Mary, University of London

2018

Statement of originality

I, Jacqueline Elizabeth Poxon, confirm that the research included within this thesis is my own work or that where it has been carried out in collaboration with, or supported by others, that this is duly acknowledged below and my contribution indicated. Previously published material is also acknowledged below.

I attest that I have exercised reasonable care to ensure that the work is original, and does not to the best of my knowledge break any UK law, infringe any third party's copyright or other Intellectual Property Right, or contain any confidential material.

I accept that the College has the right to use plagiarism detection software to check the electronic version of the thesis.

I confirm that this thesis has not been previously submitted for the award of a degree by this or any other university.

The copyright of this thesis rests with the author and no quotation from it or information derived from it may be published without the prior written consent of the author.

Signature: [can be digital signature]

Date: 01/06/2018

Details of collaboration

The first batches of Fricke gel detectors used for experiments in chapter 4 were made in collaboration with David Crossley of the National Physical Laboratory, Teddington, UK. David alongside colleagues from the Radiation Physics group at NPL had previously investigated Fricke gel dosimetry with optical-CT analysis. Subsequently all detectors were manufactured at St. Bartholomew's Hospital. It is specified in the thesis which experiments were carried out with detectors manufactured at the NPL.

The development of an OsiriX plugin for creating T_1 maps from images acquired with a Look Locker sequence was carried out with assistance from Dr. Redha Boubertakh. This is reported in Chapter 3. Redha helped and guided me with writing the code for this task.

The development of protocols for T_1 and T_2 quantification using the whole-body MRI scanner was carried out with my supervisor, Dr. Marc Miquel. Marc is the lead MRI physicist at St. Bartholomew's Hospital. Thereafter, for each experiment, I manufactured the Fricke gel detectors. Whilst I was irradiating the detectors, Marc prepared the MRI scanner for detector readout. We scanned them together; I then carried out the subsequent the analysis of the acquired scans.

Acknowledgements

Abstract

Radiotherapy involves the treatment of tumours with ionising radiation. Technological advances have improved the ability to conform dose distributions to tumours in three dimensions (3D) and thereby reduce morbidity. However, sophisticated measurement devices are required to verify these complex distributions and ensure their accuracy. Radiation-sensitive gels, including polymer and Fricke gels, are a potential solution to this 3D dosimetry problem. Scanning these detectors using imaging methods such as magnetic resonance imaging (MRI) provides quantifiable images of dose distribution.

Despite research efforts, 3D gel dosimetry has not yet been implemented as a routine dosimetry tool in clinical radiotherapy. This thesis aims to investigate the implementation of Fricke gel detectors within a clinical radiotherapy department. The existing literature was reviewed to establish what evidence already existed on the dosimetric accuracy of Fricke gel detectors. This review highlighted gaps for many important dosimetric characteristics and a lack of a systematic approach to the testing of these detectors.

Basic dosimetric characteristics were then investigated using test tube Fricke gel samples and an MR spectrometer. These experiments showed an excellent basic precision over a dose range of 3 to 20Gy. However, detectors need to be scanned within a certain time of irradiation to avoid signal drift. There was no evidence of any dependence of response on dose rate, energy or fractionation.

Larger volume detector samples were analysed using a 3T MRI scanner. Detector response was homogeneous and did not vary with volume. Post-irradiation blurring of the measured distribution due to ferric ion diffusion was within acceptable limits if detectors were scanned within 2 hours following irradiation for typical clinical dose gradients.

Finally, large volume Fricke gel detectors were used to measure complex VMAT stereotactic plans, describing the integrated dose distribution with sufficient accuracy and demonstrating clear potential to be applied to our clinical practice.

Abbreviations

#	fraction of radiotherapy
1D	one dimensional
2D	two dimensional
3D	three dimensional
3DCRT	three dimensional conformal radiotherapy
BANG	bis, acrylamide, nitrogen and gelatine; a type of polymer gel
bw	by weight
cm	centimetre
CI	confidence interval
CPMG	Carr-Purcell-Meiboom-Gill
CT	computed tomography
CTV	clinical target volume
CV	coefficient of variance
DICOM	digital imaging and communications in medicine
DTA	distance to agreement
EPID	electronic portal imaging device
Fe^{2+}	ferrous ions
Fe^{3+}	ferric ions
FXG	ferrous xylenol orange gelatin; a type of Fricke detector
g	grams
GTV	gross tumour volume
Gy	Gray (Gy), special SI unit of absorbed dose ($J\ kg^{-1}$)
ICRU	international commission on radiological units
IMRT	intensity modulated radiotherapy
l	litre
MeV	mega electron Volts
mg	milligrams
ml	millilitres
MLC	multi-leaf collimator
mM	millimolar
MR	magnetic resonance
MRI	magnetic resonance imaging
ms	milliseconds

MU	monitor unit
MV	megavolt
$M_{x,y}$	magnetisation in the x,y (transverse) plane
M_z	magnetisation along the z axis
NHS	national health service
NMR	nuclear magnetic resonance
NPL	national physical laboratory
NSA	number of signal averages
NTCP	normal tissue complication probability
OAR	organs at risk
PAG	polyacrylamide gel
PRV	planning risk volume
PTV	planning target volume
QA	quality assurance
QC	quality control
R_1	spin-lattice (longitudinal) relaxation rate
R_2	spin-spin (transverse) relaxation rate
RF	radiofrequency
ROI	region of interest
SABR	stereotactic ablative radiotherapy
SD	standard deviation
SI	Système International
SNR	signal to noise ratio
SRS	stereotactic radiosurgery
SSD	source to surface distance
T	Tesla
T_1	spin-lattice (longitudinal) relaxation
T_2	spin-spin (transverse) relaxation
TCP	tumour control probability
TE	echo time
TI	inversion time
TR	repetition time
TPS	treatment planning system
VMAT	volumetric modulated arc radiotherapy
XO	Xylenol orange

Table of Contents

9

Index of Tables

Chapter 1. Introduction

1.1   Radiotherapy

1.1.1   Introduction to Radiotherapy

Radiotherapy is the treatment of cancer with high energy ionising radiation. The aim is to destroy cancer cells while sparing adjacent normal tissue. Photon, electron or heavy particle beams may be applied to various clinical situations. This project is concerned with the use of megavoltage energy (MV) photons to treat deep seated tumours. Radiation dose has the unit of gray (Gy), defined as the amount of energy absorbed per kilogram of matter (joules per kilogram).

The aim of radiotherapy is to eradicate the tumour whilst causing minimal damage to surrounding normal tissue, more specifically to achieve a high tumour control probability (TCP) with a low normal tissue complication probability (NTCP). The therapeutic ratio refers to the ratio between the TCP and NTCP for a given radiation dose level. If the radiation dose is too low, the tumour will not be eradicated, too high and unacceptable side effects result.

One way of improving the therapeutic ratio is to divide radiotherapy treatments into small daily fractions (#) delivered over the course of a few weeks. This relies on the repair of sub-lethal damage to normal tissue and repopulation of cells, as well as increasing tumour damage due to re-oxygenation and redistribution of tumour cells. Typical radiotherapy fractionation schedules for conventional radical treatments are 1.5 to 3Gy per fraction for 15 to 35 daily fractions. Stereotactic radiotherapy involves a much higher dose per fraction over fewer fractions, up to 20Gy in a single fraction and will be discussed further in section 1.1.6.

Another way is to improve the conformity of radiation to the tumour target volume, reducing the dose received by surrounding organs and consequently allowing dose to the tumour to be boosted. Developments in radiotherapy technology over recent years have aimed to improve the accuracy and conformity with which radiation doses are delivered.

1.1.2   Target volumes and organs at risk

A critical part of the radiotherapy process is the definition of the tumour volume to be treated. The International Commission of Radiation Units (ICRU) published several reports regarding the definition of tumour volumes and organ at risk [1-3]. The Gross Tumour Volume (GTV) is defined as the palpable, visible or demonstrable tumour volume. The Clinical Target Volume (CTV) includes the GTV plus a margin for sub-clinical spread e.g. regional lymph nodes. The CTV must be adequately treated to achieve a cure. A third volume, the Planning Target Volume (PTV), is defined which includes a margin around the CTV to account for geometric uncertainties in radiation dose delivery. These include day to day variations in patient set up and internal organ motion.

Surrounding organs at risk (OARs) are also outlined for example the spinal cord, rectum and lungs. These may also have margins added to account for set up uncertainties to create Planning Risk Volumes (PRVs).

In conventional fractionation radiotherapy the aim is to deliver the prescription dose as uniformly as possible to the PTV whilst limiting dose to surrounding normal tissue. It is recommended that the PTV dose should be within 95 and 107% of the prescription dose [1]. Hotspots outside the PTV should be avoided, defined as regions outside PTV receiving at least the prescription dose. Doses to OARs should be within defined limits, either from published recommendations or data from clinical trials.

1.1.3   Radiotherapy delivery equipment

This project is limited to megavoltage photons produced by a Linear Accelerator (linac) (Figure 1.1), a brief description of which is given here. All experiments in this project were carried out with either a Varian 2100 iX or a Varian Truebeam (Varian Medical Systems, Palo Alto, CA) therefore the description here is relevant to these machines.

To produce a high energy photon beam, an electron beam is accelerated along an accelerating waveguide using microwave energy. The electron beam is guided towards a tungsten X-ray target using bending magnets. Within the target, the electrons interact with atomic orbital electrons and atomic nuclei producing characteristic X-rays and

bremsstrahlung photons. The resulting photon beam is peaked in the forward direction, therefore a flattening filter is used to create a beam that is flat at depth in tissue.

An ion chamber within the linac gantry measures the photon fluence passing through and checks for beam flatness and symmetry. It also enables calibration of the beam. Once a set number of *Monitor Units* (MU) are reached, the beam is terminated; monitor units are related to the fluence measured by the ion chamber. Each linac beam is calibrated whereby MU are related to dose to water under defined reference conditions. At St. Bartholomew's Hospital 1cGy = 1 MU at the depth of dose maximum (d_{max}), with a 10x10cm open field and 100cm source to surface distance (SSD). This reference dose is measured with a Farmer ionisation chamber with dose calibration traceable to the National Physical Laboratory according to the UK photon dosimetry code of practice [4].

The photon beam is then shaped by a series of collimators within the head of the linac which will be described in the following sections. The linac gantry rotates around a single point in space called the isocentre. The location of the isocentre is displayed visually by an optical cross hair projected from the linac head and external laser beams.

Figure 1.1 Varian linac used in this project.

The dose distribution is optimised initially by adjusting the number of beams, beam direction, relative weighting and radiation energy. Prior to the implementation of multileaf collimators (MLCs), beam shaping was limited to rectangular fields up to $40 \times 40 cm^2$ formed by the 2 pairs of tungsten secondary collimator jaws and involved the undesired irradiation of normal tissue.

1.1.4   Conformal radiotherapy

3D conformal radiotherapy (3DCRT) describes the creation of irregular beam shapes (2D) using a multileaf collimator. The multileaf collimator comprises of two banks of narrow, high atomic number leaves (usually tungsten) which move independently of each other. The Varian linacs used throughout this project have a 120 leaf MLC comprising of 2 banks of 60 leaves, the central 20 cm of which are 0.5cm width at the isocentre and outer leaves are 1cm leaf width at the isocentre. A "beams eye view" projects the MLC position on a simulated radiograph of the patient from the radiotherapy beam direction and helps design the MLC shaping to best conform to the PTV (Figure 1.2).
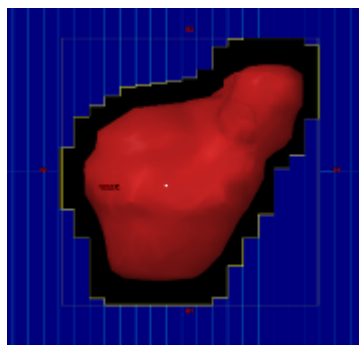
Figure 1.2: Beams Eye View showing multileaf collimator shaping around PTV.

However, conformal radiotherapy is limited in its ability to conform dose distributions to some irregular tumour volumes, particularly those that are concave in an axial plane (Figure 1.3).
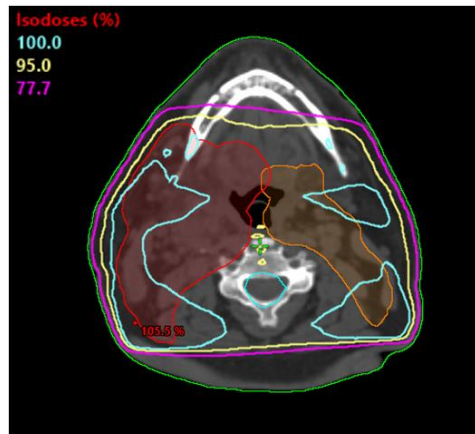
Figure 1.3: Isodose distribution for a 3DCRT plan treating a head and neck tumour with high and low dose PTVs shaded red and orange. There is a large region of normal tissue irradiated, including spinal cord.

1.1.5   Modulated radiotherapy

Modulated radiotherapy techniques such Intensity Modulated Radiotherapy (IMRT) and Volumetric Modulated Arc Radiotherapy (VMAT) have been developed to improve the conformity of dose distributions to irregularly shaped tumour volumes in 3D. They also allow the simultaneous treatment of different PTVs to different doses with a single treatment plan for example primary disease and elective lymph nodes.

IMRT involves multiple intensity-modulated static fields. The dose distribution is shaped in three dimensions by altering the intensity or *fluence* map across each beam (Figure 1.4). Delivery of these intensity modulated beams is achieved by the MLC leaves moving across the field while the beam is on or by using multiple MLC shapes per beam direction. Typically, 5 to 9 beam directions are used. The MLC shields parts of the PTV for large amounts of the treatment, therefore total beam-on time is long for IMRT (> 5 minutes) and there is an increase in scattered dose to the rest of the patient when compared with conformal techniques.

a

b
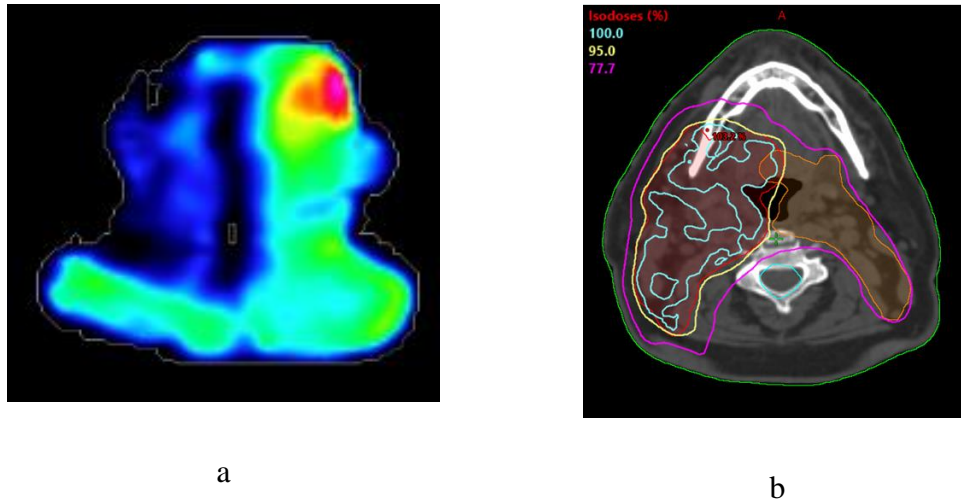
Figure 1.4: Example fluence map for an IMRT field (a) and isodose distribution (b) for a head and neck plan.

With VMAT, the linac gantry continually rotates around the patient in one or more arcs. As the gantry rotates, the MLC leaves move to define different shapes from each direction and simultaneously the linac gantry speed and radiation dose rate vary. VMAT treatments are much shorter than IMRT. Typically, 1 to 2 arcs are used, with each arc taking approximately 1 minute to deliver. As well as improving linac efficiency, shorter treatment times reduce the effects of intra-fraction organ motion and potentially allow for smaller CTV to PTV margins. RapidArc is the VMAT solution for the Varian linacs used throughout this project [5].

1.1.6   Stereotactic radiotherapy

Stereotactic radiotherapy is the treatment with high positional accuracy of small, well defined tumours. Stereotactic Ablative Body Radiotherapy (SABR) is defined as the precise irradiation of an image-defined extracranial lesion with the use of high radiation dose in a small number of fractions. Stereotactic Radiosurgery (SRS) delivers high doses of radiation precisely to intracranial lesions. Accurate tumour localisation may be achieved with immobilisation devices or by imaging during treatment delivery. A Cyberknife unit (Accuray Inc., Sunnyvale, CA, USA) is currently in use at our centre for the delivery of stereotactic radiotherapy treatments. This is a linac mounted onto a robotic arm which allows the delivery of many narrow photon beams from a wide range

of directions enabling steep dose fall off away from the tumour. Stereotactic radiotherapy can also be delivered on a conventional linac with appropriate patient immobilisation and imaging.

There has been an increased interest in stereotactic techniques over recent years. NHS England have led commissioning programs for SABR for specific treatment sites, and awarded contracts aiming to increase the number of patients with brain cancers treated with SRS.

1.1.7 Treatment planning systems

The treatment planning system (TPS) facilitates many functions in the creation of radiotherapy treatment plans, including the importing of CT and other modality images, contouring of target volumes and OARs and the calculation and evaluation of dose to the patient. CT is the imaging modality of choice, as scanners are widely available, geometrically accurate but most importantly can quantify tissue (electron) density which is necessary for accurate dose calculation.

Conformal radiotherapy plans are generally created using *forward planning*. All beam parameters are set by the planner i.e. the number, direction, energy and relative weighting of beams as well as field size and MLC shape. The dose distribution is calculated, plan evaluated and parameters adjusted iteratively until an acceptable plan is achieved.

For IMRT and VMAT, *inverse planning* is used. The number of beams, beam direction (or arc length) and energy are still commonly set by the planner but an inverse planning module determines the MLC positions and other parameters required to fulfil specified dose constraints. Within the inverse planning module, dose objectives are applied for each target volume and OAR and assigned a relative weighting. For example, PTV dose should be within 95% and 107% of the prescription dose. The optimiser determines parameters required to best achieve these constraints. For IMRT this is the MLC leaf motions for each field and for VMAT it is MLC shape, gantry speed and dose rate at each gantry angle.

1.2 Radiation dosimetry

1.2.1 Overview of dosimetry for complex radiotherapy techniques: the challenge

The verification of the accuracy of dose distributions delivered by modern radiotherapy techniques presents a significant challenge. For both IMRT and VMAT, fields are composed of many subfields of complex MLC shapes. The accuracy of dose delivery depends critically on accuracy of MLC position. For fields with small MLC gaps, sub-mm errors in MLC cause large dose errors of several percent [6]. A comprehensive commissioning programme for modulated radiotherapy techniques was recommended following a multi-centre audit of IMRT dosimetry carried out in the United States [7]. Dosimetric measurements were carried out in an anthropomorphic phantom and demonstrated that approximately one-third of irradiations failed to meet the wide criteria that were set of 7% dose agreement and 4mm distance to agreement between measurement and stated dose. A lack of a cohesive approach for the quality assessment of complex radiotherapy technologies was highlighted [8].

There are two options for the verification of the dose calculated by the treatment planning system; a dosimetric measurement or an independent dose calculation. In 3DCRT, a second check of the planned dose carried out by hand using basic beam data, or using simple spread sheets is reasonably straightforward. For IMRT and VMAT there is no simple relationship between the machine settings and dose to a point within the field. The dose to a single point cannot easily be calculated by hand from tables of basic beam data. In addition, the dose varies in 3D, therefore checking the dose accuracy at a single point is no longer adequate. Dose distributions incorporate high dose gradients which present additional challenges. More complex secondary dose calculation programmes exist, for example based on Monte Carlo calculation methods which can carry out a 3D independent dose calculation. However, this only checks part of the process, the TPS calculation, whereas the accuracy of dose delivery can depend critically on multileaf collimator leaf speed and position. Therefore any QA and commissioning programme must also test treatment delivery as well as calculation.

It was proposed that with the introduction of IMRT there should be a change in the type of verification carried out [9]. Rather than separately verifying the correct functioning of all the different hardware and software components of IMRT (and now VMAT)

delivery, it was recommended to assesses the overall accuracy and reproducibility of each IMRT technique. This should be a measurement in a phantom of the dose delivered. A radiation detector is positioned within a phantom and used to measure the dose delivered by the IMRT or VMAT plan. The dose distribution is also recalculated on the phantom within the treatment planning system and measured and calculated doses are then compared. A comprehensive QA programme for IMRT should include the initial commissioning of any software and delivery equipment, ongoing routine quality control and checks on the accuracy of calculation on a per-patient basis [9, 10].

A range of radiation detectors has been used for VMAT and IMRT dosimetry within clinical radiotherapy departments, the most common of which are described in the next sections.

1.2.2   A note regarding absolute and relative dosimetry

Reference is made in radiotherapy to relative and absolute dose measurements. Relative dose measurements are measurements which are normalised in some way. This might be at a point in the distribution or 1D scan, an example being normalising a depth dose curve to the point of dose maximum to give a *percentage* depth dose curve. With regard to the comparison of two dose distributions, this would be called a relative dose comparison if both distributions were normalised to the same point and distributions then presented as percentage values. This has commonly been carried out for IMRT and VMAT 2D dosimetry, for example with radiographic film in a US dose audit [7].

According to Low *et al* [10], "Absolute dosimeters are defined … as those whose results, for absorbed dose to water, require no adjustment or renormalization other than those done in accordance with the established dosimetry protocols". The example given is of a small volume ionisation chamber being cross-calibrated against an ionisation chamber which has a calibration traceable to a national standards laboratory.

For IMRT and VMAT dosimetry where the aim is to verify the accuracy of the dose predicted by the treatment planning system, it is standard practice to exclude any variation in linac output (calibration dose) which might vary by up to $\pm$ 2%. This is accomplished by performing a calibration reading in an open field (e.g. 10×10cm^2) and correcting for detector response according to the *expected* dose rather than the *actual* dose (e.g. as measured by a Farmer ionisation chamber). Results are still presented as

absolute dose (i.e. in Gy). Commercial software tools for dose distribution analysis, such as OmniPro I'mRT used in this project, describe absolute dose in this way. Unless stated, this is the definition of absolute dosimetry used in this dissertation.

1.2.3   Point detectors

Cylindrical ionisation chambers are the gold standard detector used in clinical radiotherapy. Their dose response is traceable to national primary standard detectors at the National Physical Laboratory according to UK dosimetry codes of practice [4]. Cylindrical ionisation chambers are used to calibrate the output of linacs and carry out many quality control tests. Their use is limited for IMRT techniques as they measure dose at a single point and are in general too large for measurement in particularly high dose gradients. However, small volume PinPoint ion chambers are often used in conjunction with film measurements whereby the ion chamber measures absolute dose at a point and the film gives spatial dose information in 2D.

1.2.4   Radiochromic film

Radiochromic film consists of a layer of radiation-sensitive dye on a thin polyester base. When irradiated, a colour change is induced and the optical density is related to the radiation dose. The film may be readout using a flatbed scanner; it is self-developing i.e. no processing is required unlike previously used radiographic film. The most commonly used types are GafChromic^{TM} EBT2 and EBT3 (Ashland, Bridgewater, NJ, USA). The optical density-dose response must be characterised by irradiating areas to known doses and plotting the calibration curve. Film dosimetry has the advantage of providing a sub-mm resolution dose information across a 2D plane.

1.2.5   Electronic portal imaging device

The electronic portal imaging device (EPID) is mounted on an arm attached the linac gantry and allows an amorphous silicon panel to be positioned behind the patient in line with the radiation beam. EPIDs were originally designed to acquire MV photon images of the beam portal just prior to or during radiotherapy treatment to verify patient position. EPID detectors consist of a thin copper layer and a scintillator to create photons which are detected by photodiode and electronics.

EPIDs may also be used for radiation dosimetry. Used in integrating mode, they can capture the whole dose information for a dynamic radiation field. They have been used for various applications including routine linac QC, pre-treatment verification of modulated radiotherapy plans and as an in-vivo dosimeter by making measurement during treatment i.e. with patient in situ (known as transit dosimetry). In terms of dosimetric tool for pre-treatment QC, the dose measured at the panel can be compared with a prediction of dose to this plane, or the EPID measurement can be used to infer the dose within the patient. The latter method results in a 3D distribution, however, software reconstruction is required are required to predict the dose within the patient or phantom.

1.2.6   2D and pseudo-3D detector arrays

There exists a range of 2D and quasi-3D electronic detector arrays. These were introduced to streamline routine linac IMRT and VMAT QC and pre-treatment patient specific verification. 2D devices consist of a 2D array of ion chambers or diodes arranged within a flat panel that can be placed on the couch, held in a mount attached to the linac gantry or positioned within a phantom. Examples include the I'mRT MatriXX (IBA Dosimetry, Bartlett, TN, USA), an array of 1020 ion chambers with 8mm spacing and the MapCheck (Sun Nuclear Corporation, Melbourne, FL), an array of 1527 semiconductor diode detectors with 7mm spacing. They are best suited to the measurement of individual IMRT fields with the device perpendicular to the beam; a large angular dependence makes the measurement of VMAT plans difficult with corrections required for non-perpendicular beam angles.

For VMAT, measurement of whole plan is more appropriate therefore different types of pseudo-3D arrays have been developed. These include the ArcCheck (Sun Nuclear Corporation, Melbourne, FL), where 1386 diode detectors with 1cm spacing are arranged in an arc geometry and the Delta4 (Scandidos, Uppsala, Sweden) where 1069 diode detectors with minimum 5mm spacing are arranged in a cross.

A selection of the devices currently used for radiation dosimetry at St. Bartholomew's Hospital is shown in Figure 1.5.
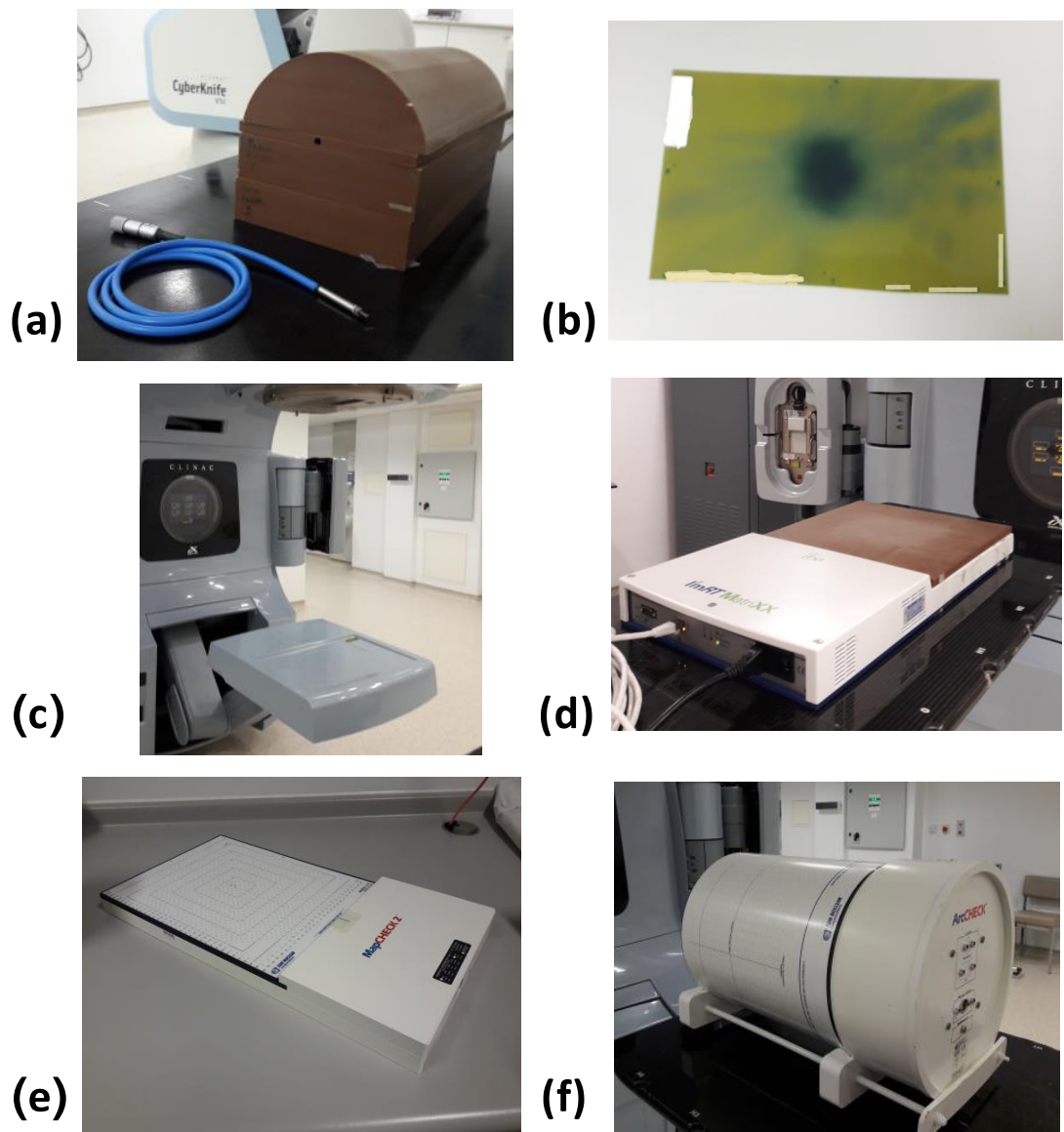
Figure 1.5: Dosimetric devices currently used at St. Bartholomew's Hospital for IMRT, VMAT and stereotactic dose measurements: (a) PinPoint chamber, (b) Radiochromic film, (c) EPID, (d) MatriXX 2D array, (e) MapCheck 2D array, (f) ArcCheck 3D array.

1.2.7   Gamma analysis

Gamma evaluation is very widely used in radiotherapy and allows the comparison of measured and calculated IMRT and VMAT dose distributions in terms of both dose difference and distance to agreement. Measured distribution may be via EPID, 2D or 3D

detector array or radiochromic film and is compared with the dose calculated by the treatment planning system. Dose difference is suitable in a low dose gradient region, but inadequate in high dose gradients where small spatial shifts result in large dose differences. In steep dose gradients, the distance to agreement (DTA) is more appropriate. Therefore, the gamma method was introduced to combine both [11, 12]. For each pixel or measurement point, the calculated gamma value gives a measure of disagreement which may be plotted on a 2D map.

For a point lying on the reference distribution, usually the measured dose plane, the compared distribution needs to contain at least one point for which the gamma value is less than 1 i.e.

$$\Gamma\left(r_c, D_c\right) \equiv \sqrt{\frac{\Delta r^2}{\Delta d_M^2} + \frac{\Delta D^2}{\Delta D_M^2}} \leq 1 \qquad \textbf{Equation 1.1}$$

where Δd_M^2 is a set tolerance for DTA and ΔD_M^2 is a set tolerance for dose difference, Δr is the distance between the reference and compared point and ΔD is the difference in dose. The gamma value is calculated for each point in the reference distribution and the presented gamma for that point is the minimum value. The Δd_M and ΔD_M criteria form an acceptance ellipsoid around the reference point. If an evaluated point it located within this surface then the reference point will pass as the gamma value is less than 1. Tolerances are set for combinations of dose difference and distance to agreement and results are commonly presented as the percentage of measured points which pass the gamma test .

1.2.8   Limitations of current systems.

As discussed in section 1.2.1, a comprehensive programme of QA measurements is required for the accurate delivery and verification of IMRT and VMAT radiotherapy, including:

- Definitive dose calibration of a linear accelerator
- Collection of beam data for input into the treatment planning system, in order to optimise the beam model e.g. depth dose curves, beam profiles and field size factors
- Verification of the accuracy of the treatment planning software

- Routine QA measurements of delivery equipment
- Patient specific quality control measurements whereby the TPS calculated dose is verified on a per-patient basis
- *In-vivo* dosimetry whereby dose measurements are carried out during treatment
- Full 3D verification of the entire planning and delivery chain
- Dosimetric audits in an anthropomorphic phantom
- 4D measurements for respiratory motion.

These different measurements have different detector requirements and therefore each radiotherapy department has a range of detectors available. This was presented as different levels of dosimetry from Level 1 involving high accuracy ionisation chamber measurements for the definitive calibration of radiotherapy beams, to Level 4 the full 3D dosimetric verification of the entire planning and delivery chain for which a multidimensional measurement is required (at least 2D) [9, 13].

Many of the measurements listed above can be adequately carried out with the detectors already in use in radiotherapy and described in the sections 1.2.3 to 1.2.6. For example, the collection of beam data for input into the TPS involves scanning in 1D, for which small volume ion chambers and diodes are suitable. Patient specific QC is carried out as a check of accuracy for every patient plan prior to the start of treatment. Fast, streamlined measurements with immediately available results are prioritised at the expense of detector resolution and this is reasonable as it is a check of an already commissioned technique. Therefore, the pseudo 3D electronic arrays or EPID based methods are suitable. A currently active area of research is investigating the use of the EPID to make dose measurements during treatment for in-vivo dosimetry (known as transit dosimetry).

However, for the commissioning of new IMRT and VMAT delivery technology, treatment planning software and new classes of treatment, a high resolution 3D measurement in a phantom is recommended in published guidance [9, 10]. A high resolution measurement is particularly important at the commissioning stage to identify any issues, for example with the beam model or MLC leaf model in the treatment planning system, with the 3D dose calculation algorithms or with the MLC calibration and performance of the MLC and other components of the treatment machine. A

measurement of the full 3D distribution would increase the confidence in the accuracy of radiation dose delivery, and potentially allow treatment margins to be reduced or doses to be escalated. The ability to position a 3D detector within geometric and patient representative phantoms would provide the ability to carry out an end-to-end test of the entire planning and delivery chain. Despite their individual benefits, for all the detectors in current use, none offer the true 3D dose measurement required for technique commissioning. In all cases the 3D dose distribution is only sampled at discrete points or across 2D planes. This prompted a search for a high resolution 3D detector.

1.3   3D chemical dosimetry

In principle, this 3D measurement can be carried out using chemical dosimetry which is based on the quantification of the extent of a chemical reaction induced by ionising radiation. For 3D measurements, chemicals are embedded within a solid structure such as a gelatine matrix. Various 3D chemical detectors have been developed including Fricke gels, polymer gels and PRESAGE^{TM}. Once irradiated, the detector is read out with a 3D imaging tool to enable quantification of the 3D dose distribution. This has most commonly been accomplished using magnetic resonance imaging or optical-CT imaging.

1.3.1   Types of 3D chemical detector

Fricke gel dosimetry was proposed in 1984 [14] and is based on the radiation-induced oxidation of ferrous ions (Fe^{2+}) to ferric ions (Fe^{3+}). Ferrous ions are present in the form of ferrous ammonium sulphate which in solution form has been used as a radiation detector for many decades [15]. When mixed with gelatine or agarose, the spatial dose information is preserved. The change in the relative concentration of ferrous and ferric ions was shown to alter the T_1 and T_2 relaxation times enabling 3D quantification of the measured dose distribution using magnetic resonance imaging (MRI) [16-20]. The radiation also induces a change in optical density, therefore others have investigated the use of optical-CT scanners to readout irradiated detectors [21-28]. The benefits of Fricke gel dosimetry are that it is based on a well-established dosimetry technique, low toxicity chemicals are used and the manufacture process is straightforward requiring only simple laboratory facilities. However, a post-irradiation diffusion of ferric ions has

been reported [17, 22, 25, 29-33] which causes a blurring of the measured dose distribution over time.

Focus then moved onto polymer gel dosimetry which is based on the radiation-induced polymerisation of monomers [34, 35]. The amount of polymerisation, related to the radiation dose, is quantified using MRI [35] or optical-CT [36]. Polyacrylamide gels or "PAGs" use acrylamide as the monomer [34, 35] but must be manufactured under a nitrogen atmosphere in order to eliminate oxygen which otherwise inhibits polymerisation. Oxygen must be bubbled through the mixture for several hours during manufacture. Other monomers have been evaluated [37]. Normoxic gels overcome this limitation by employing antioxidants to scavenge the oxygen allowing gel manufacture under normal atmospheric conditions [38]. The use of toxic chemicals, requiring more sophisticated lab facilities, is a disadvantage of polymer gel detectors versus Fricke gels. In addition, it has been shown that some polymer gel compositions suffer from poor inter-sample variation [39], volume dependence [40], and variation in response due to integration of radiation dose [41]. Despite much research effort over many years, it was recently acknowledged that polymer gel dosimetry is still largely restricted to research departments [42].

Radiochromic dosimeters which attenuate light by absorption have also been proposed. PRESAGE[TM] is a solid polyurethane based plastic material doped with a radiochromic leuco dye [43-46]. Ionising radiation causes a colour and therefore optical density change which is quantified using optical-CT. It has been reported that this detector offers low diffusion post-irradiation compared with gel based compositions [43]. Initial studies aimed to characterise some of the dosimetric properties of this detector [44-46]. Feasibility studies investigated the use of PRESAGE[TM] and optical-CT for the measurement of small field commissioning data [47] and to measure clinical dose distributions within a thorax phantom [48]. However, at the outset of our project, it was not readily commercially available nor is it straightforward to manufacture. In addition, this detector may only be analysed using an optical-CT scanner, which must also be purchased specifically.

1.3.2 Imaging systems used for 3D dosimetry read out

Various methods of 3D imaging have been proposed to quantify in 3D the measured dose distribution including MRI [16, 35], optical-CT [23, 36], X-ray CT [49, 50] and ultrasound [51]. Of these, the best results have been obtained with MRI and Optical-CT.

MRI has been used to quantify the delivered dose distribution for both Fricke gel dosimetry [14, 16, 18, 52] and polymer gel dosimetry [35, 53, 54]. The analysis method is based on a radiation-induced change in the T_1 or T_2 relaxation times, which will be described further in chapter 3. For Fricke gel dosimetry, this change is due to the different concentrations of ferrous and ferric ions which are paramagnetic. For polymer gel dosimetry, the change is due to the effect of polymerisation on the relaxation time, most commonly the T_2. The advantage of MRI is that it is a well-established clinical imaging modality, with scanners already located within hospitals. However, access to them for research purposes can be limited as they carry a heavy clinical workload.

Optical-CT scanners have been developed for the analysis of 3D chemical detectors [21, 22, 36, 55, 56]. This is similar in concept to conventional X-ray CT, although visible light rather than X-ray radiation is transmitted through the material and detected. Image contrast is formed due to light absorption by Fricke detectors, and light scattering by polymer gel detectors. The detector, for example a charge coupled device CCD camera, rotates to allow the acquisition of a series of image projections at different angles which are reconstructed to form the 3D image [55, 56]. Most recent scanners use either a parallel beam [56] or cone beam configuration [55, 57]. It is claimed that although cone beam systems are less expensive they suffer issues due to stray light artefacts [58], whereas parallel beam systems are more costly.

Optical-CT scanners must be purchased or designed specifically for gel applications. An optical-CT scanner would represent an additional investment for a clinical radiotherapy department for use specifically for 3D dosimetry, therefore this technology has thus far been limited to select research groups [59]. In any case, there are few scanners commercially available.

1.3.3 Current status

A large amount of research over many years has focused on chemical composition, gel manufacture and imaging analysis however 3D chemical dosimetry has yet to be implemented as a routine dosimetric tool in clinical radiotherapy. This was the case at the start of this project and is still true now. A recently published text book focuses on 3D dosimetry, highlighting the importance still placed on finding a suitable system for modern dosimetry [58]. Two chapters are dedicated to 3D chemical dosimetry; however, it was acknowledged that chemical dosimetry is still largely limited to academic centres. This has been attributed to factors including the need for toxic chemicals, sophisticated laboratory facilities and access to expensive or bespoke scanners [42]. In addition, it was suggested that a factor for the slow uptake of chemical dosimetry within clinical radiotherapy departments is due to a lack of confidence in the reliability of these detectors.

The accuracy of measurement of any radiation detector must first be established before it is used to measure unknown radiation distributions. Without a quantified measurement uncertainty, the level to which the detector can be trusted for measurements in complex dose distributions is not known and it is impossible to identify the cause of any discrepancies between the measured and planned dose distributions.

There is a variation in the methods and criteria previously used in the literature to evaluate 3D chemical dosimeters and compare different chemical compositions. Many authors have made comparisons of the detector sensitivity via the dose-response curve [25-27, 38, 60]. Publications describing dosimetric characteristics of 3D detectors have used a variety of factors such as variation in response with energy [61], dose rate [62] and error due to the calibration methodology [63, 64]. These individual factors are all relevant, but do not fully predict the overall performance of the detector-imaging system. A systematic method for testing new 3D chemical detectors is required for the widespread implementation of 3D chemical dosimetry in clinical radiotherapy.

1.4 Project aims

The aim of this project is to address these issues and develop a 3D gel detector that is simple to manufacture and use in a clinical radiotherapy department, that operates over

a clinically relevant dose range and has a proven dosimetric performance with quantified measurement uncertainties.

The dosimetric characteristics of the selected detector will be systematically evaluated over two dose ranges of clinical relevance: 0 to 3Gy relevant to conventional fractionation schemes and 5 to 20Gy for high dose per fraction stereotactic techniques. An emphasis will be placed on the evaluation of the basic dosimetric performance and quantification of measurement uncertainties. A logical and practical method for the testing of new 3D chemical detectors will be developed.

1.5   Thesis scope

This thesis is written by a radiotherapy physicist and prompted by difficulties encountered in verifying the accuracy of complex radiation distributions in clinical practice. It follows on from previous work by this research group, investigating a commercially available polymer gel detector which highlighted substantial uncertainties in the accurate measurement of radiation doses even in simple radiation fields [39, 40].

It was therefore decided to investigate a detector that could be manufactured in-house within a clinical radiotherapy department. We set requirements that the detector should be simple to manufacture with only basic laboratory facilities and that the irradiated detector should be readout using existing imaging equipment available within our hospital. Of the available detector types and readout methods, Fricke gels and MRI best fulfil these requirements and were therefore selected for this work. Fricke gel detectors involve only low toxicity chemicals and require very basic laboratory facilities, therefore could be manufactured in a simple lab within the radiotherapy physics department at St. Bartholomew's Hospital. Clinical MRI scanners are located in the same building.

Once manufacture and readout methods were established, our Fricke-MR system was fully commissioned as if it was a commercial product and we were the end user before application to complex VMAT distributions.

1.6   Thesis structure

This thesis is organised into 7 chapters. Chapter 2 contains a more detailed overview of Fricke gel detectors including a structured literature review of previous work carried out

on the dosimetric characterisation of Fricke gel detectors. This review highlighted areas with little evidence, and a lack of systematic approach to testing 3D chemical detectors, particularly under clinically relevant irradiation conditions.

Within chapter 3, methods for the manufacture of a Fricke gel detector are described. A literature review was carried out to identify a starting point for the detector composition used in this project. An overview of the MR theory relevant to the readout of Fricke gel detectors is presented. MR scan and measurement protocols were developed for an NMR spectrometer and a whole-body MRI scanner.

The experimental work is described in the following chapters. Detector characteristics were systematically investigated with increasingly complex dose distributions. Chapter 4 describes measurements in simple radiation fields, where small volume detectors were irradiated to known doses to establish basic detector characteristics of inter-sample variation, chemical stability, dose rate and energy dependence. Test tube samples were irradiated and read out with a bench-top NMR scanner. Experiments on large detector volumes were then carried out, analysed with the MRI scanner, and are the subject of chapter 5. The homogeneity of response and variation with detector volume were investigated as well as the post-irradiation diffusion of ferric ions.

Calibration methods were then established. The optimised detector-imaging system was then finally used to measure the delivered dose for simple and complex VMAT treatment plans, described in chapter 6. The project is summed up, including recommendations for future work, in chapter 7.

1.7   Statement of originality

A large body of work already exists on the subject of 3D chemical dosimetry and it is reviewed in chapter 2. However, the work previously carried out has largely been concentrated in research laboratories and much of it has focused on the customisation of the chemistry of the detectors, detector manufacture and imaging protocols. There has been a lack of structured approach to the testing of the final customised detector and imaging system, as would be normally carried out for any other radiation detector. This was recently acknowledged by key researchers in the field of 3D chemical dosimetry. In a recently published textbook on 3D dosimetry, it was commented in regards to polymer gel dosimetry that *"A major obstacle that has hindered the wider dissemination of*

polymer gel dosimetry in radiotherapy centers is a lack of confidence in the reliability of the measured dose distribution" [42]. A further analysis of the reasons behind the slow uptake of this dosimetry technique by clinical radiotherapy departments was presented [65]. Here it was stated that "*Despite significant progress in the capability of multi-dimensional dosimetry systems, it is striking that true 3D dosimetry systems are today largely found in academic institutions or specialist clinics*" and "*the goal of widespread clinical implementation remains elusive*". In terms of proposed reasons, the authors highlighted issues including the requirement for substantial expertise for particular detector systems, that some systems exhibit dosimetric issues including with sensitivity and stability and that there are issues with the economics and practicality of techniques in non-research settings.

The work presented within this thesis aims to address these concerns by (1) the selection and customisation of a detector-imaging system with focus on implementation within a clinical radiotherapy department and (2) a full and structured quantitative dosimetric characterisation of the detector before applying the detector to complex clinical techniques. In contrast to the previous approaches, the detector system was fully commissioned using the same approach that would be applied to a commercial detector system.

Regarding the expertise necessary to implement 3D chemical dosimetry within a clinical radiotherapy department, in this project primary considerations when selecting a detector and imaging method were the ease of detector manufacture, toxicity of chemicals, cost and the local availability of scanners. This is discussed in chapter 3 which describes the development of imaging processes and detector manufacture with a very strong focus on applicability and use within a clinical radiotherapy department.

The main area of novelty was the definition at the outset of quantified dosimetric requirements of a 3D detector and the development of a structured plan to evaluate the dosimetric uncertainty of the detector. For other detector types, such as radiochromic film, there exists published guidance for their implementation and commissioning [66]. There is currently not a similar guide for 3D chemical dosimetry. To address this an analysis of the entire detector-imaging process was first carried out in order to identify the factors which should be investigated to quantify the uncertainty for 3D chemical dosimetry (chapter 2).

A review of the existing literature on Fricke gel dosimetry was then carried out which highlighted major areas with lack of evidence and an unstructured approach to detector characterisation. Therefore, the aim of the first sets of experiments of this project was to fill in these gaps in evidence by undertaking measurements to quantify dosimetric uncertainties for this detector. This systematic characterisation for one particular detector and imaging combination has not been presented previously in the literature.

As outlined in section 1.2.8, the intended application of 3D dosimetry not currently fulfilled by existing dosimetric devices is a high resolution measurement of 3D dose distributions delivered by modulated radiotherapy techniques to a water equivalent, or patient mimicking, phantom during the commissioning stage of new technology, software or for classes of treatment. The final experimental chapter described the use of Fricke gel detectors to measure high dose per fraction VMAT plans and quantitatively compared results versus the treatment planning system. Again, because of the previously documented large range of chemical formulations proposed for chemical dosimetry, there is sparse evidence in the literature for Fricke gel measurements of VMAT plans. The measurement of complex VMAT plans with a fully commissioned Fricke gel-MR system has not been previously reported.

Results from this project have been presented at the UK Biennial Radiotherapy Meeting of the Institute of Physics and Engineering in Medicine (IPEM):

2010: The dosimetric characterisation of 3D chemical detectors (a literature review)

2018: The dosimetric characterisation of an in-house method for Fricke gel dosimetry applied to the verification of stereotactic VMAT plans

Chapter 2. The dosimetric characterisation of Fricke gel detectors: a review of the literature

2.1 Introduction

2.1.1 Aims of this chapter

An important part of the commissioning process for any radiation detector is an investigation into each of the factors which might affect its measurement uncertainty. According to the National Institute of Standards and Technology (NIST): "a measurement is only complete when it is accompanied by a quantitative statement of its uncertainty" [67]. There are many potential sources of uncertainty for radiation detectors used in radiotherapy dosimetry, such as dependence of response on radiation energy, dose rate, temporal and spatial instability and angular dependence [68, 69]. These factors are specific to each detector type and depend on the construction, geometry and operation of the detector. As highlighted in chapter 1, and previously discussed in the literature, an important reason for the slow uptake of 3D chemical dosimetry by clinical radiotherapy departments is a lack of confidence with their dosimetric performance. The aim of this chapter is to outline the potential sources of uncertainty for Fricke gel dosimetry, review the literature in terms of existing evidence and identify gaps. From this, a plan will be developed to quantify the dosimetric characteristics of a Fricke gel detector.

Before this can be carried out, the general requirements of a detector for the 3D measurement of complex radiotherapy distributions should be defined. As discussed in chapter 1, detector requirements depend on the intended application of the detector. The aim of this project is to implement a method for high resolution dosimetry as part of the pre-clinical commissioning of VMAT radiotherapy, for which it is recommended that a high resolution 3D dose measurement is carried out [9]. This should be a direct measurement of dose in a phantom, not requiring software back projection methods to predict dose to the phantom. The first basic requirements are therefore a 3D measurement and that this should be a direct dose measurement in a phantom.

The dosimetric and geometric uncertainty need to be adequate for the intended measurement and this needs to be quantified. When comparing measured to calculated dose distributions, any deviation between the two distributions has several potential

causes; uncertainty with the delivery of radiation, uncertainty with the dose calculation, or uncertainty connected to the measurement device itself. International guidance documents were reviewed with the aim of setting a tolerance for dosimetric uncertainty of a 3D measurement detector [9, 58, 70, 71]. These reports discuss the subject of uncertainty in radiotherapy in depth but, even in the more recent documents, a clear statement of uncertainty required of a 3D dosimeter is lacking. This is partly due to there being different dosimetric requirements for different types of radiotherapy treatment for example high dose per fraction stereotactic techniques versus conventional fractionations or palliative radiotherapy. There are also different requirements for different regions within one dose distribution; high dose, high dose gradient and low dose regions which will be discussed more fully subsequently [9, 70].

A comprehensive report was recently published by the International Atomic Energy Agency (IAEA) regarding uncertainty in radiotherapy [70]. The impact of dose uncertainties with radiotherapy delivery on radiobiological outcomes (NTCP and TCP) were considered. Based on this analysis, it was recommended to aim for systematic uncertainties in radiotherapy *delivery* within 1-2% and random uncertainties within 3-5%. The main focus of the remainder of this report was on what level of accuracy is currently achievable in clinical practice. The many various sources of uncertainty in the calculation and delivery of radiotherapy were considered for example (but not limited to) processes for dose calibration, QC, imaging and outlining of the target volumes and critical structures. Of relevance to this project, the uncertainty associated with treatment planning systems was split into different regions of the dose distribution; high dose, low gradient (2%), high dose gradient (2 to 4mm) and low dose, low gradient (3 to 5%). For the end to end measurement of dose verification in a phantom, incorporating errors in calculation and delivery, the suggested tolerance was 3 to 10% or 2mm.

According to Ahmed *et al* [72], there is a dilemma regarding IMRT dosimetry in that the uncertainty of the detectors used to perform dosimetric measurements is of the same order of magnitude as the desired uncertainty in the delivered dose, rather than an order of magnitude smaller as usually required for metrology. An ideal detector would have a dosimetric uncertainty of much less than 1%, and it will be seen in the next paragraphs that this is not achieved by any detector offering spatial information of dose distributions. It was presented in another way, that one of the factors limiting overall

accuracy in radiotherapy is the limit to the measurement accuracy practically achievable using today's instrumentation [58].

Requirements for the geometric uncertainty again depend on the specific technique. At St. Bartholomew's Hospital, the distance to agreement criteria when comparing measured to calculated distributions is set at 1mm for stereotactic radiotherapy and 2-3 mm for standard dose per fraction VMAT in agreement with other published dose audits [73-75]. Therefore, it might be desirable to set a sub-mm limit for the geometric uncertainty for the detector and scanner combination. For 3D chemical dosimetry, it is the scanner resolution that determines the geometric uncertainty. However, there is an inherent compromise between dosimetric uncertainty and scan resolution, as highlighted previously specifically for 3D chemical dosimetry [76]. These authors proposed a tolerance of 1mm for the spatial resolution of this dosimetry system.

An ideal detector might have a tolerance of < 1% for dosimetric uncertainty depending on the treatment technique under investigation, however it will be seen that this is not achieved by the detectors currently used for 2D or pseudo-3D dosimetry. It would therefore be reasonable to set aims for 3D dosimetry based on an assessment of dosimetric and geometric uncertainty achieved for 2D detectors currently used for IMRT and VMAT dosimetry. The performance of typical detectors currently used for IMRT, VMAT and stereotactic dosimetry were therefore reviewed and this is presented in table 2.1. There is a wide range of detectors used within radiotherapy for IMRT dosimetry and for each type of detector a variety of different models, geometry construction and measurement methodology. Presented are the detectors currently in use at St. Bartholomew's Hospital for VMAT and stereotactic radiotherapy dosimetry which are representative of the detectors used by a typical clinical radiotherapy department. Many sources of uncertainty potentially contribute to the overall detector uncertainty. These are specific to each different detector; significant effects are summarised in table 2.1. The overall dosimetric performance figures in this table were extracted from a reference text book [58] and key publications; for the PinPoint chamber [77, 78], radiochromic film [79-81], Varian EPID [82, 83].

It can be clearly seen that none of the detectors in current use comply with the basic requirement of a true 3D dose measurement. Ionisation chambers are considered the "gold standard" detector in radiotherapy in terms of accuracy and precision. However,

they only measure at a single point and are too large, even the small volume PinPoint detector presented here. The EPID does not offer a direct measurement of dose, requiring software to reconstruct the dose back onto a phantom or the patient. The measurement resolution of the ArcCheck does not fulfill requirements, with the detector spacing greater than 0.5cm. 2D radiochromic film is commonly used for the verification of dose distributions for VMAT and IMRT. Although only 2D, it is high resolution and potentially could be used to evaluate multiple planes. However, each film measurement requires a repeated plan irradiation and phantoms can normally only accommodate the film in a particular orientation. There is a practical limit therefore to the number of dose planes assessed. In terms of the dosimetric accuracy, the 2D detectors presented in table 2.1 have a typical range of up to 3%. It is therefore common to combine measurements that offer spatial dose information, for example radiographic and radiochromic film with a point dose measurement, for example with an ionisation chamber [7, 74, 84].

3D chemical dosimetry complies with the requirement to directly measure a 3D dose distribution in a range of phantoms and has the potential to offer a high resolution measurement. Considering all the factors outlined in this section regarding ideal and realistic dosimetric uncertainty, in this project it will be attempted to maintain dosimetric uncertainty for the detector measurement within 3%, for an in-plane uncertainty of 1mm. If necessary, combining a 3D gel measurement with a more precise but single point dose measurement with an ionisation chamber would be a reasonable option similar to a common approach used for 2D dosimetry.

Table 2.1 Summary of characteristics for detectors currently used for VMAT dosimetry

Characteristic		PinPoint ion chamber (0.015cc)	EBT3 GafChromic film (Radiochromic film)	Varian EPID	ArcCheck detector array
3D measurement		No	No	No	No
Direct dose measurement		Yes	Yes	No	Yes (not in high dose region. Entrance / exit dose measured)
Absolute (Gy not %)		Yes	Yes (only with strict irradiation and scanning protocols)	Yes	Yes
Water/tissue equivalent		No	Yes	No	No
Geometric uncertainty		Point dose 2mm diameter, 5mm length	Depends on scanner resolution, typically ~0.4× 0.4mm	0.4×0.4mm, but mechanical sag 1mm	1cm detector spacing
Dosimetric uncertainty	Overall	<1% repeatability but energy dependence (effect depends on field size)	2-3%	1.5-3%	2-3%
	Notable sources of uncertainty	Stem effects, energy dependence	Film orientation & position, non-uniformity, chemical instability	Missing signal, back scatter, image ghosting, pixel-to-pixel variation, energy dependence	Energy dependence, angular dependence

2.1.2 Chapter overview

The remainder of the chapter focuses on the dosimetric performance for a Fricke-MR detector system. A more detailed description of the Fricke gel detector is provided in section 2.2. The factors potentially affecting the measurement uncertainty for Fricke gel dosimetry were then identified. The whole Fricke gel process, from manufacture and irradiation to scanning and analysis, was considered to identify all sources of measurement uncertainty specifically for this measurement system. This is presented in section 2.3. The Fricke gel literature was then reviewed to identify publications which investigated each of these factors, for example variation in dose response with detector volume, radiation energy or chemical stability (section 2.4). Finally, the results of this structured review were used to develop an experimental plan for this project.

2.2 Background into Fricke gel detectors

Fricke gel dosimetry was introduced in chapter 1 and previous research has demonstrated sufficient promise with benefits such as simple manufacture to be selected for further investigation in this project. There follows a more detailed description of Fricke gel dosimetry.

Fricke gel detectors are a type of chemical detector based on ferrous ammonium sulphate. Chemical detectors require a reaction to occur which causes a measurable change, for example colour or temperature. When water is irradiated, a series of reactions occur resulting in the production of free radicals. These free radicals react with the ferrous ions to produce ferric ions. There are a series of reactions, but simplified reactions for the three main reaction channels are given below.

$$H_2O \xrightarrow{\text{Ionising Radiation}} e_{aq}^-, HO^\bullet, H^\bullet, HO_2^\bullet, H_3O^+, OH^-, H_2O_2, H_2$$
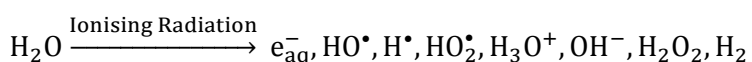
The hydroxyl $HO^\bullet$ reacts with a ferrous ion to produce a ferric ion:
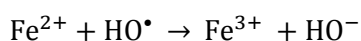
$$Fe^{2+} + HO^\bullet \rightarrow Fe^{3+} + HO^-$$

The hydrogen peroxide produces two ferric ions per molecule:

$$Fe^{2+} + H_2O_2 \rightarrow Fe^{3+} + HO^\bullet + HO^-$$
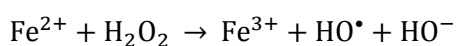
and, $Fe^{2+} + HO^{\bullet} \rightarrow Fe^{3+} + HO^{-}$

or in simplified form:

$2\ Fe^{2+} + H_2O_2 \rightarrow 2\ Fe^{3+} + 2\ HO^{-}$
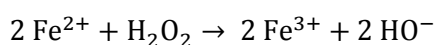
Finally, the hydroperoxyl radical can react to create three ferric ions. This reaction channel can be simplified to:

$HO_2^{\bullet} + H^{+} + 3\ Fe^{2+} \rightarrow 3Fe^{3+} + 2HO^{-}$
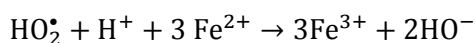
Both ferrous and ferric ions are paramagnetic species but with different relaxivities. Relaxivity is the degree to which the species enhances the MR longitudinal and transverse relaxation rates (R_1 or R_2). R_1 and R_2 are related to the concentration of ferrous and ferric ions and therefore, to the delivered radiation dose. The different concentrations of ferrous and ferric ions also affect the optical density of the sample, therefore delivered radiation dose may also be determined by quantifying the OD using optical methods. This was first made use of in Fricke solution dosimetry [15], a well-established dosimetry technique, using spectrophotometer readout.

The analysis of Fricke detectors using MRI was proposed by Gore *et al* [14]. The change in the relative concentration of ferrous and ferric ions was shown to alter the T_1 and T_2 relaxation times. Fricke solution samples were irradiated and a linear relationship between R_1 and radiation dose was demonstrated. It was then proposed that mixing the Fricke solution with a gelling agent such as gelatine or agarose would produce a solid 3D detector where radiation dose would be preserved in 3D. This was accomplished in the late 1980s [16, 85] and followed by many studies reporting the use of Fricke gel detectors with MRI for 3D radiotherapy dosimetry [17-20, 26, 29, 31, 86-88]. Optical methods have also been used to read out irradiated Fricke gels [21-28].

Many publications reported the investigation of different chemical compositions, such as varying concentrations of ferrous ammonium sulphate and sulphuric acid [28, 56, 89, 90], gelling agents [17, 19, 23, 25, 91, 92] and the use of other components such as xylenol orange [22, 28, 31] and saccharides [27]. These will be reviewed in more detail in chapter 3 in order to identify an evidence based starting point for the detector composition used in this project. Many of these focussed on optimising the dose response (i.e. detector sensitivity) when comparing the different chemical compositions.

Researchers have applied Fricke gel detectors to a variety of clinical applications for example proton beams [93], neutron beams [94] and high dose rate brachytherapy [88, 95]. In terms of external photon beams, Fricke gel detectors have been used to measure small radiation fields [96], MLC properties [97] and distributions delivered using stereotactic radiotherapy techniques e.g. Gamma Knife [98-100].

Despite promising results, Fricke gel dosimetry is still not widely used in clinical radiotherapy departments. Prior to use as a dosimetry tool for the verification of these complex distributions, a systematic analysis of dose uncertainty is required. A summary of the literature on the dosimetric testing for Fricke gel detectors is the subject of the next section.

2.3   A critical analysis of the Fricke gel measurement process.

2.3.1   Overview

It is necessary to commission any detector used for radiation dosimetry to establish its limitations in the measurement of radiation dose and determine the overall measurement uncertainty [68, 101]. Properties which dosimetrically characterise a general radiation dosimeter are described in these reference texts including precision, accuracy, energy dependence, dose rate dependence and chemical effects. These provide a starting point for the testing of 3D chemical detectors. However, sources of uncertainty are specific to each different type of detector and need to be identified for 3D chemical detectors. An AAPM report into the characterisation of radiochromic film, usefully lays out the different detector characteristics which should be considered for this 2D chemical detector [66]; no similar reference exists for 3D chemical dosimetry, however, concepts are similar therefore can be extended to 3D chemical detectors. Characteristics have been proposed for 3D polymer gel dosimetry [42] but key factors are absent for example detector homogeneity.

To identify the factors which potentially affect the measurement accuracy specifically for 3D chemical detectors, dosimetric characteristics outlined in the text books and guidance documents referenced above were considered, along with an analysis of the entire measurement process as follows. 3D chemical detectors are manufactured in batches, either in-house or as commercial products. They are then stored prior to being irradiated with the proposed radiotherapy treatment plan. Additional calibration samples

are irradiated with known radiation doses. The irradiated detector and calibration samples are then scanned with the optimised 3D imaging protocol. The dose response relationship is characterised by plotting signal versus dose for the calibration samples. This is used to convert image signal to measured dose distribution which may then be compared against the dose predicted by the treatment planning system using analysis software.

Chemical detectors may be affected by the ambient conditions during storage and therefore the time between manufacture, irradiation and scanning; there may be spatial and dosimetric instability over time. The radiation dose rate and energy delivered at the detector may vary. The homogeneity of response across large volume 3D detectors also needs to be considered. As integrating detectors, another consideration is how they integrate the dose from multiple beams compared with an identical dose delivered in a single shot. These chemical detectors must be calibrated to convert imaging signal to dose. This is accomplished by irradiating additional samples to known doses and plotting their characteristic dose-response curve. The calibration process itself may introduce measurement uncertainties depending on the number and volume of samples used and curve fitting of the dose response relationship.

A summary of these potential sources of measurement error for 3D chemical detectors is presented in Figure 2.1. A brief description of each is provided in the following section. Then the Fricke literature was then reviewed to identify publications addressing each of the factors in turn, described in section 2.4.
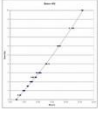
Figure 2.1: Summary of potential sources of error for 3D chemical detectors.

2.3.2 Scanner properties

Variation in the imaging response across the scan volume arises from the random fluctuations in image intensity (image noise) and unwanted signals in the image (image artefacts). There is an inherent compromise between SNR, imaging time and resolution. A variation in response of repeated scans would contribute to the overall measurement uncertainty if calibration and experimental samples are scanned sequentially.

2.3.3 Detector properties

Inter-sample variation

To characterise the dose response of chemical detectors, additional detector samples are typically irradiated to known radiation doses. It is common practice for experimental and calibration samples for a particular experiment to originate from the same batch. As such, the inter-sample variation is an important factor that should be evaluated. When evaluating the inter-sample variation, it is necessary to control all other potential contributions to measurement uncertainty. This is accomplished by irradiating samples

from the same batch at the same time, with identical radiation conditions and scanning all samples at the same time.

Dose response

The dose response i.e. the signal versus delivered dose has been commonly used to evaluate different 3D chemical detectors and to compare different chemical compositions. A steeper response allows greater differentiation between doses; uncertainties for example due to inter-sample variation will be magnified for detectors with a lower dose response. The shape of the dose response curve is also of interest. A linear response is not essential, but simplifies the calibration process requiring fewer dose points and therefore calibration samples to characterise the dose response.

Chemical effects: dosimetric stability

Chemical reactions may occur due to external factors other than irradiation, for example heat and light during storage. In addition, following irradiation chemical reactions may take some time to complete. The result of these effects is that the detector signal may vary depending on the length of time between manufacture and irradiation, and also the time between irradiation and scanning.

Short term signal instability can introduce additional measurement uncertainties for long scanning or analysis sessions. It is important to quantify and minimise uncertainties by selecting an appropriate time within which to analyse irradiated detectors. Long term signal drift, or variation in response, might limit the shelf life of these detectors i.e. the time within which a detector should be used after manufacture.

Spatial stability (post-irradiation diffusion)

Any diffusion of ions throughout the gel matrix following irradiation would cause a blurring of the dose distribution increasing with time between irradiation and readout. If significant this would require the detector to be scanned within a set time of irradiation. It would be useful to define the time within which a detector should be scanned to fulfil pre-set tolerances on spatial accuracy.

Temperature during irradiation and scanning

The temperature during irradiation can affect the response of detectors, so is a characteristic to be considered. However, if experimental and calibration samples are irradiated and scanned at the same time, any effect of irradiation or scanning temperature on measurement uncertainty should be minimal. In addition, altering the temperature of the detector during irradiation is a difficult task. This will not be considered further in this project, instead efforts made to control the room temperature during irradiation.

Radiation energy

A detector may over- or under-respond to different radiation energies if it lacks tissue equivalence i.e. if its effective atomic number is quite different to tissue (or water). Calibration samples are typically irradiated using a beam of the same radiation quality as the experimental sample. However, the radiation energy at the detector depends on both the energy set at the treatment machine and the local energy spectrum which is influenced by field size and beam modifiers. Energy dependence should be investigated over a sufficiently wide energy range for the intended clinical application.

Dose rate

Once again, where possible calibration and experimental samples are irradiated using the same dose rate set on the treatment machine. However, the set dose rate can vary considerably for some techniques such as VMAT and the dose rate deposited at the detector also depends on factors such as the distance from the source and beam modifying devices. Therefore, the dose rate dependence of 3D chemical detectors should also be considered.

Dose fractionation

The delivery of most radiotherapy techniques is via multiple treatment fields, rather than delivery the dose in a single shot. How a detector integrates the doses delivered in multiple sequential beams compared with a single shot is also a characteristic that should be investigated.

Homogeneity

Ideally, a 3D detector should display a uniform response across its volume when irradiated to a uniform radiation dose. In practice, there may be variations in signal across chemical detectors due to detector manufacture and cooling processes. It might be possible to correct for any non-uniformity with a pre-irradiation background scan, although this adds an additional step in the overall measurement process.

Volume

A difference in thermal history and therefore dose response might also occur for chemical detectors of different volume and shape. This is particularly important if small volume samples are used to calibrate large volume experimental phantoms.

Detector calibration

Finally, the calibration process potentially introduces errors. The number of samples, number of dose points and volume of samples may affect the uncertainty of the measurement as well as the methods used to model the dose response curve. If calibration of the detector is carried out using additional samples irradiated to known doses, it is imperative to assess the inter sample variation in response. In addition, if these samples are of a different volume to the experimental sample, the volume dependence must be investigated. How the characteristic dose response curve is modelled also affects the dosimetric accuracy.

2.4 Review of the literature on the dosimetric characteristics of Fricke gel detectors

2.4.1 Introduction

The Fricke gel literature was then reviewed against each of the detector characteristics outlined in the previous section. In this chapter, the focus was only on detector performance, as the scanner (MRI) performance is covered specifically in chapter 3.

Any paper describing Fricke gel detectors was initially considered. Any detector composition was included that included at least ferrous ammonium sulphate in a gelling material. Papers were included which used both optical and MRI based methods. The body of Fricke gel literature was then searched to find evidence for investigation of

each dosimetric characteristic in turn. Search tools including Medline and Google scholar were used and extensive cross checking of references was carried out, including use of Web of Knowledge.

2.4.2 Literature analysis of detector characteristics

2.4.2.1 Inter-sample variation

A systematic review previously demonstrated a lack of evidence for the basic precision of 3D gel based detectors [102]. This was found to be the case again in this review. Only one paper was found which described the inter sample variation for Fricke gel detectors [103]. The standard deviation of the optical density of 10 samples was calculated for Fricke gel detectors both pre-irradiation, and following irradiation to 10Gy using a Co^{60} source. The coefficient of variation was 3% for both unirradiated and irradiated gels.

2.4.2.2 Dose response

In contrast, many Fricke gel publications have presented the dose response for Fricke gel detectors [16, 23, 25, 28, 98]. Many studies have shown a linear dose response for doses greater than 20Gy [16, 18, 23, 25, 28, 98] which would cover the clinical range required for most radiotherapy techniques. However, others have shown a deviation from linear response beyond approximately 10-12Gy [91, 100, 104].

The dose sensitivity has been shown to vary depending on the chemical composition, for example ferrous ammonium sulphate concentration [24, 89, 90, 105], sulphuric acid concentration [18, 24, 28, 89, 90], gelling materials [16] and the addition of chelators such as xylenol orange [26, 27, 31, 32]. The impact of chemical composition on dose response will be discussed in greater detail in section 3.2.

It also varies from batch to batch [92] and with storage time and ambient conditions, as will be described in the next section. It is therefore necessary to establish the dose response for each type of Fricke gel detector and also for each batch of detectors manufactured as part of the calibration process which will be described in further detail subsequently.

2.4.2.3 Chemical stability

It has been reported in various publications that the optical density (OD) of unirradiated and irradiated Fricke gel detectors varies over time for detectors analysed using optical methods [22, 23, 25, 27, 28, 91, 92, 106]. This may be quantified by repeating measurements of unirradiated or irradiated Fricke gel detectors.

An initial rapid increase following irradiation due to reaction completion [23, 28, 91, 92] is followed by a slower increase in signal caused by reactions induced by factors other than radiation [22, 27, 28, 86, 92, 106]. A range of reaction completion times of 10 -15 minutes [23, 91], up to 90 minutes [92] and 2 hours [28] have been reported. Waiting 1.5 to 2 hours to carry out the imaging of a detector might not be practical, particularly if there is a post-irradiation diffusion of ions that would require detectors to be scanned within a short time of irradiation.

The longer term drift has been quantified and was shown to be approximately 1 to 2% per hour; for a ferrous benzoic acid XO gelatine gel (unirradiated and irradiated to 8Gy) [22] and for a ferrous xylenol orange gelatine (FXG) detector irradiated to 6Gy analysed with optical methods [23]. It has been shown to vary with chemical composition [27, 28]. Storing detectors at lower temperatures (5 to 10^oC) reduced the longer term drift in signal either pre- or post-irradiation [25, 92, 106], but it was not clear whether these samples were also in the dark when in the fridge. Effect of visible light has not been specifically investigated however studies where detectors were stored in the dark showed low drift of signal versus time [28, 107].

In summary, a range of reaction completion times has been previously shown up to 2 hours and this should therefore be confirmed for the detector in our study. A longer term slow drift in signal of approximately 1-2% per hour has been shown to be reduced by storage in a refrigerator, however an investigation into the effect of ambient light would be a useful study.

2.4.2.4 Spatial stability (diffusion of ferric ions)

The post-irradiation diffusion of ferric ions has been widely reported [19, 22, 25, 29-33, 87, 90, 108-110] which causes a blurring of the measured dose distribution over time. Much of the literature has concentrated on the determination of the diffusion coefficient for ferrous ions [29-32, 87, 90, 108-110]. Despite a variety of experimental methods employed, there is a reasonable agreement between the published diffusion coefficients.

The diffusion coefficient was between 1.0 and 1.9 $mm^2 h^{-1}$ for agarose based detectors (1 to 1.5% by weight, bw) [29, 30, 32, 90, 108] and 0.7 and 1.5 $mm^2 h^{-1}$ for gelatine based detectors (4 to 5% bw) [31, 32, 108]. It was shown that this diffusion coefficient may be reduced with the addition of xylenol orange [31, 32, 108, 110] or with an increase in gelatine concentration [31], however both these steps also cause a reduction in the MR dose response. One study showed relatively low diffusion coefficients for gelatine based detectors which had been stored at a temperature of $10^{o}C$ [31].

According to Tseng 2002 (and is logical) "despite good agreement in the measured ferric ion diffusion coefficients, it remains unclear in what time scale the degradation of initial dose profile becomes apparent" [33]. The degree of blurring over time will be dependent on the initial dose gradient [33, 86] therefore any effect might be less pronounced for a conventional dose fraction, than for a stereotactic radiotherapy delivery.

The impact of the ferric ion diffusion on a measured dose gradient has been modelled [29, 30, 90] and investigated experimentally [19, 22, 32, 33, 87], mostly in terms of a visual inspection of dose profiles instead of any quantitative analysis. The modelling studies predicted a noticeable loss of edge sharpness for a theoretical step function even within 30 minutes to 1 hour of irradiation [30, 90] however this is not particularly clinically relevant. The effect on a more realistic radiation penumbra was much less pronounced at 1 hour [30] and it was also reported that a 14MeV electron beam could be scanned up to 2 hours post-irradiation with little loss of edge information [29]. Optical density profiles were measured across a Fricke-agarose detector irradiated with a narrow 70kV x-ray beam (2Gy) at 40 minutes and 2 hours post-irradiation and showed a visible blurring in the profile over this time frame [22]. These authors suggest scanning "within an hour or so".

There were few papers which attempted to quantify the degree of spatial uncertainty versus dose gradient and time. One study attempted to quantify the degree of blurring of the measured distribution for different delivered dose gradients of up to 0 to 40Gy and different times post-irradiation [87]. Scans up to 3 hours post irradiation were compared with a reference scan in terms of gamma analysis. Gamma failures (3% 2mm) were seen only at 3 hours for the steepest dose gradient of 0 to 40Gy. However, the reference profile used for comparison was, by the authors' admission, measured with a detector

that was too large, resulting in a less sharp reference profile for comparison. In addition, the distance tolerance was 2mm which is potentially too large for precise applications such as stereotactic radiotherapy. Tseng *et al* quoted different scan time limits for different dose gradients (0.5h for 4Gy mm^{-1} and 2 hours or more for 2Gy mm^{-1}) [33], however analysis was based on a single Fricke gel detector irradiated with a steep stereotactic plan (40Gy in the centre); they looked at blurring in different dose gradient regions of the one distribution.

In summary, there has been a great deal of work carried out investigating the post-irradiation diffusion of ferric ions, which has been reported as a factor limiting the use of these detectors. However, varying conclusions have been reached in the literature, from scanning within 0.5 hours [33, 90], 1 hour [22], 2 hours [29], greater than 3 hours [87] or even that the ferric ion diffusion makes the use of Fricke detectors impractical altogether [110]. Having to scan within half an hour would limit the practicality of this dosimetry technique.

To conclude, it appears that it is not necessary to repeat experiments establishing diffusion coefficient as there is much evidence and good agreement in the literature. A useful study to add to the existing body of evidence would be to quantify spatial error versus time by comparing measured and known dose profiles versus time post irradiation. Two papers have attempted to answer this question, but there were experimental weaknesses with both. This should be carried out for a range of clinically relevant dose gradients. Results can be used to decide on the time within which detectors should be scanned to maintain a defined spatial accuracy.

2.4.2.5 *Energy*

It has been suggested that Fricke gel detectors are reasonably water equivalent [111, 112], based on analysis of their effective atomic number [111] and theoretical, Monte Carlo based, analysis of their radiological properties [112]. This would suggest an energy dependence of dose response is unlikely. No energy dependence was seen for a Fricke detector irradiated with a range of different quality kV X-ray beams [111]. Energy dependence was also investigated for a FBX with polyvinyl alcohol (PVA) dosimeter for a range of MV energies (6-15MV) [104] and no effect was seen.

Whilst no energy dependence has been demonstrated in the literature, only one paper has described the experimental investigation of energy dependence for MV photon

energies relevant to our study and for only one detector composition. It is recommended this is confirmed for our detector and megavoltage energies.

2.4.2.6 Dose rate dependence

Dose rate dependence has been previously investigated by several authors [16, 90, 91, 93, 104]. This has been carried out by changing the dose per pulse [16, 104] and also the distance between the source and the detector [16, 90]. This has been studied for detectors based on gelatine [16], agarose [90, 91] and PVA [104]. There was no evidence of a dose rate dependence of Fricke gel dose response in any of these studies.

2.4.2.7 Dose fractionation

There were no papers found which described the dose integration for Fricke gel detectors. Although the lack of dose rate effect demonstrated in the previous section might suggest that there would also be no effect of dose fractionation, this should still be investigated.

2.4.2.8 Homogeneity and cooling effects

It was suggested that for certain agarose based Fricke detectors there exists a dose variation across large volumes due to the difference in cooling rate at the edge of the phantom compared with the centre [89]. This was attributed to the breakdown of the agarose chain structure by sulphuric acid which is dependent on temperature. Different types of agarose with lower melting points were then investigated. To evaluate homogeneity, the dose sensitivity was compared for small vials cooled in the air (representing rapid cooling) to those cooled in the centre of a liquid (representing slow cooling rate). This was shown to be greater than 5% for most combinations of agarose, but reduced for a particular composition. In a further study, it was shown that adding certain saccharide additives reduced the non-uniformity, again with similar analysis comparing the dose sensitivity of test tube samples [27]. Agarose has a high melting point when compared with gelatine. Therefore, non-uniformity might be less of an issue for gelatine based detectors which require heating to much lower temperatures.

Homogeneity should in fact ideally be evaluated by scanning large volume detector samples, with a similar geometry to the phantoms to be used for clinical experiments. This should be carried out for both unirradiated gels and also gels irradiated with as uniform a dose distribution as possible. One paper was found which analysed the uniformity of unirradiated ferrous gelatine samples [20]. Uniformity was quantified by

calculating the standard uncertainty of the signal in several ROIs positioned across an MR scan of the unirradiated detector and was within 1.5%.

Few studies were found which investigated the homogeneity of response of uniformly irradiated detectors. In one, a ferrous sulphate agarose gel was irradiated with a 3 field plan (1 anterior plus 2 lateral beams) which was designed to produce a uniform distribution over a dummy PTV region [113]. However, the measured distribution was compared with the TPS in terms of the isodose distribution instead of via any quantitative measure of uniformity. Elsewhere, the uniformity of response was investigated for a ferrous gelatine detector analysed optically both unirradiated and irradiated with a parallel opposed beam arrangement [92]. Standard deviation in signal in a large region of interest was within 1.5%; the uniformity of dose distribution delivered to the detector was not described for context.

In summary, surprisingly few publications were found which investigated the uniformity of response of large volume detectors irradiated with uniform dose distributions. It has been suggested that uniformity might depend on the cooling method [89], but possibly more significant for agarose detectors. Results from two studies using gelatine based detectors suggest that the detector uniformity is adequate for these detectors [92, 114], but in one only was the detector actually irradiated with a uniform dose distribution [92]. Therefore, this would benefit further investigation.

2.4.2.9 *Volume dependence*
No studies were found which investigated volume dependence of Fricke gel dose response. This is despite the fact that results would influence whether small volume samples can be used to calibrate large experimental samples.

2.4.3   Summary

The characteristics of Fricke gels were outlined which might affect their dosimetric performance and therefore which should be investigated. These were identified from a critical analysis of the whole Fricke gel process, basic text books and published guidelines and similar analysis for other 2D and 3D chemical detectors. The aim then was to review the Fricke gel literature to identify any publication which describes the investigation of any of these characteristics. Detectors were considered as long as they incorporated at least ferrous ammonium sulphate and a gelling agent. It was hoped to

build up a picture of evidence for dosimetric performance versus detector composition. Although there has been a great deal of effort in evaluating Fricke gel detectors, this proved a difficult task for the following reasons.

Firstly, there exist many different chemical compositions. Previous publications have not tended to systematically investigate many characteristics for a particular recipe. It is clear that many characteristics do depend on detector composition, for example the gelling agent has been shown to affect the dose response, diffusion and homogeneity. Many additives have also been used in different recipes for example, saccharides and benzoic acid. Different manufacture methods have been used including cooling methods and storage conditions.

In particular, significant gaps have been highlighted in this review, which is summarised as follows. The dose response has been widely investigated, and has been shown to be linear over the clinically relevant dose range, to vary from batch-to-batch and with time post manufacture, therefore calibration is required for each measurement session. It has been shown to depend on chemical composition, therefore needs to be characterised for each different composition. The chemical stability has also been the subject of several publications which show evidence for a change in the detector response over time. It was shown that storing detectors in the fridge reduces the ongoing signal drift, however whether ambient light conditions affect the response has not been fully explored. A range of reaction completion times has been previously presented, which might depend on whether XO is incorporated, this should be investigated for our detector to provide clarification.

The detector response with dose rate has been investigated; with no effect seen. However, the detector response versus radiation energy, fractionation and detector volume has not been widely studied, nor has inter-sample variation. The homogeneity has been considered, with non-uniformity suggested for agarose based detectors, however this has often been investigated using test tube samples with different cooling methods rather than actually irradiating a large volume detector with a homogeneous dose distribution. This would also benefit from additional investigation. Finally, ferric ion diffusion has been investigated in many publications, but further work is required elucidate the impact of this on the post irradiation blurring of measured dose distributions.

2.5   Development of an experimental plan

From this review, an experimental plan was developed as follows. Firstly, a detector composition will be selected based on practical considerations and evidence for dosimetric performance that does exist; this will be described in chapter 3. A systematic characterisation of all detector properties will be carried out according to the plan laid out in Figure 2.2.
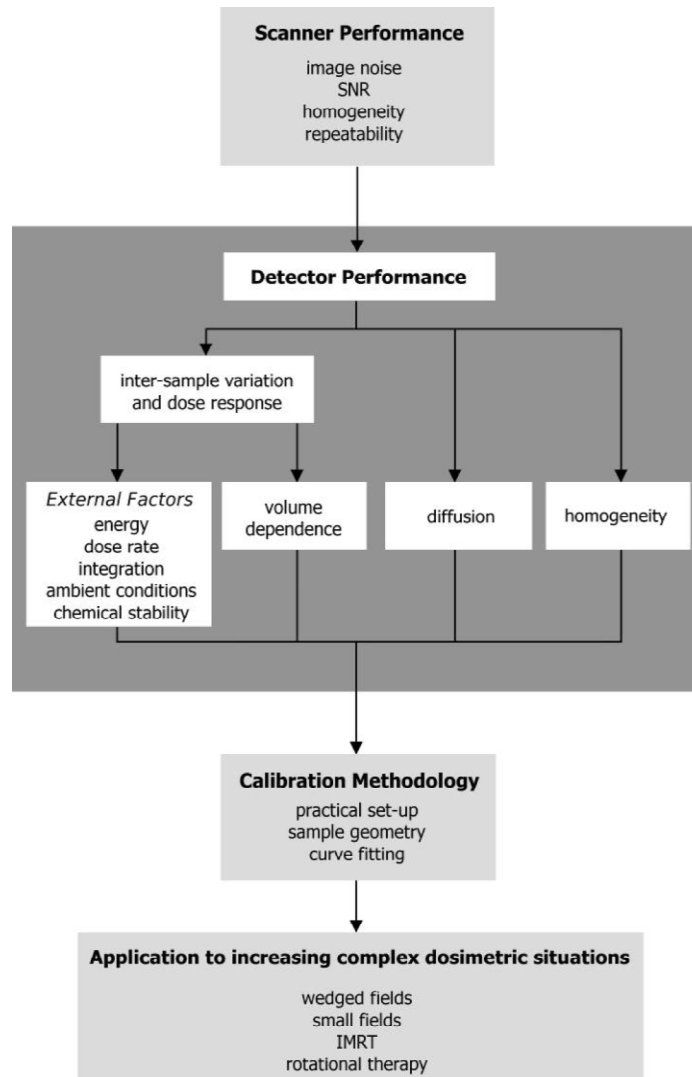
Figure 2.2:   Experimental plan for the dosimetric characterisation of Fricke gel detectors in this project.

In chapter 3, the scanner performance will be established and the detector manufacture will be streamlined. Experiments into the basic characteristics will then be carried out using test tube samples analysed with an MR spectrometer, including inter sample

variation, dose rate response, fractionation, energy dependence and chemical stability. These are the subject of chapter 4. The work will then be extended to larger volume samples analysed in a whole-body MR scanner, including volume dependence, inter sample variation of larger samples, homogeneity of response to uniform radiation distributions and the impact of ferric ion diffusion on clinically relevant dose distributions. These are the subject of chapter 5. If the detector performance is adequate, the detector will then be applied to increasingly complex radiation scenarios and compared against existing detector measurements and is the subject of chapter 6.

2.6   Conclusion

In this chapter, a broader overview of the Fricke gel literature was followed by a structured literature review of detector characteristics. The absence of a systematic approach was demonstrated along with a lack of evidence for many factors. An experimental plan was then developed aiming to address this lack of evidence for a Fricke gel detector in this thesis.

Chapter 3. Development of experimental methodology: Fricke gel manufacture and MR analysis methods

3.1 Introduction

3.1.1 Aims of this chapter

The aim of this chapter was to set up the practical methodology related to the manufacture and readout of the Fricke gel detectors before moving onto systematic testing of an optimised system.

Firstly, the exact composition of the Fricke gel detector needed to be decided. In order to do this, a literature review was carried out to identify publications which analyse the different chemical constituents in terms of dosimetric properties, for example detector sensitivity. The focus was on simplicity and obtaining a composition with few, low-toxicity, constituents and a simple manufacture processes in order to be accessible to radiotherapy departments with no or limited access to a chemistry laboratory. The aim was to provide an evidence based starting point for the detector composition. With the detector composition established, the manufacture process was then optimised and streamlined again with simplicity and time as a focus.

The second part of this chapter concentrates on the readout and analysis methods. In this project, test tube Fricke gel samples were analysed using a bench top NMR spectrometer and larger volume samples analysed using a whole-body MRI scanner. As described in chapter 2, the readout of the irradiated detector has the potential to introduce measurement errors and uncertainty due to non-uniformity in response across a scanner, noise and lack of reproducibility in repeated measurements. There is a trade-off between signal to noise ratio (SNR), measurement time and spatial resolution with any imaging system [76]. An important step in setting up the Fricke gel process was to design and optimise spectrometer and scan protocols and to evaluate residual measurement uncertainties.

Inversion recovery and CPMG pulse sequences were used for the T_1 and T_2 quantification of test tube Fricke gel samples using the NMR spectrometer. Sequences were compared and optimised using copper sulphate quality control samples. Methods were then developed for the MR scanning and analysis of irradiated Fricke gel

detectors. Pulse sequences were customised for the T_1 and T_2 quantification of larger Fricke gel samples. Image analysis software was developed by modifying plugins within OsiriX, an open source image analysis platform [115]. Larger volume copper sulphate samples were prepared for the evaluation of scan protocols via well-established measures of signal to noise ratio, image homogeneity and repeatability.

3.1.2 Chapter overview

Firstly, a structured review of the literature was carried out to identify an evidence based starting point for the composition of the Fricke gel detector; this is described in section 3.2. The manufacture process is described in section 3.3; this was streamlined to fulfil our aim of creating a quick and simple method for Fricke gel manufacture.

The remainder of the chapter focuses on NMR/MRI methods. A very brief overview of the MR theory relevant to this thesis is summarised in section 3.4. Work to commission an NMR spectrometer for the analysis of test tube Fricke gel samples is described in section 3.5. The optimisation of pulse sequences on the whole-body MR scanner and the development of image analysis software is described in section 3.6.

3.2   Fricke gel composition

3.2.1   Overview of Fricke gel composition

The basic components of a 3D Fricke gel dosimeter are ferrous ammonium sulphate, sulphuric acid, water and a gelling agent. Ferrous ammonium sulphate provides the ferrous ions which are oxidised by the free radicals produced when water is irradiated. Ferrous ions are not soluble in neutral solutions [89] therefore, an acidic medium is required usually in the form of sulphuric acid. Finally, a gelling agent is necessary to spatially fix the ferrous and ferric ions to produce a 3D representation of the irradiated dose.

Benzoic acid and sodium chloride were components of Fricke solution dosimeters and consequently have been incorporated in some gel based recipes. Other chemicals have been investigated for example xylenol orange (XO) to allow optical analysis and decrease ion diffusion and saccharide additives to increase the sensitivity.

The literature was reviewed to select a starting composition for the Fricke gel detector. In the following sections, each chemical constituent is briefly reviewed in terms of published information on dosimetric performance and ease of manufacture.

3.2.2   Analysis of Fricke gel components

3.2.2.1 Ferrous ammonium sulphate

Previous investigations compared the detector sensitivity for different concentrations of ferrous ammonium sulphate [24, 89, 90, 105]. It was demonstrated that optimum concentrations in terms of detector sensitivity were in the range 0.5 to 2mM with two studies agreeing that 0.5mM gave the greatest dose response [24, 89]. A concentration of 0.5mM was therefore selected for this project.

3.2.2.2 Sulphuric acid

There was slightly conflicting evidence in the literature on the variation in detector sensitivity with sulphuric acid concentration with some showing peak sensitivity at concentrations of 25mM to 50mM [24, 28, 90] where others demonstrated improvements using concentrations of greater than 100mM [18, 89]. However, any improvements in sensitivity at these high concentrations were slight and also reported to be accompanied by a greater effect of cooling rate on detector homogeneity [89]. From a practical perspective, a lower concentration would be desirable to reduce the detector toxicity. As there appears to only be small improvements, if any, in the dose response for sulphuric acid concentrations greater than 25mM, this concentration was selected.

3.2.2.3 Gelling agent

Different gelling materials have been used, most commonly agarose [17, 19, 85, 90, 114] and gelatine [23, 28, 92, 105] but also alternatives such as polyvinyl-alcohol (PVA) [25]. Agarose has been shown to improve the dose response compared with gelatine [16] but at the expense of a more significant ferric ion diffusion [32]. In addition, the manufacture process for standard agarose types requires heating the gel mixture to 95°C compared with 45°C for gelatine. Oxygen must then be bubbled through the solution for at least 5 minutes to replace that lost during heating. Also, a non-uniform sensitivity over large detector volumes has been attributed to the variation in cooling rate at the centre and edge of the detector [89]. To overcome this, detectors using agarose with a lower melting point alongside other additives were proposed [89].

Gelatine was selected for our detector due to its ease of manufacture and its reported lower post irradiation diffusion. A gelatine concentration of 3-5% by weight (bw) has been shown to be optimal in terms of detector strength and dose sensitivity by several studies [16, 18, 28, 31]. 5% was selected for this work.

3.2.2.4 Sodium chloride

Sodium chloride was often used in Fricke solution dosimeters to counteract the effects of organic impurities which is important for absolute dosimetry. Although early studies on Fricke gels did include sodium chloride [16, 17, 105, 114], it was soon suggested that this is not effective for gel based dosimeters due to the intentional presence of an organic gelling material anyway. Fricke gel detectors are not intended as absolute dosimeters. In fact a decrease in sensitivity was demonstrated when sodium chloride was added [19]. Consequently, this was not added to the detector recipe.

3.2.2.5 Benzoic acid

Similarly, benzoic acid was added to Fricke solution detectors to increase the chemical yield in a controlled way. Several studies have demonstrated little or no improvement in the dose response for Fricke gelatine detectors [18, 32, 52] and again this was not included.

3.2.2.6 Chelating agent

Xylenol orange and other chelating agents have been investigated to attempt to increase the optical-CT dose response and reduce the post irradiation diffusion [31, 32]. A reduction in diffusion was normally accompanied by a reduction in the detector sensitivity, with the best compromise achieved with xylenol orange. This is now commonly added to detectors analysed using optical CT [24]. However, a reduction in the MR response has been demonstrated [26, 27, 31, 32]. Xylenol orange was investigated in an initial experiment, described in section 4.2.3, but not used thereafter.

3.2.2.7 Saccharide additives

Olsson *et al* demonstrated a variation in sensitivity with cooling rate for agarose based Fricke gels causing an inhomogeneous response across large volume detectors [89]. This is particularly seen with agarose due to the high temperatures used during manufacture. By adding a non-gelling polysaccharide purified from locust bean gum (SeaGel) the dependence of sensitivity on cooling rate was reduced for two types of agarose. Saccharide additives were also incorporated into a Fricke-agarose-xylenol

orange (FAX) detector [27]. Various additives were investigated and all increased the optical density-dose sensitivity although the effect on R_1-dose sensitivity was moderate [26]. This was therefore not included to simplify the manufacture process.

3.2.3 Summary

The chemical composition used throughout this work was selected based on the results of this review. The basic components of this detector are ferrous ammonium sulphate, sulphuric acid, gelatine and distilled water. Concentrations were selected from the literature review based on optimised dose response. Although it is recognised that these may not combine linearly, in the literature the impact of different chemical components on dose response has been investigated independently of each other. This summary is based on the best evidence available. Gelatine was selected as the gelling agent for ease of manufacture, lower diffusion and fewer anticipated issues due to cooling. Other additives were not incorporated due to a lack of evidence for any benefit.

The final composition of the Fricke gel dosimeters used throughout this thesis was 0.5mM ferrous ammonium sulphate, 25mM sulphuric acid and 5% gelatine (bw). 0.1mM xylenol orange was added in an initial experiment, described in chapter 4, to establish the effect on dose response, but not used thereafter.

3.3 Fricke gel manufacture

3.3.1 Introduction

The next step was to define the process for the manufacture of Fricke gel detectors. For the first few batches of Fricke gel a collaboration with the radiation physics group at the National Physical Laboratory (NPL) was set up. Their group had previous experience with Fricke gel dosimetry as they had been investigating a similar detector with optical-CT analysis methods. For these batches, the manufactured gel had to be transferred by public transport from the NPL across London to St Bartholomew's Hospital. It was felt that this added an extra potential uncertainty with regards to consistency of storage and temperature history which was not necessary in the first instance. Should this project be successful, it would be a useful future study to see if the detectors could be transferred to other radiotherapy departments for irradiation. However, for the remainder of this project, detector manufacture was carried out within a simple laboratory within the

radiotherapy department at St Bartholomew's Hospital, thus keeping manufacture, storage, irradiation and imaging within the same location. Following manufacture, the detectors could be immediately placed in the most appropriate storage environment, in the dark, or refrigerated.

3.3.2   Manufacture process

The final manufacture process for Fricke gels manufactured in the radiotherapy department is detailed in the following section, with illustrations in Figure 3.1 and a work instruction in Figure 3.2. Batches of Fricke gels were manufactured, producing 1.05l per session.

Firstly, two 1000ml volumes of 25mM sulphuric acid were prepared. For each, 50ml of 0.5M stock solution of sulphuric acid (Fisher Scientific, Loughborough, UK, CAS No. 7664-93-9) was added to a 1000ml volumetric flask and made up to 1000ml with distilled water obtained from a still at St Bartholomew's Hospital (Autostill 4000X, Jencons Scientific Ltd, UK). 4.1g of ferrous ammonium sulphate (Fisher Scientific, Loughborough, UK, CAS No. 7783-85-9) was weighed and dissolved in one of the sulphuric acid volumes. The other sulphuric acid sample was poured into a 2000ml beaker. 52.5g gelatine powder (gelatine from porcine skin, gel strength 300, Sigma Aldrich CAS No. 9000-70-8) was added and allowed to dissolve for 15 minutes. This mixture was heated to 45°C whilst being constantly stirred using a magnetic stirrer after which the gelatine had completely melted. The mixture was then removed from the heat and allowed to cool to 32°C whilst continuing to stir. Finally, 50ml of ferrous ammonium sulphate solution was added and the mixture thoroughly stirred.

The Fricke gel was poured into the desired containers, either bottles or test tubes, details of which are given in subsequent chapters. Different storage conditions were investigated in chapter 4 and chapter 5, in particular the impact of ambient light and cooling methods on the dosimetric properties of the Fricke gel.
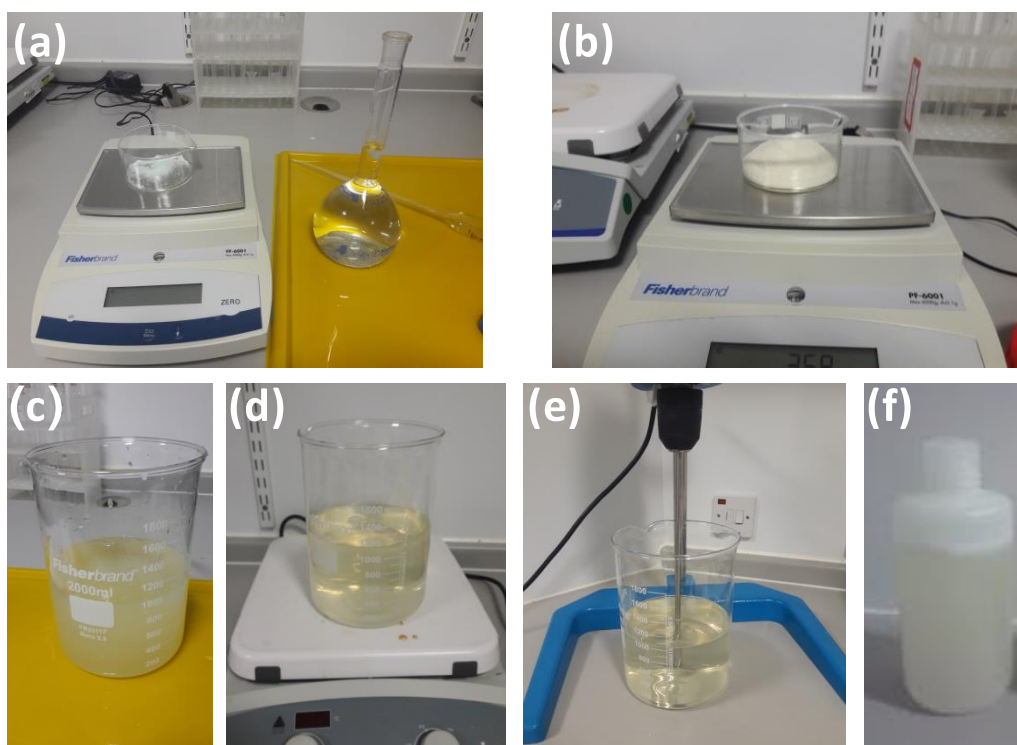
Figure 3.1: Steps in the manufacture of Fricke gel detectors (a) preparation of ferrous ammonium sulphate solution (b) weighing the gelatine powder (c) the gelatine is dissolved in sulphuric acid (d) the mixture is stirred and heated to 45°C (e) the gelatine is removed from the heat and allowed to cool to 32°C whilst continuing to stir. (f) ferrous ammonium solution added and mixture poured into the required containers.

3.3.3   Summary

The Fricke gel composition has been selected and the manufacture process designed. The Fricke gel is manufactured from readily available, cheap chemicals with low toxicity. The manufacture can be carried out in a laboratory within a clinical radiotherapy department and requires only basic equipment. The entire process takes 2 hours plus cooling time. This is a notable benefit over other chemical detectors which involve more toxic chemicals e.g. acrylamide of Polymer gels, which require a fume hood, require heating to higher temperatures such as Fricke-agarose or require bubbling through with oxygen following manufacture (Fricke agarose and BANG gels.

Plan for the manufacture of Fricke gel detectors at Barts

This makes a 1050ml volume of Fricke gel detectors with composition 0.5mM ferrous ions, 5% b.w. gelatin and 25mM sulphuric acid.

Step A: Preparation of a 1000ml 10.5mM ferrous ammonium sulphate stock solution

A1. Make up 1000ml of 25mM H_2SO_4

Measure 50ml of the 0.5M stock H_2SO_4 solution and add to a measuring cylinder. Make up to the 1000ml mark with distilled water.

A2. Add ferrous ions
Weigh 4.1g of ferrous ammonium sulphate powder into a weighing dish. Transfer some to a small beaker, add some of the 25mM sulphuric acid solution and dissolve. Pour into a 1L bottle. Repeat with all of the ferrous ammonium sulphate powder. Add the remaining sulphuric acid solution and mix until fully dissolved.

Label and store in the dark.

Step B: Manufacture of Fricke gels

B1. Make up 1000ml of 25mM H_2SO_4

Measure 50ml of the 0.5M stock H_2SO_4 solution. Add it to distilled water in a measuring cylinder or volumetric flask. Make up to the 1000ml mark with distilled water. Pour into a 2000ml beaker.

B2. Add gelatin

Weigh 52.5g of gelatin into a large weighing dish. Add the gelatin to the sulphuric acid and leave for 10-15 minutes in which time the gelatin will start to dissolve.

B3. Heat to 45°C and allow to become liquid.

Place the beaker onto the hot plate / magnetic stirrer and heat to 45°C. Stir slowly using a magnetic stirrer. Remove from the heat and allow to cool to approximately 32°C, still stirring.

B4. Add 50ml of the stock ferrous ammonium sulphate solution

Measure 50ml of the stock ferrous ammonium sulphate solution and add to the gelatin mixture.
Pour into the desired containers immediately and cool in the fridge.

Figure 3.2: Process for the manufacture of Fricke gel detectors.

3.4   Brief NMR theory relevant to this thesis

3.4.1   Introduction

The next step was to develop methods to read out the irradiated detectors using an NMR spectrometer and whole-body MR scanner. The MR analysis of Fricke gel detectors is based on T_1 or T_2 quantification. This dissertation is intended primarily for radiotherapy physicists and in this section, a basic theory of relaxation and quantification techniques relevant to Fricke gel analysis are discussed. For a more detailed description of the principles behind MRI, the reader is directed towards standard text books [116, 117]

3.4.2   Introduction to relaxation

A hydrogen nucleus consists of a single proton and is of interest in MRI due to its abundance in water and human tissue. The proton can be thought of as spinning on its own axis. As protons are positively charged, this results in a magnetic dipole moment; the proton acts like a tiny magnet. When a static magnetic field is applied (B_o) the proton dipoles align at 54.7^o to the field in a parallel or anti-parallel direction (Figure 3.3), also referred to as "spin up" or "spin down". Therefore it experiences a torque which causes it to precess around the axis of the magnetic field. The frequency of precession is called the Larmor frequency.

There is a slight excess of spins in the spin-up state resulting in a small net magnetisation (M_0) in the direction of the magnetic field, depicted along the z-axis. The protons precess out of phase with each other which means there is no net magnetisation in the transverse (xy) plane (Figure 3.4). To obtain a measurable signal, the net magnetisation is tipped away from the longitudinal axis by applying a radiofrequency (RF) pulse perpendicular to B_0 and oscillating at a frequency equal to the resonance Larmor frequency. The flip angle is the angle through which the net magnetisation is tipped.
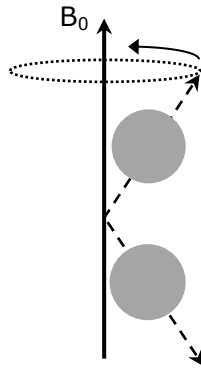
Figure 3.3: Parallel and anti-parallel spin states of hydrogen nucleus.
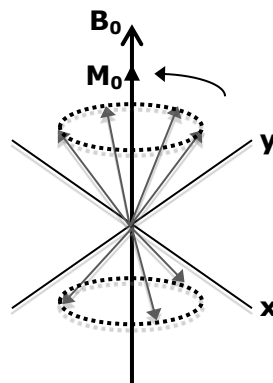
Figure 3.4: Net magnetisation in the longitudinal (z) direction.

For example, a 90° RF pulse tips the net magnetisation vector into the transverse plane where it precesses around the axis of the static field and induces a signal in a receiver coil. Following the pulse, the transverse magnetisation (M_{xy}) and therefore signal amplitude rapidly decreases to zero as the protons dephase, this is known as the "Free Induction Decay" (Figure 3.5). The process by which the transverse magnetisation returns to zero, is known as spin-spin or transverse relaxation and is associated with the time constant T_2.

The longitudinal component of the net magnetisation (M_z) increases exponentially back to its equilibrium value. This process is known as spin-lattice or longitudinal relaxation and is associated with time constant T_1. T_1 and T_2 relaxation times are inherent properties of the measured sample (e.g. different tissues in the body will have different

T_1 and T_2 values). MRI involves the development of RF *pulse sequences* to enhance the difference in T_1 and T_2 between different tissues hence, creating tissue contrast. This project is concerned with the T_1 and T_2 quantification of irradiated detectors and this is described in the next sections.
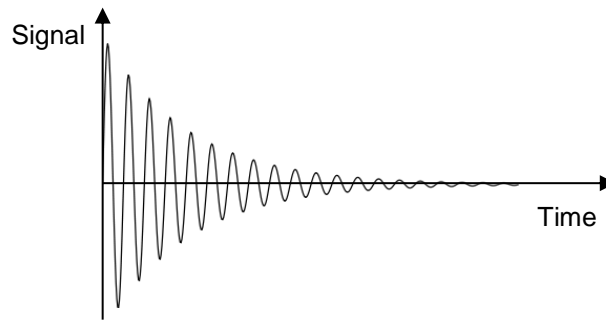
Figure 3.5: Decay of signal and transverse magnetisation following RF pulse.

3.4.3 T_1 relaxation

Immediately after the initial RF pulse, the longitudinal component of net magnetisation is altered from its equilibrium value ($+M_o$). The exponential recovery of M_z following an RF pulse is described by the time constant T_1 known as the spin-lattice relaxation time (Figure 3.6) with T_1 being the time required for the longitudinal magnetisation to reach $(1-\frac{1}{e})$ or about 63% of its maximum value (M_o). T_1 relaxation is due to the loss of energy back to the surrounding environment or "lattice". The T_1 relaxation time is dependent on the molecular environment surrounding the proton spins, therefore T_1 depends on the tissue or material type.
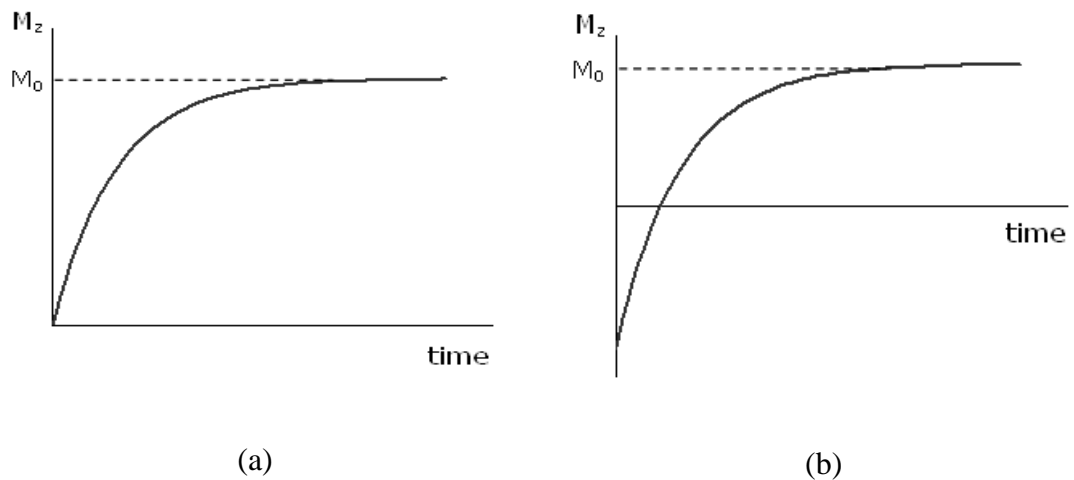
Figure 3.6: Exponential longitudinal saturation recovery (a) and inversion recovery (b) following 90° and 180° RF pulses.

For a $90°$ *saturation* pulse, the longitudinal magnetisation is zero immediately following the pulse, then recovers according to the equation:

$$M_z(t) = M_0\left(1 - e^{-t/T_1}\right)$$ **Equation 3.1**

For a $180°$ *inversion* pulse, the longitudinal magnetisation is $-M_0$ immediately following the pulse, then recovers according to the equation:

$$M_z(t) = M_0\left(1 - 2e^{-t/T_1}\right)$$ **Equation 3.2**

The spin-lattice relaxation rate is defined as $R_1 = \dfrac{1}{T_1}$.

3.4.4   T$_2$ relaxation

The exponential decay of the transverse magnetisation is due to the interaction of neighbouring proton spins. It is described by the time constant T_2 and is known as spin-spin or transverse relaxation. T_2 is the time required for the transverse magnetization to fall to approximately 37% (1/e) of its initial value.

Following an initial $90°$ RF pulse, proton spins experience slightly different local magnetic fields which causes them to precess around the axis of the static magnetic field at slightly different frequencies. The spins become increasingly out of phase and the net transverse magnetisation decreases. The local magnetic field experienced by

68

each proton varies due to both inhomogeneities in the static field and the magnetic moment of neighbouring protons. T_2^* ("T_2 star") describes the loss of phase coherence due to both of these effects. The T_2 relaxation time describes the loss of coherence due to spin-spin interactions only and is of interest as this depends on the molecular environment surrounding the proton.

To separate T_2 from T_2^*, signal echoes are created (Figure 3.7 and Figure 3.8). Some time after the initial 90° pulse, a further 180° RF pulse is applied. This has the effect of reversing the phase of the spins so that faster spins that had a positive phase now have a negative phase and vice versa. The spins eventually refocus resulting in a signal echo at time known as the echo time (TE).

This spin echo sequence compensates for the loss in phase coherence due to the inhomogeneities in the static field by reversing the phase with the 180° pulse but not for the time-varying effects of spin-spin interactions.

The equation for transverse magnetisation decay following an initial 90° pulse is:

$$M_{XY}(t) = M_0 e^{-t/T_2}$$ **Equation 3.3**

The spin-spin relaxation rate is defined as $R_2 = \frac{1}{T_2}$.
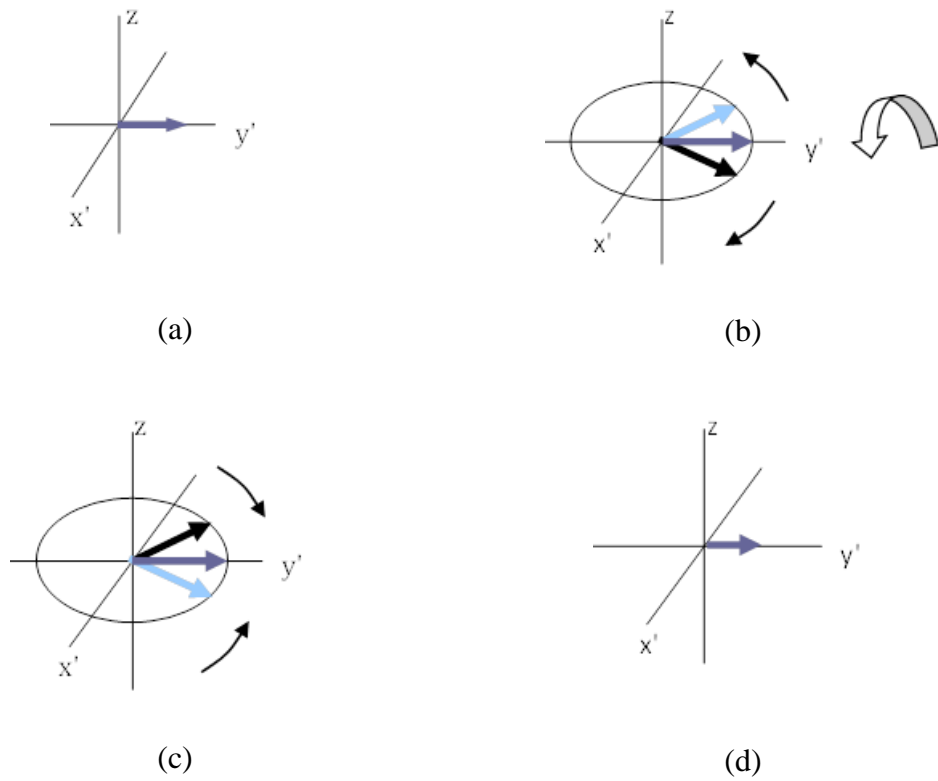
Figure 3.7: Spin echo formation: (a) after 90⁰ RF pulse, (b) after TE/2, loss of phase coherence, (c) immediately after 180⁰ pulse and (d) after TE, a signal echo forms.
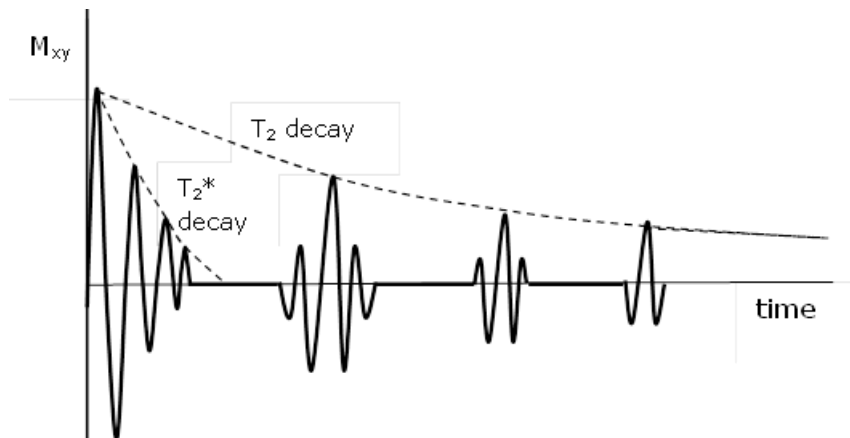
Figure 3.8 Transverse decay due to T_2* and T_2 following a 90⁰ RF pulse.

3.4.5 Overview of pulse sequences used for T_1 and T_2 quantification

If one makes abstraction of spatial localisation, pulse sequences to quantify T_1 and T_2 are essentially the same on a spectrometer and on an imager. However, for the latter, a series of images are acquired and the T_1 or T_2 values are determined on a pixel by pixel basis to create a synthetic image known as a T_1 or T_2 map. Pulse sequences are designed to alter the net magnetisation from the equilibrium situation, then measure the magnetisation to allow T_1 and T_2 relaxation curves to be plotted from which T_1 and T_2 are quantified.

For T_1 quantification, an initial inversion or saturation pulse is applied, tipping the longitudinal net magnetisation through 90° or 180°. The benefit of inversion pulse is a doubling of the dynamic range. Following the initial inversion pulse, a further 90° pulse is applied after an inversion time (TI) to allow the residual magnetisation to be measured. This sequence was used for the T_1 quantification of test tube samples by the spectrometer, and is described in more detail in section 3.5.4.

The inversion recovery sequence is slow as there is only one measurement made after each inversion pulse. After the measurement, it is necessary to wait for the longitudinal magnetisation to fully recover before applying the next inversion pulse. The measurement times for single measurements with the spectrometer are manageable (a few minutes), however, inversion recovery sequences for MR scanning are prohibitively long. According to an example presented by Crawley *et al*, an inversion recovery sequence with 10 points, TR of 2.5s and matrix of 256×128 would take 53 minutes [118]. Therefore alternative sequences have been developed. In this project, a modified Look Locker sequence was used for the T_1 quantification of larger Fricke gel samples as it was available on the scanner [117, 119-121]. This sequence is usually used in cardiac imaging to determine appropriate inversion times for myocardium nulling in perfusion imaging. However, it can be easily modified to obtain a series of images that can be used for off-line T_1-mapping. This is described in more detail in section 3.6.5

For T_2 quantification an initial 90° pulse tips the net magnetisation into the transverse plane. This is followed by a series of 180° pulses forming a series of spin echoes according to Figure 3.7. The signal amplitude of each echo is plotted versus echo time (TE) giving the T_2 relaxation curve from which the T_2 may be determined according to Equation 3.3. The Carr Purcell Meiboom Gill (CPMG) sequence applies a modification

to compensate for imperfections in the 180° refocusing pulses [122, 123]. If the initial 90° degree pulse is applied on the x' axis, the train of 180° pulses is applied on the y' axis. Due to the imperfections in the 180° pulse, every odd numbered pulse will be too small, but even pulses are correct. Therefore, only even numbered pulses are sampled. In this project, the CPMG sequence was used for both T_2 quantification of test tube Fricke gel samples with the spectrometer and large samples using the MR scanner (sections 3.5.5 and 3.6.6).

3.5   Commissioning an NMR spectrometer for the analysis of test tube Fricke gel samples

3.5.1   Overview

A low field 40MHz (~ 1T) minispec mq-40 MR spectrometer (Bruker, Karlsruhe, Germany) was used for the analysis of small test tube samples of Fricke gel. The measurement probe assembly has a circulating water supply which allows the temperature in the sample probe to be varied. This was controlled by a Julabo F25 refrigerated-heating circulator (Julabo GmBH, Seelback, Germany). Dedicated software includes a range of pre-programmed pulse sequences for T_1 and T_2 quantification which may be customised for specific applications.

In the first instance, pulse sequences were selected based on those that were already pre-programmed in the spectrometer software for T_1 and T_2 quantification. It should be noted that absolute T_1 and T_2 values are not required in this project, merely that the values are repeatable and reproducible and that the R_1 or R_2 (or any other MR signal parameter) is linearly related to dose for the Fricke gel detector. Pulse sequences for T_1 and T_2 quantification were customised and evaluated in terms of measurement precision, linearity and measurement time using copper sulphate quality control samples, as described in the following sections.

3.5.2   Preparation of copper sulphate QC samples

Copper sulphate solution samples are often used as MR test objects due to the linear relationship between Cu^{2+} concentration and relaxation rate [117]. Initial test experiments showed expected T_1 range of Fricke gels (irradiated over a range of 0 to 20Gy) to be approximately 900 to 1700ms and the T_2 range approximately 600 to

1250ms. Copper sulphate samples were prepared with a range of concentrations from 0.8mM to 10mM selected to cover the range of relaxation rate expected for Fricke gels. A 0.1M stock solution of CuSO4 was first prepared by weighing 25g of $CuSO_4·5H_2O$ (Sigma Aldrich, CAS No. 7758-99-8) and making up to 1000ml with ultrapure water (deionised, distilled, Fisher Scientific, UK). A series of dilutions were then carried out to reach the required concentrations. They were poured into 6mm inner diameter MR test tubes (borosilicate glass) (Bruker UK Ltd, UK).

3.5.3   Measures of pulse sequence performance

The linearity between relaxation rate and concentration was checked by plotting R_1 and R_2 versus copper sulphate concentration over the range 0.8mM to 10mM. Measurement precision (repeatability) was quantified by making 10 repeated measurements of copper sulphate samples with concentrations of 0.8mM (approx. T_1 1700ms, T_2 1500ms) and 4mM (approx. T_1 300ms, T_2 250ms) and calculating the coefficient of variation (CV).

3.5.4   Inversion recovery sequence for T_1 quantification

An inversion recovery pulse sequence was used for T_1 quantification with the spectrometer. In this sequence, an initial 180° inversion rf pulse is first applied and the longitudinal magnetisation is let to recover during an inversion time (TI) which varies. A 90° rf pulse is then applied to tip the residual longitudinal magnetisation into the transverse plane where it can be detected (signal detection, SD). This is repeated with different TIs, resulting in a series of data points of M_z versus TI which allow the T_1 relaxation curve to be plotted as in figure 4.5(b). The NSA is the number of signal averages i.e. how many times the sequence is repeated per TI. N is the number of different TI values sampled. The sequence can therefore be summarised as:

$$[[180^o - TI - 90^o - SD]_{NSA}]_N$$

T_1 was calculated from the exponential signal recovery curve (Equation 3.2).

Pulse sequence parameters were set as follows. The TI range was set to adequately sample the T_1 recovery curve. The initial and final TI are set by the user, and the software automatically calculates TI intervals which vary to ensure there are more data points at short TIs where the slope of the recovery curve is steep. TR was set to be approximately $5 \times T_1$ to ensure full longitudinal recovery between excitations, the NSA

was set to 4 and N was set to 10. Sequences were evaluated in terms of measurement precision (repeatability) and measurement time. Final settings for the parameters of the inversion recovery sequence for T_1 quantification are summarised in Table 3.1.

Table 3.1 Inversion recovery protocol for T_1 quantification

Parameter	Value
NSA	4
N	10
TI (ms)	50-100 to 2000-5000*
TR (ms)	3000-7000*

*dependent on the approximate T_1 of the sample

The coefficient of variation (CV=standard deviation / mean $\times$ 100%) for 10 repeated T_1 measurements was <0.2% across the T_1 range evaluated. T_1 versus copper sulphate concentration was linear as shown in Figure 3.9 (R^2>0.999). As mentioned, the inversion recovery sequence is long; for the longest T_1 values expected in this project, the approximate measurement time was 5 minutes.

3.5.5   CPMG sequence for T_2 quantification

In a CPMG sequence, an initial 90° pulse tips the net magnetisation into the transverse plane. This is followed by a train of N $\times$ 180° pulses forming a series of spin echoes separated by a time tau (τ). The amplitude of each echo is measured (SD, signal detection) and used to determine the T_2 according to Equation 3.3. A number of dummy echoes (DE) are not sampled before each measured echo. This whole sequence is repeated a number of times (NSA) and the signal averaged:

$$[90^o - \tau - [(180^o - \tau -)_{DE} (180^o - \tau -)SD - \tau -]_N]_{NSA}$$

Pulse sequence parameters were set and evaluated using the copper sulphate QC samples. The TR was set to be greater than 5xT_1 to ensure full longitudinal magnetisation recovery between each excitation and the NSA was 4. This gave adequate precision with sufficiently short measurement times. DE, τ and N were varied to optimise measurement precision and ensure adequate sampling of the T_2 relaxation curve within the constraints that τ is recommended to be <1ms and N is limited to a

maximum of 250 within the Minispec software. The final settings are presented in Table 3.2.

Table 3.2 CPMG protocol for T_2 quantification

Parameter	Value
NSA	4
N	250
τ (ms)	1.0
Dummy echoes	5-13*
TR (ms)	7000

*depending on approx. T_2

The CV for 10 repeated T_2 measurements was < 0.1% over a T_2 range of 115ms to 1300ms. The relationship between relaxation rate and $CuSO_4$ concentration was again linear for R_2 as seen in Figure 3.9 (R^2 >0.999).
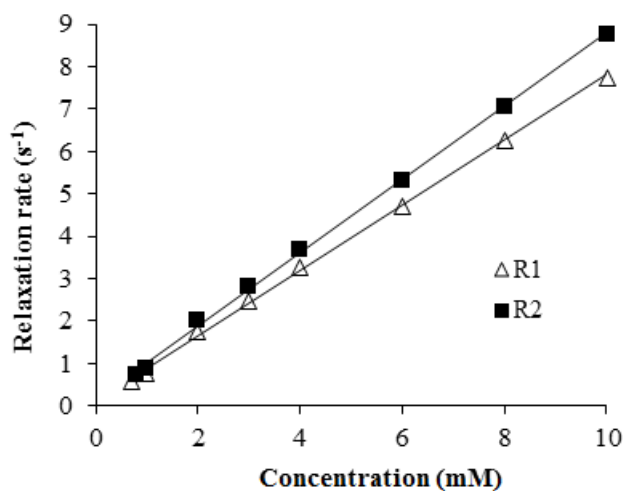
Figure 3.9: Relaxation rate versus $CuSO_4$ concentration for R_1 and R_2.

3.5.6 Summary

Pulse sequences have been designed for the T_1 and T_2 quantification of test tube Fricke gel detectors using an NMR spectrometer and evaluated using copper sulphate QC samples resulting in a precision (CV <0.2%) and linearity (R^2 > 0.999) adequate for the determination of R_1 and R_2 in this project when considered with regard to the 3% aim

for overall uncertainty. This was evaluated over the R_1 and R_2 ranges anticipated for Fricke gel dosimetry.

3.6 Commissioning an MRI scanner for analysis of large volume Fricke gel samples

3.6.1 Overview

A Philips Achieva 3T Tx MRI scanner in conjunction with an 8-element head coil (Philips Medical System, Best, The Netherlands) was used to image larger volume Fricke gel samples for investigations into the homogeneity of Fricke gel detectors and the diffusion of ferric ions.

The aim of this section was to develop methods for the mapping of larger volume Fricke gel samples. For now, this was limited to 2D dose maps, sufficient for the basic characterisation work in this project with the aim to extend it to 3D in the future.

Pulse sequences were optimised to carry out 2D T_1 and T_2 quantification in acceptable times. Software was required for the analysis of the acquired image set, converting images to T_1 maps then dose maps. The development of bespoke analysis software was carried out within OsiriX image analysis platform. Pulse sequences were evaluated using copper sulphate QC samples.

3.6.2 Preparation of copper sulphate QC samples

Copper sulphate QC samples were again used for the comparison and optimisation of T_1 and T_2 quantification scan sequences. In addition to the test tube samples described in section 3.5.2, larger QC samples were prepared. 1l samples of $CuSO_4$ were created with approximate concentrations of 0.5mM, 1.5mM, 4mM and 7mM.

3.6.3 Parameters for evaluation of pulse sequences

Parameters used to evaluate different pulse sequences were the scan repeatability, linearity, image uniformity, scan time and a measure of the signal to noise ratio (SNR) according to international guidance [124]. The test tube copper sulphate samples were used to assess the linearity of R_1 and R_2 versus copper sulphate concentration. It is known that R_1 and R_2 should be linear versus $CuSO_4$ concentration therefore, this was evaluated as a test of pulse sequence performance. Three larger volume $CuSO_4$ samples

(concentrations 1.5mM, 4mM and 7mM) were used to evaluate the image uniformity, image noise and SNR, see Figure 3.10.
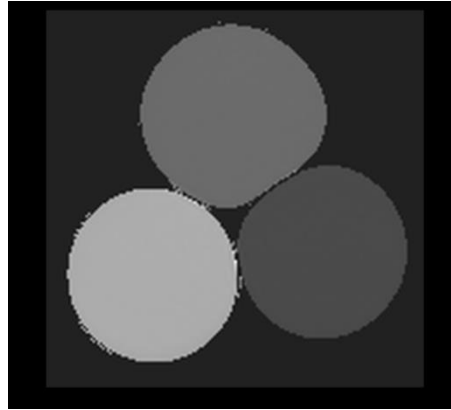
Figure 3.10: Scan of 1l volume copper sulphate samples used for pulse sequence evaluation.

The scan uniformity was determined by positioning a $1cm^2$ ROI in the areas of minimum signal intensity and maximum signal intensity and calculating the percentage image uniformity (PIU) [124]:

$$PIU = 100 \bullet \left[1 - \frac{\left(\overline{S}_{max} - \overline{S}_{min} \right)}{\left(\overline{S}_{max} + \overline{S}_{min} \right)} \right] \qquad \textbf{Equation 3.4}$$

The repeatability is the coefficient of variation of the mean signal within a ROI of 10 scans. The image noise, and therefore SNR, would usually be assessed using regions of interest (ROI) in the background region of the image, outside of the samples. T_1 and T_2 maps are synthetic rather than an acquired image, where the signal outside of the copper sulphate or Fricke gel samples was set to zero to limit computation. It is therefore not possible to carry a standard SNR measurement against the background. Instead, the ratio of the mean signal to the standard deviation within a $45cm^2$ ROI positioned in the phantom was used as an indication of the SNR. It is recognised that this include effects due to the T_2 fit, image artefacts and inhomogeneity in the sample itself. In the final assessment of the optimised T_1 and T_2 scan protocols, the inverse was used to provide an indication of scan uncertainty i.e. the s.d./mean expressed as a percentage. These will be referred to as SNR and scan uncertainty (%).

3.6.4   Development of image analysis software for T_1 and T_2 quantification

Image processing software was required to convert acquired MR images into T_1 or T_2 maps. The scans acquired are a series of images at different inversion times for T_1 quantification and different echo times for T_2 quantification where the pixel values represent the residual magnetisation at that time.

This software was required to carry out the following functions:

- Import the MR image series in DICOM (digital imaging and communications in medicine) format.
- For every pixel in each acquired image, extract the magnetisation signal creating a series of data points of signal versus time.
- From this data, calculate the T_1 or T_2 for each pixel. This step will be described in further detail under the sections on T_1 and T_2 quantification.
- Display the T_1 or T_2 map and allow this to be saved, analysed and exported.
- Optionally convert to R_1, R_2 map or a dose map, depending on the test.

OsiriX is a multi-modality, open source imaging platform based on the objective-C programming language [115]. The basic software enables standard image processing functions such as importing and exporting images, plotting profiles or performing analysis using regions of interest. Additional software plugins are available to carry out more specialised functions and the user can also develop their own plugins to fit specific requirements.

There already existed plugins for T_1 and T_2 quantification which had some basic functionality but required modifications for our pulse sequences and applications. Two plugins were developed to carry out T_1 and T_2 quantification of irradiated Fricke gel detectors. This is described in further detail in Appendix A, and specifics of T_1 and T_2 sequences are described in the next sections.

3.6.5   Look Locker pulse sequence for T_1 quantification

The Look Locker sequence was developed to carry out fast T_1 quantification and is usually used in cardiac imaging to determine appropriate TI for myocardial signal suppression [119, 120, 125]. In the Look Locker sequence, each initial inversion pulse is followed by a series of pulses with a small flip angle (e.g. 10°). The residual net

magnetisation is tipped by this small angle away from the z-axis resulting in a small component in the transverse plane which may be measured. This component and the transverse signal depend on the TI (time between inversion pulse and the small flip angle pulse).

In contrast to the inversion recovery sequence, many points on the inversion recovery curve are sampled following each inversion pulse, greatly reducing scan times. However, the application of small flip angle pulses perturbs the recovery of the longitudinal magnetisation and results in a different signal recovery curve. The time constant characterising the recovery is no longer T_1, but instead is termed *T1 effective* (T_{1eff}) [117].

For this work, it is sufficient to know that the signal equation is of the form:

$$M_z = A - B \exp (-TI / T_{1eff})$$

where A and B are unknown parameters. This is less straightforward to program when compared with an exponential curve. From the data series (TI, M_z), a non-linear least squares fitting routine is used to find the three unknown parameters A, B and T_{1eff}. The T_1 plugin in OsiriX was modified to incorporate a Levenberg-Marquardt non-linear least squares routine to determine T_{1eff}. T_1 can be calculated from the T_{1eff}, TI, and knowledge of the flip angle but this is not necessary for our work. An accurate determination of the T_1 value is not required. T_{1eff} will suffice as it is related to dose in a similar, linear way, which is confirmed in a subsequent experiment.

Look Locker pulse sequence parameters to be set were: flip angle, number of data points/phases (N), number of signal averages (NSA), slice thickness, pixel size, TI interval and TR. A clinical cardiac pulse sequence was used with a simulated heart trace. The R-R interval determined the TR which was 2s. The slice thickness was set to 5mm throughout. The impact of other sequence parameters on the signal to noise ratio was investigated in a series of investigations using the copper sulphate QC samples as follows. Default parameters were: flip angle 7°, N = 25, NSA = 3 and pixel size 1.4mm then each parameter was varied in turn. The flip angle was varied between 3° and 15°, N was varied: 15, 25, 51 and different combinations of pixel size and NSA were investigated. Results are shown in Table 3.3 to Table 3.5.

Table 3.3 SNR versus flip angle

Flip angle (^{o})	SNR		
	Sample A $T_1 \approx 800ms$	Sample B $T_1 \approx 420ms$	Sample C $T_1 \approx 230ms$
3	222	168	129
5	347	234	194
7	361	248	234
10	315	300	334
15	259	261	332
30	86	122	N/A artefacts

Table 3.4 SNR versus N

N	SNR		
	Sample A $T_1 \approx 800ms$	Sample B $T_1 \approx 420ms$	Sample C $T_1 \approx 230ms$
15	334	219	145
25	139	190	109
51	148	219	115

Table 3.5 SNR versus pixel size and NSA for sample B ($T_1 \approx 420ms$)

Pixel size (mm)	NSA	SNR
1.4×1.4	3	219
1.4×1.4	1	120
1.0×1.0	5	30
1.0×1.0	3	16

These investigations demonstrated an improved SNR with flip angle of 7° to 10°, therefore 7 was used thereafter. SNR versus N was optimal for N = 15. In terms of the flip angle dependence, a larger flip angle transfers more signal into the transverse plane. For a long enough TR, it will directly increase the SNR and reduce the uncertainty on

the fit. For shorter, T_1 full relaxation might not occur between excitation and this will affect the calculated T_1 values. Similarly, in terms of T_1 dependence on N, increasing N should improve the fit of the T_1 curve and reduce the standard deviation, however, it also compromises the SNR of the acquired images which in turn influences the quality of the map. Experiments in this project involved steep gradients across the image plane, therefore a high in-plane resolution (small pixel size) was required, ideally 1mm or less. However, smaller pixel sizes results in lower SNR as demonstrated here. SNR may be increased by increasing the NSA, but at a cost of increased scan time. These results show that for the Look Locker sequence, it was difficult to maintain adequate SNR for the sub-mm pixel size required in this project.

3.6.6 CPMG pulse sequence for T_2 quantification

A CPMG sequence was used for T_2 quantification of large volume samples using the scanner. A 90° pulse is followed by a series of 180° pulses at regular intervals (echo times TE) to create spin echoes. The resulting image set is a series of 2D images at varying TE. The OsiriX plugin plots the magnetisation signal in each pixel versus time and uses the signal decay curve (equation 3.3) to quantify T_2. From this, a T_2 map was calculated which may be converted to a dose map if the relationship between T_2 and dose is known. A copper sulphate sample of 0.5mM concentration was used for this experiment.

Parameters to be set for this sequence were: number of data points (N), number of signal averages (NSA), slice thickness, pixel size, TE, TR and refocusing angle. Throughout, the TR was set to 2s, echo train length was 32, NSA was 1 and the slice thickness was 5mm. The impact of refocusing angle, TE interval and pixel size on SNR was investigated. Default parameters were refocusing angle 170° and TE interval 40ms. The refocusing angle was varied between 160° to 180°, a TE of 30 vs. 40ms was compared and the pixel size was varied. Results are shown in Table 3.6 to Table 3.8.

Table 3.6 Effect of TE on SNR in sample with $T_2 \approx 1350$ms (pixel size = 0.4mm)

TE (ms)	SNR
30	124
40	152

Table 3.7 Effect of refocusing angle on SNR in sample with $T_2 \approx 1350$ms (pixel size = 0.9mm)

Refocusing angle	SNR
160°	210
170°	250
180°	210

Table 3.8 Effect of pixel size on SNR (sample $T_2 \approx 1350$ms)

Pixel size (mm)	SNR
0.35×0.35	150
0.94×0.94	250
1.0×1.0	280

The results demonstrate that SNR is increased for a TE of 40ms compared with 30ms. There was little difference in SNR for different refocusing angles; 170° was used thereafter. In contrast with T_1 quantification using the Look Locker sequence, it is possible to acquire T_2 maps with much greater SNR, even with pixel sizes of less than 1mm^2 and NSA of 1.

The final sequence for T_2 quantification used a refocusing angle of 170°, slice thickness of 5mm, 32 measured echoes, NSA of 1, TE of 40ms and TR of 2000ms.

3.6.7 Comparison between T_1 and T_2

A direct comparison between T_1 and T_2 scan results was carried out. Pixel size and slice thickness were set to be the same for both scan types (1.0×1.0mm^2 and 5mm). Otherwise optimized parameters were set, as described in the previous sections. One large 0.5mM copper sulphate solution sample was surrounded by test tube sample of varying T_1 and T_2. Scans were repeated 10 times. Results were compared in terms of SNR, image uniformity, repeatability and linearity.

Example T_1 and T_2 maps of the CuSO$_4$ solution samples are shown in Figure 3.11. The results of the scan uncertainty, homogeneity and repeatability for the optimised scan sequences are shown in Table 3.9.

<center>(a)   (b)</center>
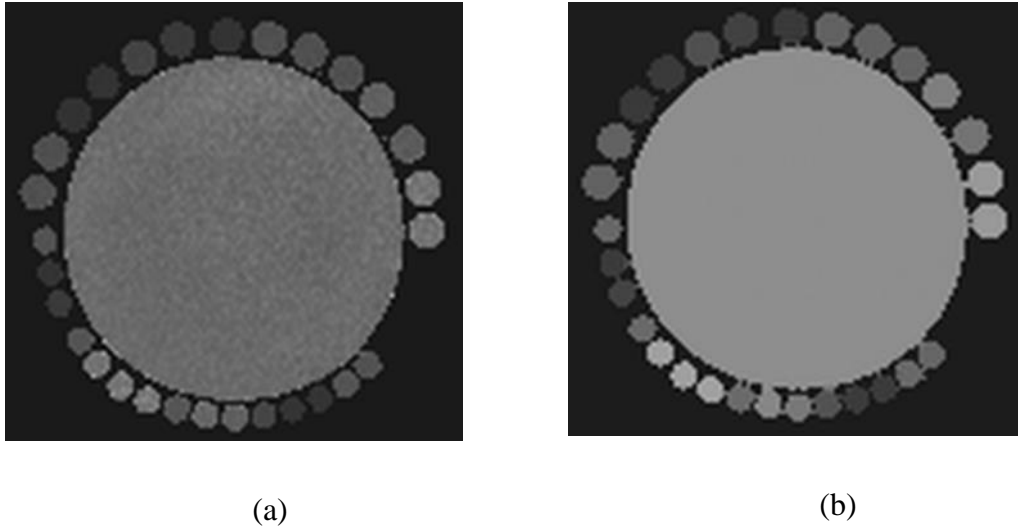
Figure 3.11: Example T_1 (a) and T_2 (b) maps of CuSO$_4$ test samples.

Table 3.9 Scan performance for T_1 and T_2 quantification sequences

Parameter	T_1 sequence	T_2 sequence
Scan uncertainty (%)	6.0	0.5
Image uniformity (%)	96.8	99.8
Repeatability CV (%)	1.5	0.5

The relationship between relaxation rate and CuSO$_4$ concentration was linear (R^2 >0.999) for both R_1 and R_2 (Figure 3.12 and Figure 3.13).
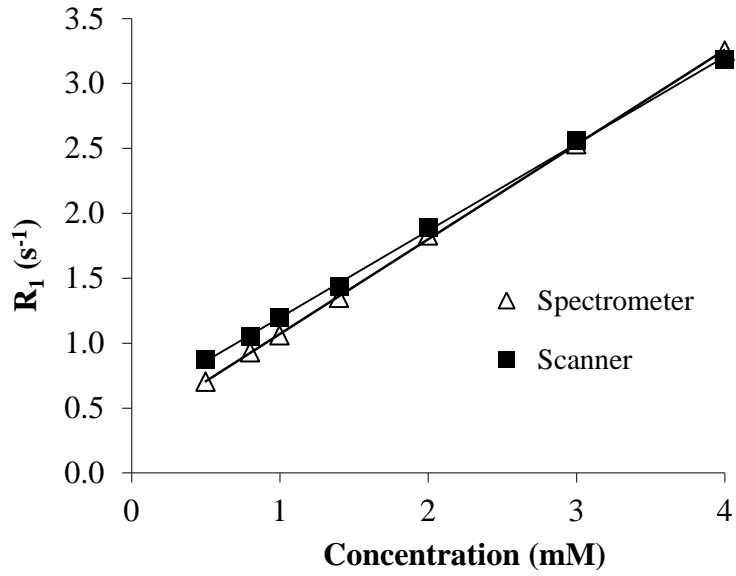
Figure 3.12: Relaxation rate versus CuSO$_4$ concentration for R$_1$.
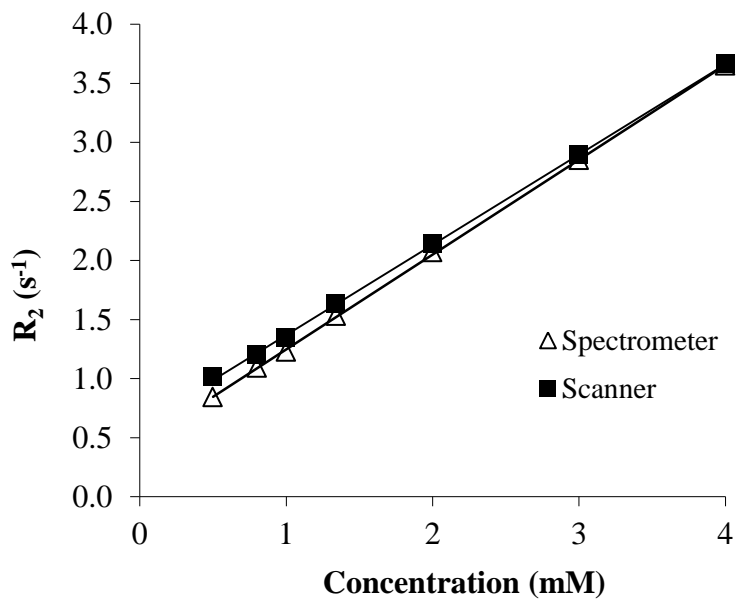
Figure 3.13: Relaxation rate versus CuSO$_4$ concentration for R$_2$.

The T$_2$ quantification method produced images with much superior signal to noise compared with the Look Locker sequence for the same spatial resolution and improved image uniformity. The slope of the relaxation rate versus CuSO$_4$ concentration was similar for both T$_1$ and T$_2$ quantification methods. T$_1$ versus T$_2$ quantification for Fricke gel dosimetry will be investigated further in chapter 4.

3.7 Summary of chapter

In this chapter, the methodology was developed for the manufacture of the Fricke gel detectors and the MR processes for the analysis of irradiated detectors. In order to decide on a detector composition, the literature was reviewed to find evidence regarding the dosimetric performance of different composition Fricke gel detectors. In the absence of a systematic evaluation of any one composition, as highlighted in chapter 2, focus was mostly on the dose response. Previous investigations tended to compare detector compositions in terms of their sensitivity i.e. slope of the dose response curve. An optimum composition was selected: 0.5mM ferrous ammonium sulphate, 25mM sulphuric acid, 5% gelatine and distilled water.

A manufacture method was then streamlined within a basic laboratory in a clinical radiotherapy department making approximately 1l batches of Fricke gel each session which could be poured into test tubes or larger volume containers. The whole process takes 2 hours plus cooling time, which will be the subject of further investigation in chapter 5.

Focus then turned to the MR analysis methods. An NMR spectrometer and whole-body MRI scanner were commissioned for the T_1 and T_2 quantification of test tube and larger volume Fricke gel samples. For the NMR spectrometer, an inversion recovery sequence was selected for T_1 quantification and pulse sequence parameters were set to measure T_1 with adequate measurement precision within a practical measurement time of less than 10 minutes per sample. A CPMG sequence was then used for T_2 quantification and appropriate pulse sequence parameters were set. Sequences were evaluated using copper sulphate QC samples with T_1 and T_2 covering the range expected for unirradiated and irradiated Fricke gels. Both resulted in a measurement precision of repeated measurements of <0.2%.

Pulse sequences were then customised for a Philips Achieva 3T MRI scanner. Analysis software was written within OsiriX, an open source image analysis platform, for the creation of T_1 and T_2 maps and dose maps. A Look Locker sequence was used for T_1 quantification and pulse sequence parameters were set to optimise the sequence in terms of SNR. A CPMG sequence was used for T_2 quantification, and again, settings selected to maximise SNR. Once again, copper sulphate samples were prepared for the

evaluation of sequences. The optimised sequences were more fully evaluated in terms of scan uncertainty, homogeneity and repeatability. Overall, scan uncertainty was lower for optimised protocol for T_2 quantification when compared with the optimised (and available) T_1 protocol for scan times of similar duration. The image uniformity was also improved for the T_2 CPMG sequence. There has been disagreement in the literature over the use of T_2 quantification for the analysis of Fricke gel detectors with many authors recommending T_1 despite issues with adequate SNR for small pixel sizes for available scan sequences. Therefore a direct comparison between T_1 and T_2 quantification results for small volume Fricke gel detectors should be carried out and will be described in chapter 4.

Chapter 4. Evaluation of the dosimetric performance of small volume Fricke gel detectors

4.1   Introduction

4.1.1   Aim of this chapter

Having established processes for the manufacture of Fricke gel detectors, and MR analysis of irradiated detectors in chapter 3, the optimised system could now be commissioned. This involves investigating all potential sources of measurement uncertainty. The literature review described in chapter 2 highlighted a lack of systematic approach to the dosimetric characterisation of 3D chemical detectors and a lack of evidence for many factors including inter-sample variation, volume dependence and integration. This was used to create an experimental plan for the full dosimetric characterisation of the Fricke gel-MR system used in this project (Figure 2.2) following a similar approach to that which would be taken if a commercial radiation detector was being commissioned for use within the department. According to this plan, basic characteristics of inter-sample variation, chemical stability, dose rate dependence, dose integration and energy dependence should be quantified first before moving onto uncertainties related to larger detector volumes such as homogeneity of response. These are the subject of this chapter.

Many previous investigations into Fricke gel detectors have involved large radiation doses and in particular there is very little published information over the 0 to 3Gy range, as summarised in chapter 2. The aim of this experimental chapter was to therefore to investigate basic dosimetric characteristics of the Fricke gel detector focusing on two clinically relevant dose ranges: 0 to 3Gy to cover conventional fractionation schedules and 5 to 20Gy to cover stereotactic techniques. All experiments in this chapter were carried out using small volume (test tube) detector samples readout using the MR spectrometer. T_1 and T_2 relaxation times were quantified using optimised protocols developed in chapter 3. This avoids introducing any uncertainties caused by performing relaxometry of larger samples on a whole-body scanner, for example artefacts and non-uniformity of scanner response and inhomogeneity of the detector response itself.

Before characterisation measurements were commenced, an initial experiment was carried out to examine the impact of adding xylenol orange on the detector response.

This has been previously shown to reduce the effect of ferric ion diffusion, but at the expense of a much decreased MR response (R_1 or R_2 versus dose). Dose response curves for detectors with and without xylenol orange were compared.

The first characterisation experiment was the pre- and post-irradiation chemical stability of the Fricke gel detector. As described in the literature review of chapter 2, the chemical stability has been previously quantified for detectors readout with optical methods and has demonstrated a short term increase in signal due to reaction completion [23, 28, 91, 92] followed by a longer term signal drift [22, 27, 28, 92, 106]. There was some variation in the reaction completion times quoted in the literature of between 10 minutes to 2 hours, which would have an impact on the time following irradiation that a detector should be scanned. A long reaction completion time might conflict with any requirement to scan detectors quickly to avoid blurring due to ferric ion diffusion. It was also not clear from the literature whether longer term signal drift could be reduced by storing the detectors in the dark. Chemical stability was investigated in terms of R_1 or R_2 versus time.

The literature review highlighted a lack of evidence of the inter-sample variation of Fricke gel detectors (section 2.4). This is an important factor as 3D chemical detectors are usually calibrated whereby the dose response is characterised by irradiating additional samples with known radiation doses. Establishing that different samples from the same detector batch respond similarly is therefore a crucial step. Therefore, the next investigations quantified inter-sample variation for this Fricke gel detector by irradiating multiple detector samples to the same radiation doses, for a range of doses between 0 and 20Gy.

Results from the inter-sample variation experiment were also used to plot dose response in terms of relaxation rate versus dose. Whilst a linear dose response is not absolutely necessary, it simplifies calibration as a simple linear regression can be used. A linear response has previously been demonstrated for Fricke gels in some studies [16, 23, 25, 28, 98] whereas others have shown a deviation from linearity [91, 100, 104]. Dose response was analysed for this detector in terms of its linearity. In addition, dose response was compared for several different batches of detector in order to perform a gross check on the consistency of the manufacture process. It is fully expected for chemical detectors to perform a calibration for each batch and measurement session.

This experiment was repeated with different times between detector manufacture and irradiation to investigate the shelf life of a Fricke gel detector.

A further aim was to compare T_1 and T_2 quantification methods in terms of their dose response and measurement precision. The acquisition of 2D or 3D T_1 maps with an adequate signal-to-noise ratio (SNR) and high measurement accuracy within a reasonable scan time presents a challenge, as was highlighted in chapter 3. Fast T_1 quantification methods, such as the Look-Locker sequence inherently suffer from a lower signal-to-noise ratio (SNR) when compared with inversion recovery techniques [117]. T_2 quantification is more straightforward and was shown in the previous chapter to more easily produce T_2 maps with higher SNR, lower noise and improved uniformity when compared with the optimized Look Locker sequence. However, early studies on Fricke gel detectors showed a lower dose response for R_2 compared with R_1 [111] and elsewhere a similar response but poor R_2 precision [14]. More recently, Marrale *et al* showed negligible R_2 response but a good R_1 response, albeit for neutron irradiation [126]. In contrast, others have used T_2 quantification successfully [19, 88]. In the next experiment, T_1 and T_2 methods were directly compared in terms of their inter-sample variation and dose response to clarify this issue.

The final set of experiments investigated the effect of radiation dose rate and energy on the detector response. Ideally detectors would be independent of dose rate and energy as both dose rate and energy spectrum may vary during a clinical delivery. Previous literature reviewed in chapter 2 demonstrated that the Fricke gel response was independent of dose rate [16, 90, 91, 93, 104] although there was little evidence for the effect of energy for MV photon beams [104]. None of these previous experiments have been carried out following a baseline inter sample variation experiment to allow results to be analysed in the context of the basis precision. Dose rate and energy dependence were investigated for this Fricke gel composition and extended to include experiments on dose integration by delivering radiation dose with several beams to mimic a clinical radiotherapy plan.

4.1.2   Chapter overview

Fricke gel detectors were manufactured according to the optimum composition established from the literature (section 3.2.2). Experiments were then carried out using

batches of Fricke gel detectors. The aim of this set of experiments was to perform the basic characterisation of the Fricke gel detector itself. For each experiment only the characteristic under investigation was altered with all other variables controlled. Detector samples originated from the same batch and were irradiated, analysed and stored together in the same ambient conditions. Analysis was carried out with the spectrometer to reduce any additional uncertainty in T_1 and T_2 quantification introduced using a whole-body scanner for example image uniformity and artefacts.

Experiments were carried out in a logical order with the chemical stability investigated first in order to establish whether there were any limitations on when detectors should be analysed or on the ambient storage conditions. The inter sample variation was then evaluated to establish a baseline precision ahead of experiments to investigate dose rate and energy dependence. Statistical analysis was then used to assess energy and dose rate dependence. Results for all these experiments were assessed in the context of the overall target of 3% for the dosimetric uncertainty for this detector set out in chapter 2.

An initial experiment investigating the effect on the dose response of adding xylenol orange to the composition was carried out (section 4.2.3). The chemical stability was investigated, both long term signal drift for light versus dark storage conditions and short term reaction completion, described in section 4.2.4. T_1 versus T_2 quantification methods were compared in terms of dose response and precision across a dose range of 0 to 20Gy. This was carried out over several batches of Fricke gel so dose response could be compared as a check of manufacture processes (section 4.2.5). Dose response and precision experiments were repeated at different times between manufacture and irradiation, to characterise the shelf life of the detector (section 4.2.6). Finally, dose rate, integration and energy dependence were investigated (sections 4.2.7 and 4.2.8).

4.2   Methods

4.2.1   Gel manufacture

The composition of the Fricke gel dosimeters used throughout this chapter was 0.5mM ferrous ammonium sulphate, 25mM sulphuric acid and 5% gelatine (bw). Batches of Fricke gels were manufactured, according to the process described in section 3.3 producing 1.05l each session. The Fricke gel was poured into 6mm inner diameter MR

test tubes (borosilicate glass, Bruker UK Ltd). Unless otherwise stated, the samples were placed in a refrigerator at 4$^{\text{o}}$C until 2 hours prior to analysis or irradiation.

4.2.2 Irradiation

All irradiations were carried out with a Varian Clinac iX linear accelerator (Varian Medical Systems, Palo Alto, CA) as described in section 1.1.3. This linac has 6 and 15MV photon beams and is capable of delivering radiotherapy plans using both IMRT and VMAT (known as RapidArc by this manufacturer). The linear accelerator output (dose per monitor unit under reference conditions) was measured before gel experiments using a Farmer ionisation chamber with calibration traceable to the UK National Physical Laboratory [4]. The precision of the radiation dose delivery has been previously measured and is better than 0.1%.

A Perspex block with inserts for four test tubes was manufactured to allow the simultaneous irradiation of multiple samples (Figure 4.1). The Fricke gel samples were irradiated with 6MV photons at 600 MU.min^{-1} in a 20×20cm^2 field. By positioning the test tubes within the central 6cm of this field, the variation in dose across the samples was kept within ±0.25% of the set dose. The Perspex phantom was sandwiched between two 5cm thick blocks of WT1 water equivalent material (St. Bartholomew's Hospital, London, UK) which provided full scatter equilibrium. The monitor units to deliver the required dose were calculated and corrected for linac output. The temperature during each irradiation session was monitored and was stable to within ± 0.2$^{\text{o}}$C.
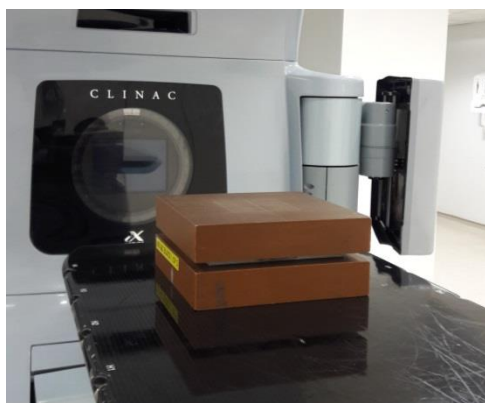
<div align="center">(a)</div>
<div align="center">(b)</div>

Figure 4.1: Phantom used for the irradiation of Fricke gel samples with (a) and without (b) build up material block.

4.2.3 Investigation into the effect of xylenol orange on dose response

The dose response of Fricke gel detectors with and without xylenol orange were compared. Two batches of Fricke gel were prepared during the same session at the NPL, one with 0.1mM xylenol orange added at the same time as the ferrous ammonium sulphate solution. A 100ml stock solution of 0.1mM xylenol orange was prepared by adding 0.76g of xylenol orange powder to 100ml of the 25mM sulphuric acid solution. Otherwise, manufacture was carried out as described in section 3.3. Samples from each batch were irradiated in pairs to doses of up to 15Gy and the T_1 was measured. The irradiation and T_1 measurements of all samples were carried out at the same time to ensure all detectors had the same thermal and light exposure history. R_1 was plotted versus dose.

4.2.4 Chemical stability

Two experiments were carried out to investigate the chemical stability of this Fricke gel detector over time. The aim of the first was to quantify for our detector composition the slow increase in gel reading previously reported for other Fricke gel detectors and to investigate the effect of visible light. T_1 and T_2 measurements were repeated over a period of 3 hours for two unirradiated Fricke gel samples from the same batch. One of the samples was stored in normal room light conditions between measurements and the other in a light-tight container. The detectors were at a constant temperature of 23°C

throughout. R_1 and R_2 were plotted versus time for both samples and the rate of change in the relaxation rate was quantified.

The second experiment was designed to investigate the variation in R_2 following irradiation. Three Fricke gel samples were irradiated to doses of 2, 8 and 15Gy. T_2 measurements were commenced immediately after irradiation and repeated for 3 hours, initially at short intervals to investigate the reaction completion time. Samples were stored in the dark in between measurements for this experiment.

4.2.5 Inter-sample variation and dose response: T_1 vs. T_2 quantification

The R_1 and R_2 measurement precision were quantified for doses over the range 0 to 20Gy and dose response curves were compared. Two batches of gels were manufactured on separate occasions. 32 test tube detector samples were prepared from each batch. Pre-irradiation T_2 values were measured for all 32 samples and the baseline coefficient of variation was calculated. Samples were then irradiated in groups of 8 to known doses. For the first batch, gel samples were irradiated to doses of 0 to 3Gy in 1Gy increments and for the second batch gel samples were irradiated to doses of 5 to 20Gy in 5Gy increments. For both batches, additional pairs of samples were irradiated to enable the dose response curves to be compared. The gel samples were all stored together in the dark and irradiated during the same session. To reduce measurement uncertainties due to signal instability established in the previous experiment, all MR measurements were commenced at least 10 minutes after irradiation and were completed within 3 hours.

4.2.6 Time post-manufacture (shelf life)

The experiments into precision and dose response were repeated with different intervals between gel manufacture and irradiation. Two batches were manufactured on separate occasions. Samples from the first were irradiated and read out on days 1 and 7 post manufacture. Samples from the second batch were irradiated on days 2, 16 and 22 post-manufacture. For each measurement session, T_2 of all remaining unirradiated samples was quantified prior to irradiation. Two samples were irradiated to doses of 0, 10 and 15Gy to plot the dose response curve and 8 samples were irradiated to doses of 3 and 20Gy to evaluate the precision.

4.2.7 Variation in detector response with radiation dose rate and integration

The dose rate and dose integration were investigated using samples from the same batch, irradiated and measured during the same session. For each set of parameters, four samples were irradiated simultaneously, the T_2 quantified, converted to R_2 and the mean R_2 was calculated. In the first set a dose of approximately 5Gy was delivered to the Fricke samples. The dose rate was varied (100, 400 and 600 MUmin^{-1}) with 500 MU delivered in one shot. To investigate how the detector integrates multiple beams and mimic a clinical delivery, a further set of samples were irradiated with 500MU split into 5×100MU beams, delivered at 60 second intervals. To mimic the delivery of high doses with multiple fields, a further set of samples were irradiated to a dose of approximately 20Gy (2000MU); in a single shot, 5×400MU (60s intervals) and 10×200MU (45s intervals).

4.2.8 Variation in detector response with radiation energy

The effect of radiation energy was also investigated using samples from the same batch, irradiated and measured during the same session. Again, four samples were irradiated simultaneously, the T_2 quantified and the mean R_2 was calculated. The irradiation conditions were the same as previously, however the energy was varied (6MV and 15MV) and measurements were also made at larger depths for each energy to confirm no effect of low energy scattered radiation. The monitor units required to deliver a dose of 5Gy were calculated for each experiment, and corrected for linac output, to enable comparison between 6MV and 15MV beams.

4.3 Results

4.3.1 Investigation into the effect of xylenol orange on dose response

R_1 was plotted versus dose (Figure 4.2). Error bars were calculated (2 s.d.) however they are too small to visualise udner the data markers. This is demonstrated as an example in Figure 4.8 of section 4.3.3. The Fricke gel detectors without XO demonstrated a greater dose response than those with XO which agrees with results reported in the literature [27, 31]. The benefit of xylenol orange is the reported reduction in the ferric ion diffusion post irradiation. The ferric ion diffusion for this detector will be investigated at clinically relevant dose levels in chapter 5. As the dose

response has been shown to be markedly worse, and we are not using optical methods, xylenol orange was excluded for subsequent experiments subject to the results of an investigation into ferric ion diffusion experiment.
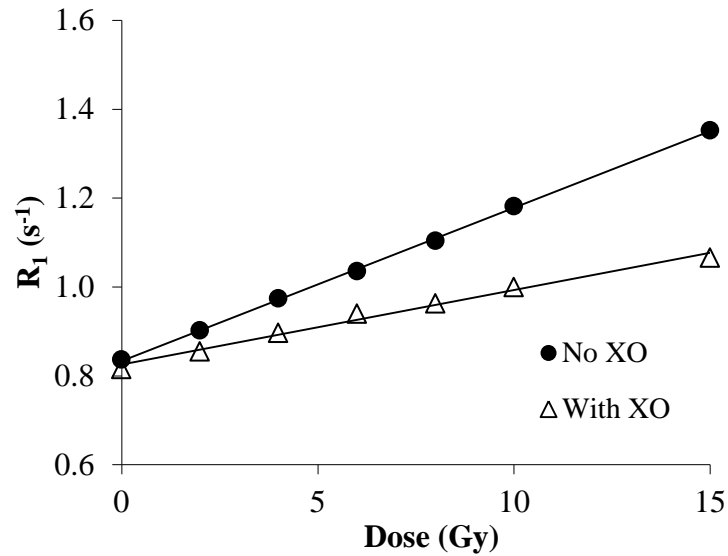
Figure 4.2: R_1 versus dose for Fricke gel samples with and without xylenol orange.

4.3.2   Chemical stability

The variation in R_1 and R_2 relaxation rate with time was compared for unirradiated Fricke gel samples stored in normal indoor light conditions and in the dark (Figure 4.3). Once again error bars were too small to visualise. The relaxation rate increased steadily for samples stored in normal ambient light conditions by 2% per hour. When stored in the dark, the rate of oxidation for unirradiated gels was reduced to 0.2% per hour which indicates that visible light induces an oxidation reaction. During all subsequent experiments, Fricke gel samples were stored in the dark and completed within 3 hours.
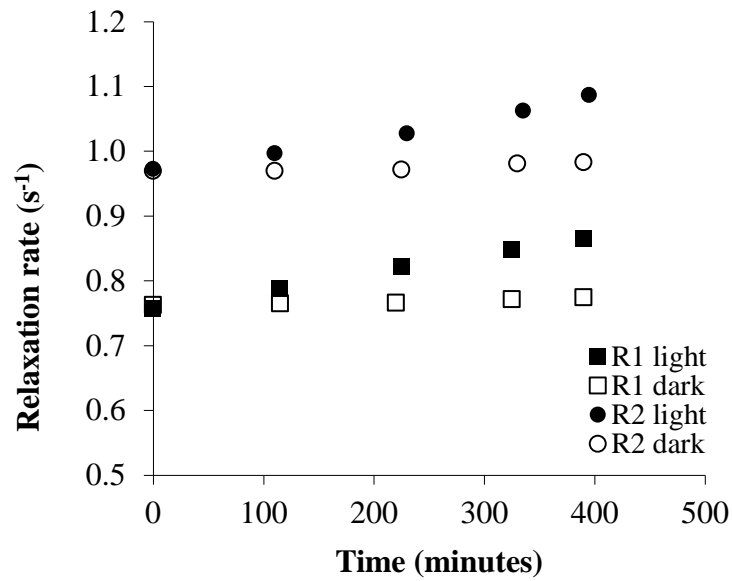
Figure 4.3: Variation in signal with time for unirradiated Fricke gel samples stored in different ambient light conditions.

The stability of the R_2 signal following irradiation for detector samples irradiated to 2, 8 and 15Gy is plotted in Figure 4.4 and as the rate of change in R_2 versus time in Figure 4.5. These detectors were stored in the dark between measurements. A steep increase in relaxation rate was seen immediately following irradiation. The reaction completion time was dependent on radiation dose, but was within 12 minutes for all doses investigated. Thereafter the R_2 signal increased by less than 0.2% h^{-1}.
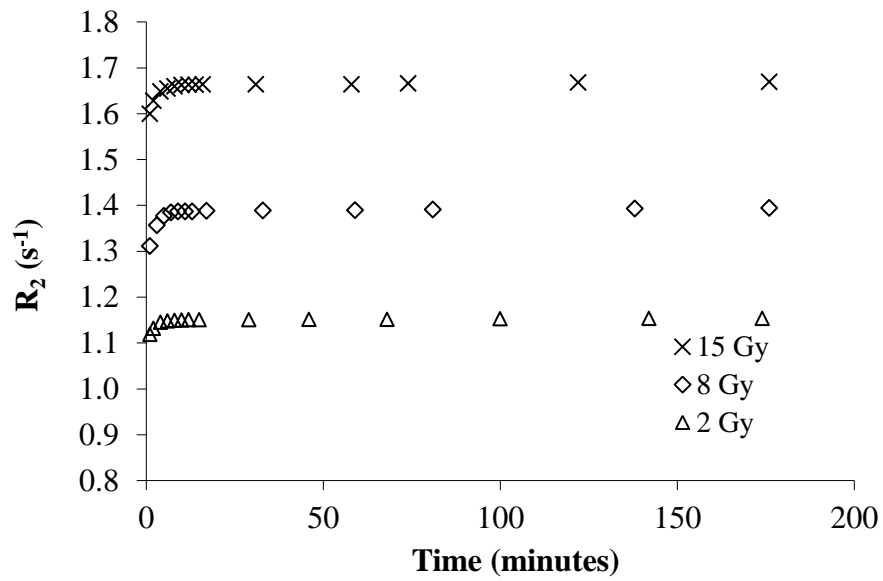
Figure 4.4: R_2 signal versus time post-irradiation.
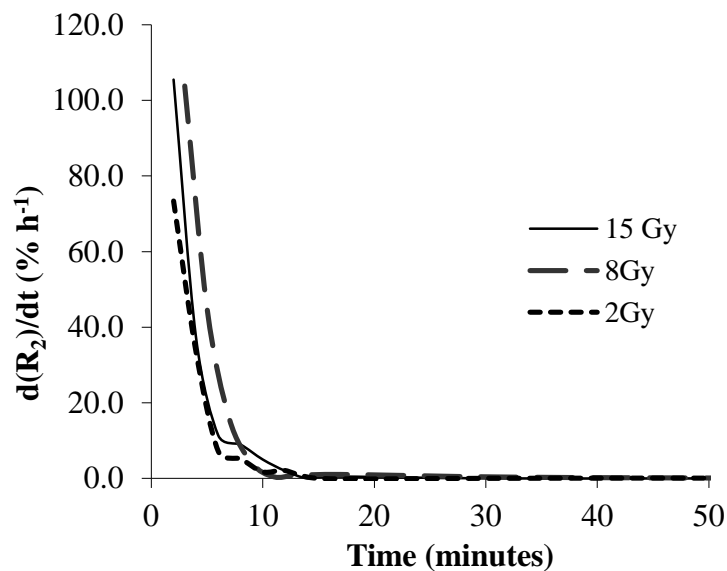
Figure 4.5: Rate of change of signal with time for unirradiated Fricke gel samples stored in different ambient light conditions.

4.3.3 Inter-sample variation and dose response: T_1 versus T_2 quantification

The CV in R_2 of 32 Fricke gel samples prior to irradiation was less than 0.5% for both gel batches indicating an excellent consistency of the gel (mean R_2 0.828, s.d. 0.003 for the first batch, mean R_2 0.850, s.d. 0.004 for the second batch). For groups of samples irradiated to the same dose, the CV was also less than 0.5% for both R_1 and R_2 for all

dose levels investigated in the range of 1 to 20Gy. All individual R_1 and R_2 values were within 1% of the mean value for each dose level (Figure 4.6 and Figure 4.7). This sets the baseline precision for subsequent experiments on dose rate and energy dependence which will involve multiple samples irradiated under different conditions.
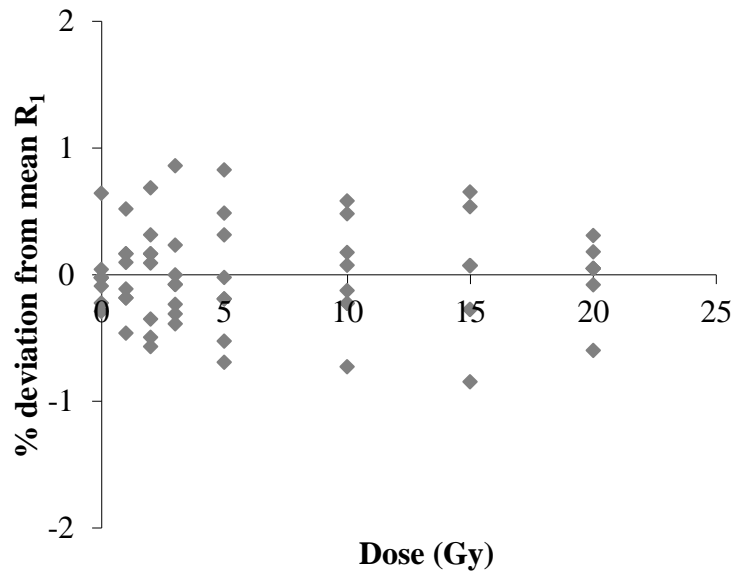
Figure 4.6: Deviation from the mean R_1 for each sample.
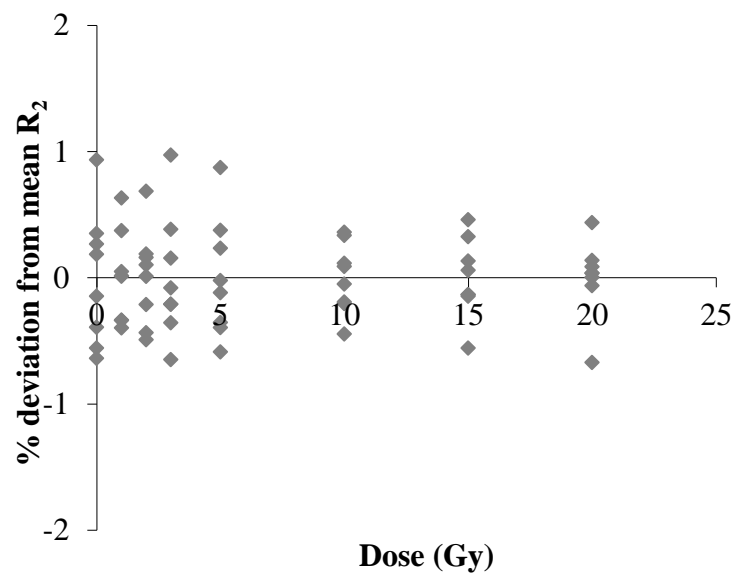
Figure 4.7: Deviation from the mean R_2 for each sample.

The dose response curves for both Fricke gel batches and for both R_1 and R_2 versus dose are shown in Figure 4.8. A linear relationship between dose and signal was demonstrated for both R_1 and R_2 ($r^2 > 0.999$ in all cases). There was a very slight improvement in the R_2 dose sensitivity compared with R_1 with the slope for batch C for $R_1 = 0.0314$ s^{-1} Gy^{-1} and $R_2 = 0.0403$ s^{-1} Gy^{-1} as an example. The dose response for the two batches was similar and this is investigated further in section 4.3.7.
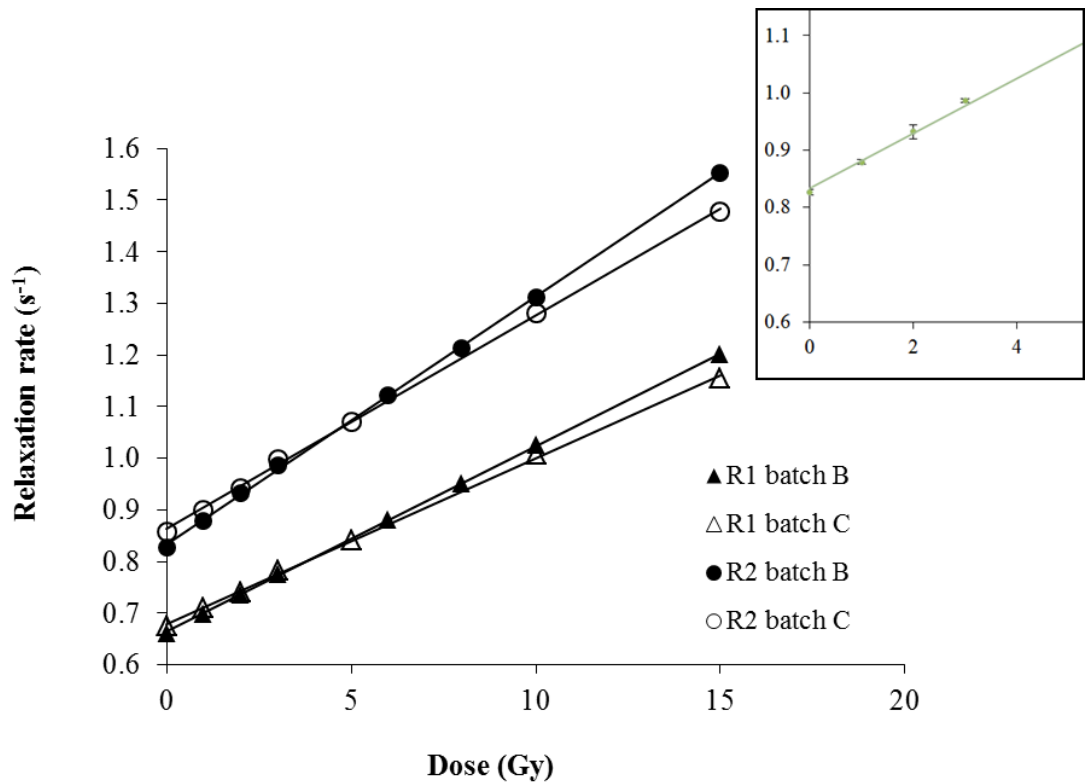
Figure 4.8: R_1 and R_2 versus dose for two Fricke gel batches. The insert shows a small section of the Batch B R2 results with 2 s.d. error bars displayed. These are too small to visualise when data markers are added.

To estimate the impact of the results of R_1 and R_2 uncertainty on the uncertainty in the calculated dose, the linear regression equations were used to convert the measured R_1 and R_2 values for each individual gel sample to dose. The CV of calculated dose was determined for each dose level as a percentage of the planned dose (Table 4.1).

Table 4.1: CV in measured dose for 8 samples irradiated to different dose levels

Dose (Gy)	CV dose (%)	
	R_1 analysis	R_2 analysis
0	n/a	n/a
1	6.1	7.1
2	4.4	3.6
3	2.8	3.0
5	2.7	2.5
10	1.3	0.9
15	0.5	0.8
20	0.3	0.6

There was negligible difference in the precision in measured dose for R_1 and R_2. The CV decreases with increasing dose and is within the set limit of 3% only over a dose range of 3 to 20Gy. Below 3Gy, the CV is greater than 3%. This is only one potential source of uncertainty, if subsequent experiments highlight any other significant contributions to measurement uncertainty, this dose range may need to be reconsidered.

4.3.4   Time post-manufacture (shelf life)

The dose response curves for gel samples from a single batch but irradiated at different times post manufacture are plotted in Figure 4.9. It can be seen that the R_2 increases over time due to the long-term signal drift previously demonstrated, despite being refrigerated at 4°C and kept in the dark. However, the slope only decreased from 0.0369 $s^{-1}Gy^{-1}$ (2 days) to $0.0357s^{-1}G^{-1}$ (22 days).
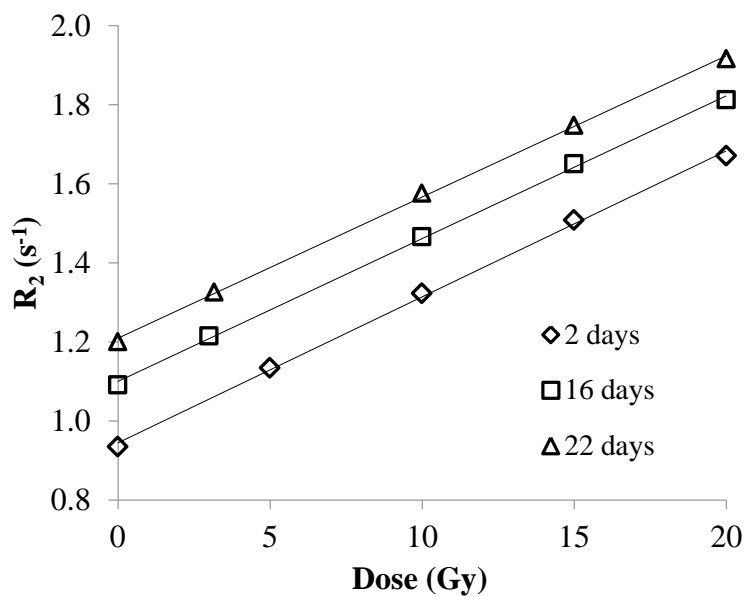
Figure 4.9: R_2 dose response at different times post-manufacture.

In terms of the inter-sample variation versus time between manufacture and readout or irradiation, the CV in R_2 of all unirradiated samples was within 1.0% for each measurement session and the CV for the 8 samples irradiated to 3Gy and 20Gy was within 0.5% for every measurement session. All individual R_2 values were within 1% of the mean value for each dose level and every measurement session. This would indicate that Fricke gels could be used up to 3 weeks after manufacture. However, the T_2 range decreases with time post manufacture (Figure 4.10) therefore variations in T_2 that occur across an MRI scanner due to inhomogeneity and image artefacts may have more impact.
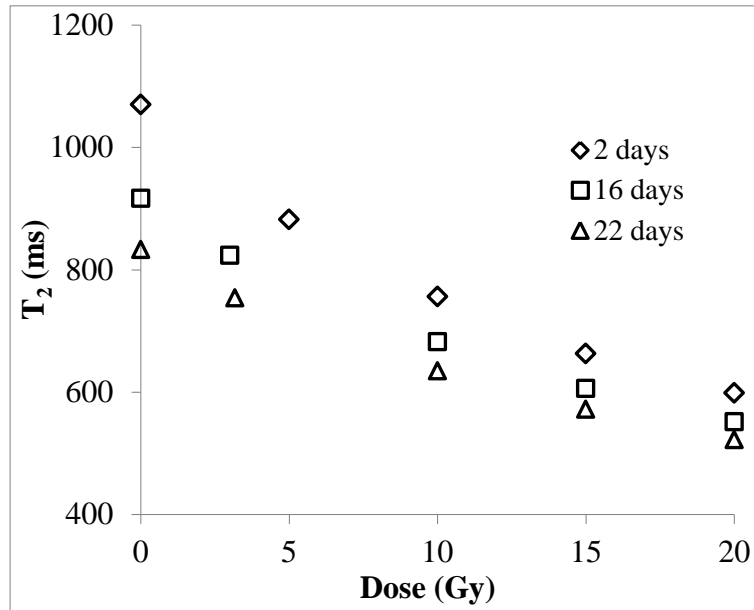
Figure 4.10: T$_2$ dose response at different times post manufacture.

4.3.5   Variation in detector response with radiation dose rate and integration

The variation in R$_2$ versus dose rate is presented in Table 4.2. The R$_2$ values presented are the mean of four samples irradiated for each set of conditions along with 95% confidence intervals (CI) calculated using the t-distribution. Results were all within 0.3% of the mean value, there was no trend with dose rate and the 95% confidence intervals overlapped. Therefore there was no evidence of dose rate or dose integration on dose response.

Table 4.2: Variation in R_2 with dose rate and dose integration

Planned dose (Gy)	Dose rate (MU/min)	Integration	R_2 (s^{-1}) [95% CI]	Normalised to mean
5	600	Single shot	1.021 [1.013-1.029]	0.998
5	100	Single shot	1.024 [1.016-1.032]	1.000
5	400	Single shot	1.023 [1.015-1.031]	1.000
5	600	5×100MU (60s)	1.026 [1.018-1.034]	1.002
20	600	Single shot	1.557 [1.544-1.577]	0.997
20	600	5×400MU (60s)	1.564 [1.551-1.577]	1.002
20	600	10×200MU (45s)	1.563 [1.550-1.576]	1.001

4.3.6   Variation in detector response with radiation energy

Results of detector response versus energy are shown in Table 4.3 along with 95% confidence intervals. Within each set energy, confidence intervals overlap and there is no trend with depth. Therefore there is no evidence of any effect of low energy scattered radiation which increases with depth for large field sizes. However, there is possibly a small effect seen between 6MV and 15MV beams as shown by the 95% confidence intervals for the mean of all measurements. However, in practice, experimental and calibration samples would all be irradiated using one set energy, usually 6MV for VMAT and stereotactic techniques. Therefore this is not of practical concern.

Table 4.3: Variation in R_2 with energy and depth (5Gy planned dose)

Energy (MV)	Depth (cm)	R_2 (s^{-1}) [95% CI]	Normalised to mean R_2
6	1.5	1.243 [1.233-1.253]	0.995
6	5.5	1.243 [1.233-1.253]	0.995
6	10.5	1.243 [1.233-1.253]	0.996
6	15.5	1.244 [1.234-1.254]	0.997
6	20.5	1.250 [1.240-1.260]	1.001
6MV Mean	N/A	1.244 [1.240-1.248]	N/A
15	3.0	1.247 [1.237-1.257]	0.999
15	5.5	1.251 [1.241-1.261]	1.002
15	10.5	1.258 [1.248-1.268]	1.008
15	15.5	1.253 [1.243-1.263]	1.004
15	20.5	1.252 [1.242-1.262]	1.003
15MV Mean		1.252 [1.248-1.256]	N/A

4.3.7   Consistency of gel manufacture

Finally, the dose response was compared for 6 different Fricke gel batches manufactured at St. Bartholomew's Hospital. It is emphasised that for chemical dosimetry it is standard practice to characterise the dose response for every batch of detectors and commonly for each measurement session, therefore differences between batches are expected and are accounted for in the calibration process. However this inter-batch comparison of dose response was carried out as a general check of the consistency of the manufacture process. All batches were irradiated within a few days of manufacture. A comparison between different batches is shown in Figure 4.11. The slope of the R_2 versus dose relationship for all 6 batches was within the range 0.0335 to 0.0380 $s^{-1}Gy^{-1}$ (mean 0.0358$s^{-1}Gy^{-1}$). The intercept was more variable, but as demonstrated in section 4.3.2 this is due to chemical reactions vs. time.
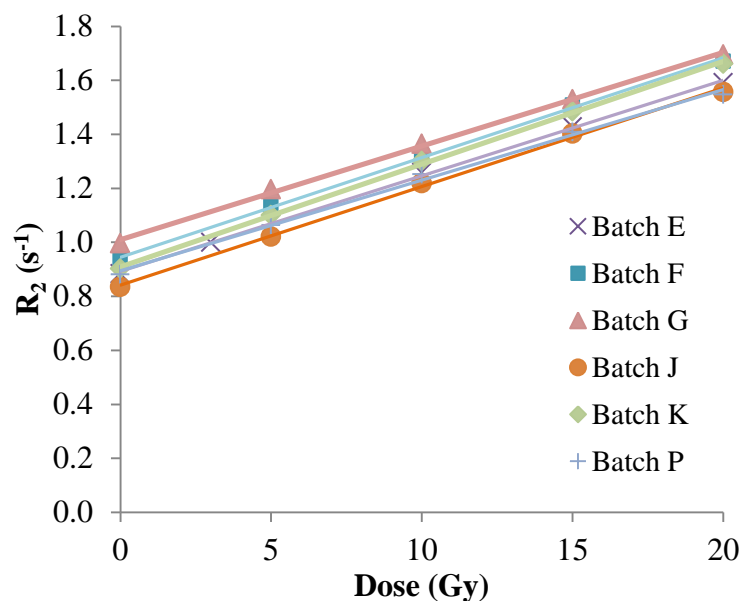
Figure 4.11: Dose response relationship for different Fricke gel batches manufactured at St. Bartholomew's Hospital.

4.4   Discussion

This chapter described systematic investigations into some of the basic properties of our Fricke–MR system using test tube samples analysed using an NMR spectrometer. Investigations into the chemical stability of this detector demonstrated a sharp increase in relaxation rate immediately following irradiation due to reaction completion, in agreement with previous reports [23, 28, 91, 92]. It is likely due to reactions taking place in the organic matrix as free radical production in the water is completed within a very short time of irradiation (<<1s). Reaction completion time was longer for larger radiation doses. Reaction completion times of between 10 minutes and 2 hours have been previously reported. Our results showed that waiting for at least 12 minutes after irradiation before commencing measurements ensures that the ferrous to ferric ion reaction has fully completed even for the highest dose investigated here (15Gy). There followed a slower increase in relaxation rate over time, which again agrees with previous reports [22, 25, 27, 92, 106]. By storing the detectors in the dark container, the increase in the relaxation rate over time for unirradiated samples was reduced from 2% to 0.2% per hour. This indicates that visible light induces a reaction, as might be expected. Other investigators have shown an effect of storage temperature [25, 92, 106] and suggested storing the gels at temperatures of 5 to 10°C. We have shown that simply controlling the ambient light conditions reduces this ongoing drift to an acceptable level

for the experiments in this project which were all completed within 2.5 hours of irradiation, introducing less than 0.5% difference in results. In practice for the measurement of clinical plans, all experimental and calibration samples will be scanned simultaneously therefore chemical instability does not contribute to measurement uncertainty.

The precision in the measured R_1 and R_2 relaxation rates was less than 0.5% for unirradiated samples and for samples irradiated to known doses of 1 to 20Gy demonstrating chemical consistency throughout the batch. This provided a baseline for the subsequent experiments on shelf life, dose rate and energy dependence. In comparison, similar analysis for a polymer gel dosimeter reported a coefficient of variation of up to 5% in R_2 over the same dose range [39]. One paper described the inter-sample variation for a Fricke gel detector analysed optically [103] and reported a CV of 3% in optical density for 10 detectors both unirradiated and irradiated to 10Gy. The results presented here demonstrated a much lower CV than this previous study.

The dose response was characterised over the dose range 0 to 20Gy. The dose response was linear ($R^2 > 0.999$), which is a benefit when compared with other types of chemical detector as it simplifies detector calibration. Only two dose levels are required to characterise the dose response relationship reducing number of samples and irradiations required, further streamlining the process. A comparison between the dose response relationships of different batches showed some variation in detector sensitivity between batches, emphasising the need to calibrate each batch with known doses.

The dose response relationship was then used to convert relaxation rate to dose for every Fricke gel sample in order to estimate the uncertainty in the measured dose at each dose level. At doses used in conventional radiotherapy of 0 to 3Gy, the dose uncertainty was greater than 3%. Despite the measurement precision of only 0.5%, when converted to dose, this translated to dose uncertainties for radiation doses of less than 3Gy which exceeded the 3% set limit. However, this detector shows potential over the dose range of 3 to 20Gy where the uncertainty in the measured dose was within 3%. This suggests that this detector is particularly suitable for higher dose per fraction techniques such as stereotactic radiotherapy (SABR and SRS).

It is a limitation that the detector cannot be applied to all VMAT techniques. Currently, standard of care for many treatment sites including breast, prostate, head and neck,

gastrointestinal tract and brain lesions involves conventional fractionation radiotherapy schedules (1.5 to 3Gy per fraction). However, there has been a shift towards higher dose per fraction techniques over recent years. Stereotactic radiotherapy programmes have been implemented across the UK to treat intracranial and body sites. In addition, recent trials have investigated hypofractionated treatment schedules for two of the most common malignancies; breast and prostate cancer. The results of the FAST trial for breast cancer were recently presented at the American Society for Radiation Oncology (ASTRO) annual meeting, demonstrating no significant increase in normal tissue toxicity for a treatment schedule of 5 (weekly) treatment fractions of 5.7 Gy compared with 25 fractions of 2Gy. The PACE trial for prostate cancer is still in progress with the experimental arm involving 5 fractions of 7.27 Gy. Stereotactic and high dose techniques involve steep dose gradients often abutting critical normal tissue for which verification of the accuracy of the full 3D dose distribution is a crucial step in the commissioning. In addition, it is these techniques in particular where technology and treatment techniques are still evolving, again requiring 3D dosimetry for their validation. Therefore Fricke gel dosimetry can still perform an important function within clinical radiotherapy dosimetry.

The experiments into the precision and dose response were repeated using both T_1 and T_2 quantification to enable a comparison between the two methods. There was negligible difference in terms of dose response and measurement precision. Over the range of doses evaluated here, average dose uncertainty was identical (2.6%) for both quantification methods . This is in contrast to some previous studies [14, 111, 126] which showed worse sensitivity or detector precision for T_2 quantification. Instead, it was demonstrated here that either method may be used for the analysis of irradiated Fricke gel detectors. The choice between T_1 and T_2 quantification methods on an MRI scanner may therefore be based on practical factors such optimising the signal-to-noise ratio and reducing the scan time. T_2 protocols are more widely available on clinical scanners and in chapter 3 it was demonstrated that on ours, T_2 maps with superior SNR and image uniformity were more easily produced.

Experiments into precision and dose response were repeated for samples from a single batch irradiated at various times following manufacture to investigate the shelf life of the detector. The R_2 precision was still within 0.5% even at 3 weeks. However, the T_2 range decreases with time, which would increase the effect of T_2 variations across a

clinical scanner with time. All subsequent experiments in the thesis were carried out within 2 days of manufacture, however there would be little effect on results if this is not practically achievable.

Finally, there was negligible dependence of detector response on the radiation dose rate or energy, agreeing with previous studies [16, 90, 93, 104, 111]. Additional analysis of dose integration also showed no effect of delivering the same dose with multiple beams compared with a single shot. This is another benefit of the Fricke gelatine detector as no corrections are required for dose rate and energy.

4.5   Conclusion

This investigation demonstrated the potential of our Fricke gel detector for the measurement of radiation dose over the 3 to 20Gy range, whilst keeping the dose precision within 3%. A systematic investigation into basic characteristics for a Fricke gel detector demonstrated many benefits of this detector system. Batches of Fricke gel are simple and quick to manufacture, requiring only simple lab facilities and involve nontoxic chemicals. There was negligible difference seen in the dose response and precision of T_1 and T_2 quantification methods, therefore detector readout can be optimised based on practical factors such as measurement time and optimisation of SNR; T_2 protocols may be used. An inter sample variation of less than 0.5% indicated chemical consistency throughout a gel batch. Dose response was linear which simplifies the calibration as only two dose levels are required to characterise the dose response for each batch. Although the dose response will be calibrated for each different batch of detectors, the dose response of 6 different batches was compared to demonstrate consistency in the manufacture process only. The Fricke gel detector was also shown to be independent of both dose rate and local variations in the energy spectrum.

However, a relatively low dose response may limit this detector to high dose techniques such as SABR and this is where efforts will be concentrated for the remainder of the thesis. This detector shows sufficient promise to move onto investigations using large volume detector samples which will be described in chapter 5.

Chapter 5. Evaluation of the homogeneity and volume dependence of Fricke gel detector response

5.1   Introduction

5.1.1   Aim of this chapter

Having established basic dosimetric properties for test tube detector samples, the aim of the next set of experiments was to investigate factors which might affect the uncertainty of measurement for larger volume detectors. Experiments were all carried out using large volume Fricke gel samples analysed with a whole-body MRI scanner. In the previous chapter, it was demonstrated that in terms of the inherent precision and dose response of Fricke gel detectors there is negligible difference between T_1 and T_2 quantification methods. In chapter 3, it was demonstrated that the SNR for a T_2 CPMG pulse sequence was far superior to that for a Look Locker sequence for T_1 quantification with comparable scan time and pixel size. Therefore, T_2 quantification was used here and in all subsequent experiments.

An important requirement for accurate 3D dosimetry is a uniform dose response across the detector volume. During Fricke gel manufacture, the mixture is first heated to melt the gelatine or agarose, then allowed to cool and finally put in a refrigerator to set. It has been reported for agarose gels, that the gel sensitivity varies considerably across large volume detectors because of the difference in cooling rate between the centre and edge [89]. In general agarose detectors are heated to much higher temperatures than gelatine (for example 90°C versus 45°C) due their high melting point, therefore a lesser effect might be expected for the gelatine based detector used in this thesis. It was demonstrated that the variation in sensitivity could be reduced by selecting agarose types with a lower melting point and using a polysaccharide additive. However, this analysis was based on the dose response for small vials of detector material cooled in air and in the centre of a gel phantom, rather than investigating the uniformity of a large volume gel detector itself. A large volume unirradiated Fricke agarose detector has been previously shown to exhibit adequate uniformity [114] and in only one study was a gel detector irradiated with a uniform radiation field [92]. The aim of the first experiment in this chapter was to evaluate the uniformity of the Fricke gelatine detector both for

unirradiated detectors and samples irradiated with a homogeneous radiation dose. Different cooling methods were compared.

Similarly, detectors of different volumes might respond differently to equal doses as smaller samples cool more rapidly than large ones. This has previously been demonstrated for a commercial polymer gel detector where there was up to 35% dose error in the dose measured between test tube samples and larger volumes [40], but not investigated for Fricke gels. This is important as it would be beneficial to plot the dose response curve using samples of a much smaller volume than the experimental sample. This is only possible if detector response does not vary with sample volume. The detector response versus detector volume was investigated.

In the literature review of chapter 2, it was shown that many previous publications had explored the issue of post irradiation diffusion of ferric ions. The diffusion coefficient has been determined by several groups for both agarose and gelatine based Fricke detectors with reasonable agreement [29-32, 87, 90, 108, 109]. However, the impact of ferric ion diffusion on clinically relevant dose gradients has not been fully quantified in terms of the spatial uncertainty versus time. In this study, the blurring of a range of clinically relevant dose gradients was investigated over time in order to determine the time within which irradiated detectors should be scanned to maintain a defined and acceptable spatial accuracy.

5.1.2   Chapter overview

The aim of this set of experiments was to extend the detector characterisation to larger detector volumes. Therefore analysis was with the whole-body MRI scanner. The homogeneity of response of larger detectors was first investigated (section 5.2.1). It was intended to investigate the impact of detector cooling processes following manufacture on the homogeneity. Due to the focus for this detector on simplicity of manufacture and use, only two cooling regimes were investigated in the first instance; simply leaving the detector at room temperature versus placing it in a water bath. Should there be any evidence of inhomogeneous response in this experiments, other cooling regimes would then be investigated further. The homogeneity of T_2 across two unirradiated detectors manufactured using the two different cooling methods was assessed and compared. A further sample manufactured using the optimised cooling method was then irradiated with a uniform dose distribution across the detector volume and the homogeneity of T_2

response was assessed (section 5.2.2). For this experiment, a radiotherapy plan was designed in combination with a rectangular phantom in order to deliver as uniform a dose as possible to the detector. The homogeneity of dose delivery depends on the number, energy, direction and relative weighting of radiation beams along with the phantom cross section (i.e. depth of the detector in the phantom); these were adjusted to produce a plan which delivered a dose across the detector which was uniform to within $\pm 0.5\%$, which is as uniform as practically achievable. A tolerance of 1% will be set for detector homogeneity in line with the homogeneity of other 2D detectors used in the department.

This same radiotherapy plan was then delivered to five samples with a range of detector volumes (8ml to 500ml) and the response versus volume was established (section 5.2.3). The aim of this experiment was to establish whether small volume samples could be used to calibrate large volume samples, therefore detector volumes were selected to represent potential calibration and experimental samples. The phantom was modified with inserts to accommodate the selected samples to enable the detectors to be irradiated under identical conditions. Results were assessed in the context of baseline precision established in chapter 4. Ideally there would be no volume dependence. The dose response of Fricke gels scanned with the 3T scanner was compared with the spectrometer response by irradiating gel samples to known doses, and was also compared for several different batches (section 5.2.4), once again purely as a check of the manufacture process.

Finally, an investigation into the diffusion of ferric ions post-irradiation was carried out for a range of clinically relevant dose gradients. Analysis focussed on establishing the time within which an irradiated detector should be scanned to maintain spatial accuracy to within defined limits in terms of distance to agreement between measured and calculated dose profiles (section 5.2.5). Typical dose gradients likely in stereotactic radiotherapy were considered and this experiment was designed to irradiate a detector with dose gradients which at least as steep than those encountered in clinical practice. For this experiment, the MRI scan protocol was adjusted to increase the in-plane spatial resolution as the steep dose gradient was in this plane. This was at the expense of an increased slice thickness. Results were presented in terms of distance to agreement between measured and reference profile versus time for each dose gradient. The

imaging time to maintain DTA within 1mm and 2mm was quantified; a sub-mm discrepancy over a typical imaging session of 1 hour post irradiation would be ideal.

5.2   Methods

5.2.1   Homogeneity of unirradiated Fricke gel detectors versus cooling method

To investigate the effect of cooling on detector uniformity, a 1050ml batch of Fricke gel detector was manufactured according to the optimised recipe and manufacture process described in chapter 3. Two 500ml volume cylindrical Nalgene bottles (7.3cm diameter) (Fisher Scientific, Loughborough, UK) were filled with the Fricke gel mixture. One bottle was left at room temperature for 3 hours following manufacture before being refrigerated at 4°C. The other sample was placed in a water bath, also for 3 hours prior to refrigeration. The initial temperature of the water bath was set to be 32°C, which is the final temperature of the gel during manufacture; the water was then allowed to cool naturally. The aim was to reduce the difference in cooling rate between the centre and outside of the sample by creating an even temperature across the bottle. Both bottles were removed from the refrigerator the night before being scanned at 3T using the optimised CPMG sequence described in chapter 3. T_2 maps were created using the OsiriX plugin and the homogeneity of T_2 was evaluated and compared using profiles and region of interest analysis.

5.2.2   Homogeneity of response of a uniformly irradiated Fricke gel detector

The comparison between cooling methods demonstrated no difference between the two cooling methods and adequate detector uniformity for unirradiated samples for both (see section 5.3.1). For ease, for all subsequent experiments Fricke gel samples were left at room temperature for 3 hours following manufacture before being placed in the fridge. The next step was to quantify the homogeneity of detector response to a uniform radiation dose distribution. A batch of Fricke gel was manufactured and used to fill one 500ml bottle.

The aim of this experiment was to deliver a uniform dose of 10Gy to the sample. In order to accomplish this, a water equivalent phantom and a 4 field radiotherapy treatment plan were designed to create as uniform a dose distribution across the sample as possible. A 10cm (W) $\times$ 15cm (H) $\times$ 18cm (L) rectangular phantom was

manufactured at the workshop at Barts from WT1 water equivalent material (St. Bartholomew's Hospital, London, UK) and is shown in Figure 5.1.

Figure 5.1: Phantom used for homogeneity experiments. 2.5cm WEP blocks were added on top and beneath the phantom.

The design allowed the 500ml bottle to be positioned in the centre of the phantom, with additional inserts to accommodate smaller bottles for the subsequent experiment on detector volume. 2.5cm thick WT1 blocks were added on top and underneath the phantom to create a cube of cross sectional area 15cm × 15cm. A four field radiotherapy plan was created. Four orthogonal 10x10cm 6MV beams were applied and the isocentre (intersection point) was positioned at the centre of the bottle. The plan was normalised to deliver 10Gy to the isocentre. The dose was calculated using Eclipse TPS and the isodose distribution for the central axial plane is shown in Figure 5.2. The resulting dose within the central 6cm length of the bottle was within ± 0.5% of 10Gy.
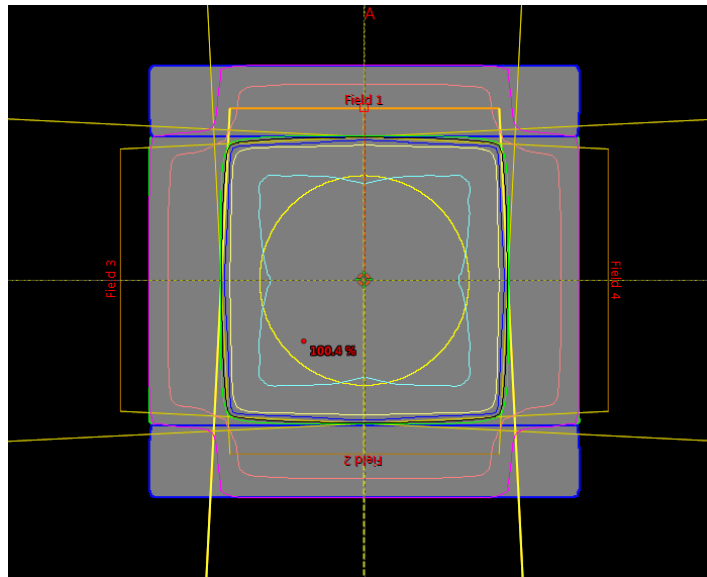
Figure 5.2: 4 field plan used for homogeneity and volume dependence experiments. The cyan isodose line is the 10Gy (100%) isodose and the yellow circle indicates the diameter of the 500ml bottle.

The Fricke gel sample was removed from the refrigerator several hours prior to irradiation and allowed to acclimatise to room temperature (air conditioned, 22°C). The sample was irradiated with the plan using the Clinac 2100iX linear accelerator. The detector was scanned immediately with the optimised CPMG sequence; scanning was complete within 40 minutes of irradiation. A T_2 map was created within OsiriX and analysis of detector uniformity was carried out via profiles and region of interest analysis.

5.2.3   Investigation into the effect of detector volume

The aim of this next experiment was to investigate the volume dependence of Fricke gel detector response in order to establish whether small volume samples may be used to calibrate large volume experimental samples. 5 bottles were investigated, the geometry and volume of which is summarised in Table 5.1. The 250 ml and 500ml bottles represented potential experimental sample geometries, and 8, 15 and 30ml samples were selected to assess suitability as calibration samples.

Table 5.1 Geometry of cylindrical bottles used for volume dependence experiment

Volume	Diameter (cm)	Height (cm)
500ml	7.3	17.0
250ml	6.1	13.3
30	3.4	6.1
15	2.5	5.8
8	2.5	4.5

The same phantom and radiotherapy plan was used as for the homogeneity experiment, again aiming to deliver 10Gy to each sample. The phantom was modified with inserts to accommodate each sample (Figure 5.3).
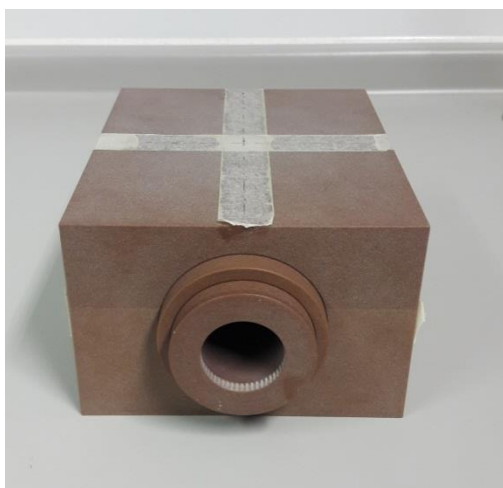
Figure 5.3: Phantom modified with inserts to accommodate other geometry bottles.

One batch of Fricke gel was manufactured and used to fill each of the bottles. 2 additional 15 ml bottles were filled and left unirradiated to allow the dose response to be assessed. All samples were removed from the refrigerator several hours before irradiation and were stored together in an air-conditioned room in the dark. All 5 samples were irradiated during the same session. The 7 samples were then scanned simultaneously within 45 minutes of irradiation with the optimised CPMG sequence. T_2

maps were created and the T_2 within regions of interest positioned at the centre of each bottle was compared.

5.2.4 Dose response analysis

The dose response was plotted using the results of the volume experiment; the unirradiated Fricke gel samples and samples irradiated to 10Gy. Additional test tube samples were prepared from this same batch, and irradiated to known doses over the range 0 to 10Gy according to the method of section 4.2. The test tube samples were readout using the spectrometer. Dose response curves for the scanner and spectrometer were compared.

5.2.5 Investigation into the effect of ferric ion diffusion

The aim of this experiment was to investigate the post-irradiation blurring of the dose distribution for a series of steep but clinically relevant dose gradients. A batch of Fricke gel was manufactured and poured into 5 small ($8 \times 5 \times 3$cm) rectangular containers. A WT1 water equivalent block (St. Bartholomew's Hospital, London, UK) was manufactured to accommodate these containers and enable them to be irradiated with a single radiation field (gantry 0°). Irradiation was carried out with a Varian Clinac iX linear accelerator (Varian Medical Systems, Palo Alto, CA, USA). Each sample was placed in turn in the WT1 water equivalent phantom with 1.5cm of build-up material added above and 5cm WT1 material beneath (Figure 5.4).

A half beam block was created by setting one jaw to 0 cm in order to create the steepest possible dose gradients. The field junction was positioned at the centre of the sample. The other three jaws were set to 10cm. Three samples were irradiated with this half-blocked field only, with the open portion receiving 20, 12.5 and 5 Gy (6MV). The remaining two samples were irradiated with this field followed a 20×20cm^2 open field to create dose differences across the junction of 20 to 10Gy and 20 to 5Gy.
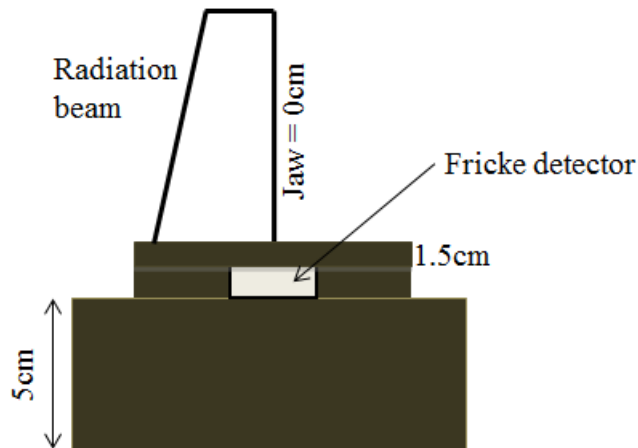
Figure 5.4: Irradiation set up for diffusion experiments. Gel container in centre of a water equivalent block, half irradiated by half beam block field.

Due to the main scanner being unavailable for this experiment, the irradiated Fricke gel samples were scanned on a 1.5T MRI scanner (Philips Achieva) in conjunction with an 8-channel receive head coil (both Philips Medical System, Best, the Netherlands). The imaging requirements for this experiment were different to all other experiments in that spatial information was needed across a steep gradient only; therefore scan uncertainty was less relevant. Therefore acquisition was designed with a high resolution was desirable in the direction of the steep dose gradient and the scan time was limited to a few minutes to allow multiple repeated scans post irradiation. As it can be assumed that the diffusion in the perpendicular direction is identical throughout the irradiated thickness, the imaging slice thickness was increased to 20mm. The sequence details are given in Table 5.2.

Table 5.2 CPMG sequence parameters for the scanner

Parameter	Value
Slice thickness (mm)	20
Pixel size (mm)	1.0×1.0 acquired, 0.6×0.6 reconstructed
TR (ms)	1800
TE (ms)	30
Echo train length	32
TE interval (ms)	30
NSA	4
Scan duration (min)	3

All five samples were positioned together in the scanner. Scans were acquired over the course of 5 hours following irradiation at approximately 10 minute intervals. T_2 maps were created and analysed within OsiriX as follows. For each scan analysed, a T_2 profile was plotted across the steep dose gradient and exported. The profile was imported into Excel and T_2 values were converted into R_2. A reference profile was also exported from Eclipse TPS, which had previously been verified by measurement with diodes and small volume ionisation chambers.

Measured R_2 was converted to dose. R_2 values at $\pm$ 2cm from the beam central axis of the measured profile (under the open and shielded part of the field and away from the steep gradient) were noted. The expected dose at these points was determined from the reference TPS profile and used to characterise the dose-response relationship. This was then used to convert R_2 values to dose for the entire measured profile.

At each time point, the maximum distance to agreement between the measured and reference profiles was determined in the steep part of the profile i.e. the largest difference in distance between the two profiles.

5.3 Results

5.3.1 Homogeneity of unirradiated Fricke gel detectors versus cooling method

The T_2 map for two unirradiated 500ml samples cooled at room temperature and in a water bath is shown in Figure 5.5. Alongside are two smaller samples (30ml bottles).
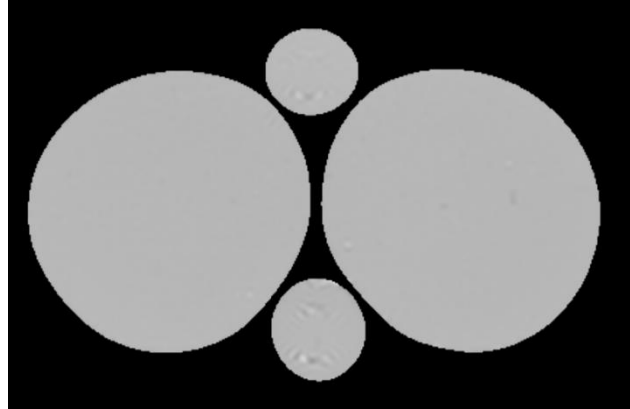
Figure 5.5: T_2 map for unirradiated Fricke gel samples (large samples). Left: cooled at room temperature, right: cooled in a water bath.

A series of horizontal and vertical profiles were plotted across the axial image of each Fricke sample. The central horizontal profile is shown as an example in Figure 5.6. There was no noticeable dip in the profiles for either cooling method and the T_2 values were all within $\pm 1\%$ of the mean. The mean and standard deviation in T_2 within a large circular region of interest ($22cm^2$, 5cm diameter) centred on the bottle was also calculated and results are presented in Table 5.3. The CV of $< 0.5\%$ indicates low variation between pixels in the region. Finally, the mean and standard deviation of 8 small ($2cm^2$) regions of interest placed in different locations across each bottle was 619.3 ± 0.9 ms (CV $= 0.2\%$) and 619.4 ± 0.9 ms (CV $= 0.2\%$). The detector homogeneity was within the set limit of 1% and therefore deemed acceptable. The homogeneity of response to a uniform dose was investigated for a sample cooled at room temperature in the next section.
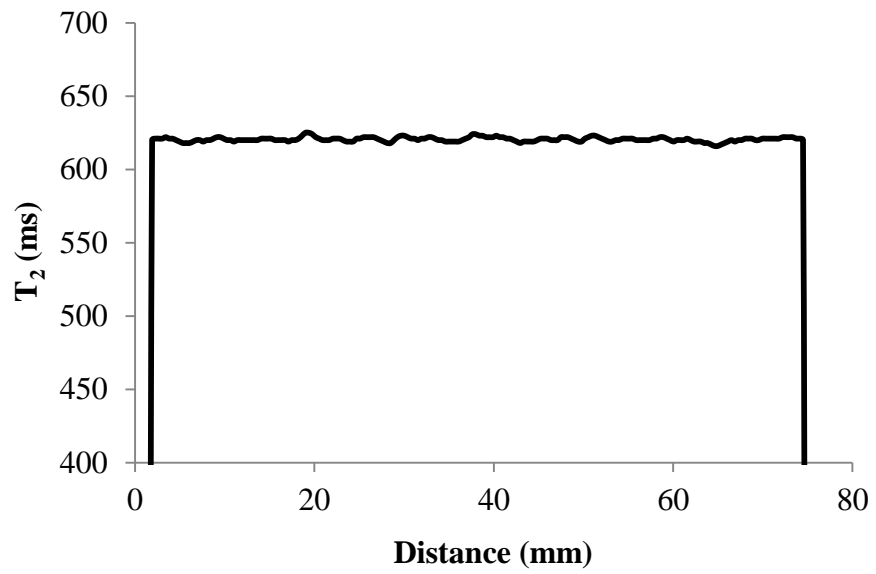
(a)
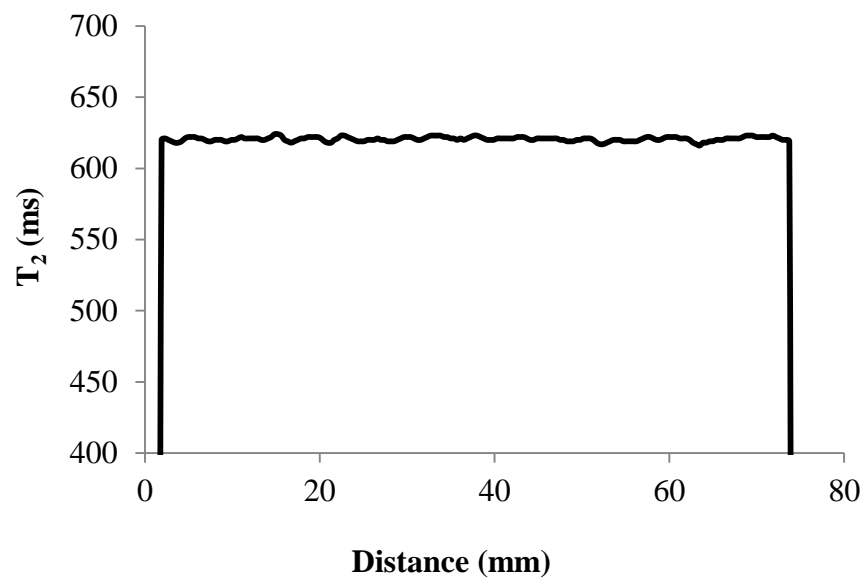
(b)

Figure 5.6: T$_2$ profiles across unirradiated samples which had been cooled at room temperature (a) and in a water bath (b).

Table 5.3 Mean and standard deviation in T_2 for unirradiated samples within a 22cm^3 ROI.

Sample	Mean T_2 (ms)	Sd (ms)	CV (%)
Room temp.	619	1.9	0.3
Water bath	620	1.7	0.3

5.3.2   Homogeneity of response of a uniformly irradiated Fricke gel detector

A representative horizontal T_2 profile across a 500ml sample from a different batch cooled at room temperature and irradiated with 10Gy is shown in Figure 5.7. Again, there was no noticeable dip or inhomogeneity in the profile and T_2 values were within 1% of the mean. The mean and standard deviation within a 22cm^2 region of interest was 459.8 ± 1.7 ms (CV = 0.4%). The mean and standard deviation in T_2 of 8 small regions of interest (2cm^2) positioned at various locations across the sample was 459.8 ±0.7 ms (CV = 0.1%).
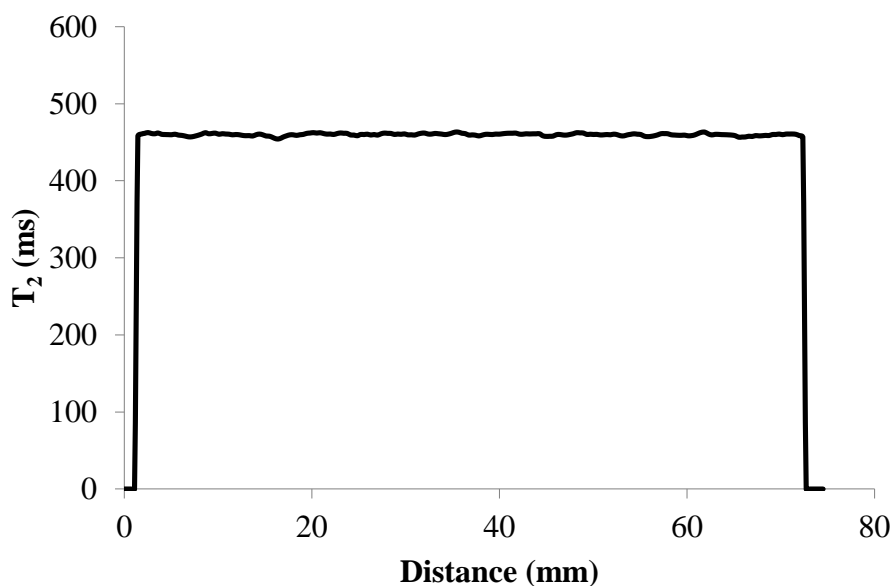
Figure 5.7: T_2 profile across sample irradiated to 10Gy which had been cooled at room temperature.

Again, the detector inhomogeneity was within the set limit of 1%. It was therefore decided to cool the gel for 3 hours at room temperature prior to refrigeration for all subsequent experiments.

5.3.3 Investigation into the effect of detector volume

A T_2 map of Fricke gel samples of different volumes irradiated to 10Gy is shown in Figure 5.8. Shown also are an additional two 15ml gel samples which were unirradiated to enable the dose response to be plotted. The mean and standard deviation in T_2 within a region of interest (1.8cm^2) centred on each bottle was calculated and compared (Table 5.4).
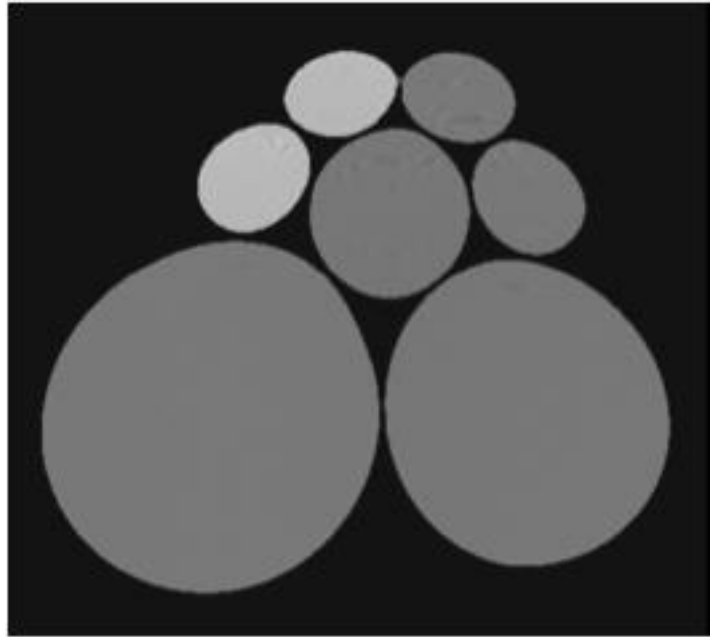
Figure 5.8: T_2 map of different volume samples irradiated to 10Gy (two additional samples unirradiated).

Table 5.4 Mean T_2 within a region of interest centred on different volume samples

Sample volume (ml)	Dose (Gy)	Mean T_2 ($\pm$ 2 s.d.) in ROI (ms)	Deviation from mean of all bottles (%)
8	10	461 ($\pm$ 8)	0.7
15	10	458 ($\pm$ 6)	-0.4
30	10	453 ($\pm$ 6)	-1.0
250	10	455 ($\pm$ 4)	0.1
500	10	460 ($\pm$ 4)	0.7

The mean T_2 was within 1% for the different volume samples and importantly there was no trend in T_2 with volume. This indicates no evidence of volume dependence for the Fricke gel detector.

5.3.4 Dose response analysis

The dose response for one batch of Fricke gel samples was compared for test tube samples analysed in the spectrometer and larger volume samples readout with 3T scanner (Figure 5.9).
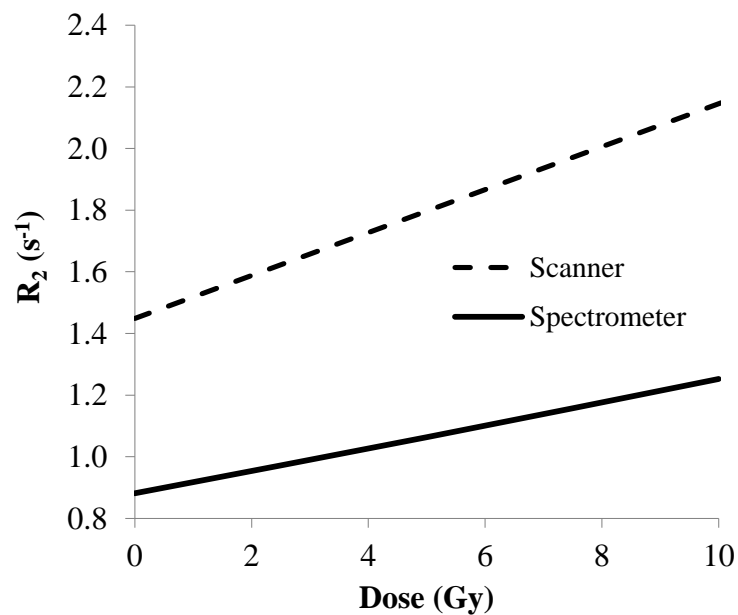
Figure 5.9: R_2 versus dose for samples analysed in the spectrometer versus the scanner.

There was a difference in dose response for samples analysed in the scanner compared with the spectrometer. Some mechanisms of T_2 relaxation, for example chemical exchange and molecular diffusion, are more efficient at higher fields, particularly due to proximity to iron, causing a reduction in the T_2 (increase in R_2). The dose response is greater with the 3T scanner, which is a benefit of this readout method.

5.3.5 Investigation into the effect of ferric ion diffusion

Figure 5.10 shows an example T_2 map is shown for the five Fricke gel samples irradiated with different dose gradients and scanned at approximately 20 minutes post irradiation.
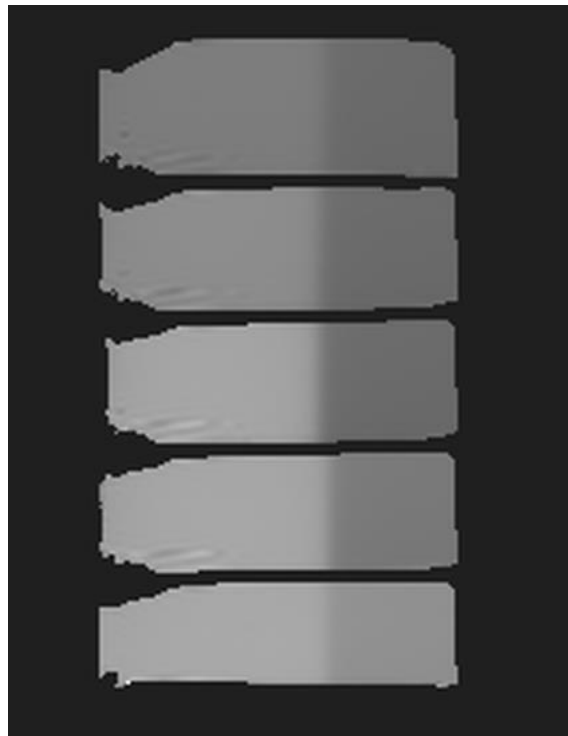
Figure 5.10: Example T_2 map for the five samples irradiated with different dose gradients, scanned at 20 minutes post-irradiation. From the top: 10 to 20Gy, 5 to 20Gy, 0 to 20Gy, 0 to 12.5Gy, 0 to 5Gy.

Profiles across the radiation beam edge were plotted for scans acquired approximately every 30 minutes up to 5 hours 20 minutes post-irradiation (a subsection are shown in Figure 5.11). There is an apparent blurring of the measured dose over this time period. This was quantified as follows. The maximum distance between the reference and measured dose profiles was calculated for each scan time (within the steep dose gradient region). This was plotted vs. time for the five different dose gradients (Figure 5.12). As expected, the DTA increases over time, and more rapidly for the steepest dose gradient of 0 to 20Gy.
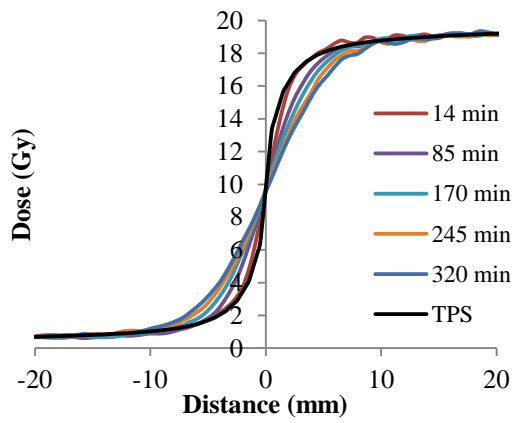
(a)
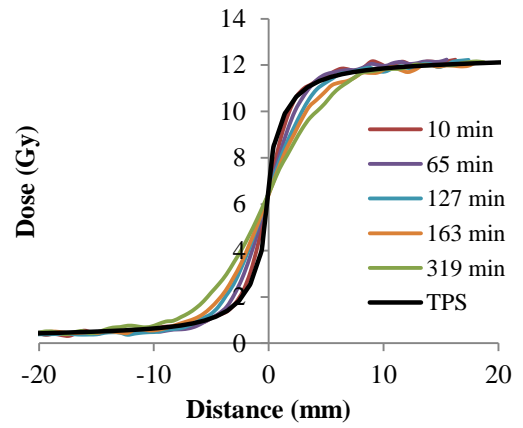
(b)
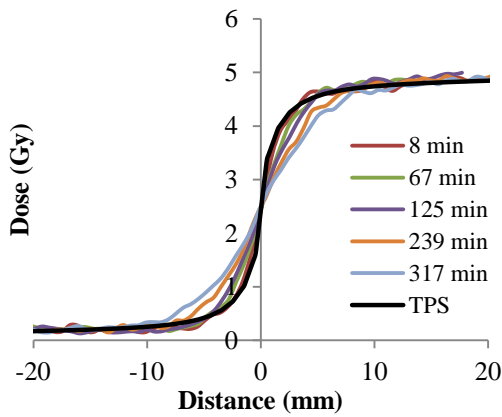
(c)
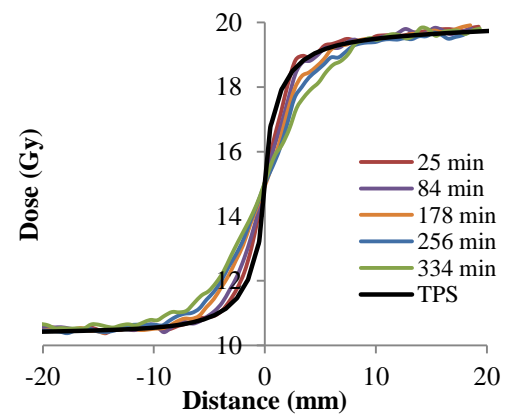
(d)
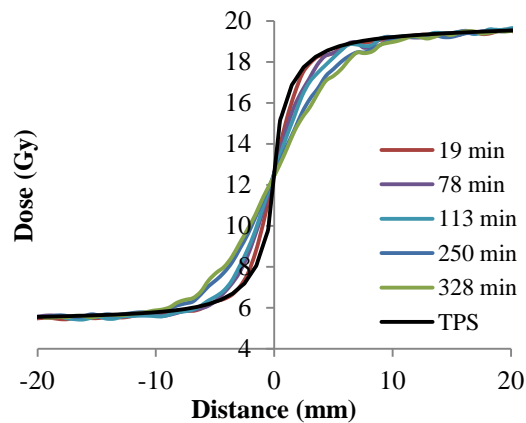
(e)

Figure 5.11: Profiles at various times post irradiation for different dose gradients: 0 to 20Gy (a), 0 to 12.5Gy (b), 0 to 5Gy (c), 10 to 20Gy (d) and 5 to 20Gy (e). TPS = treatment planning system reference profile
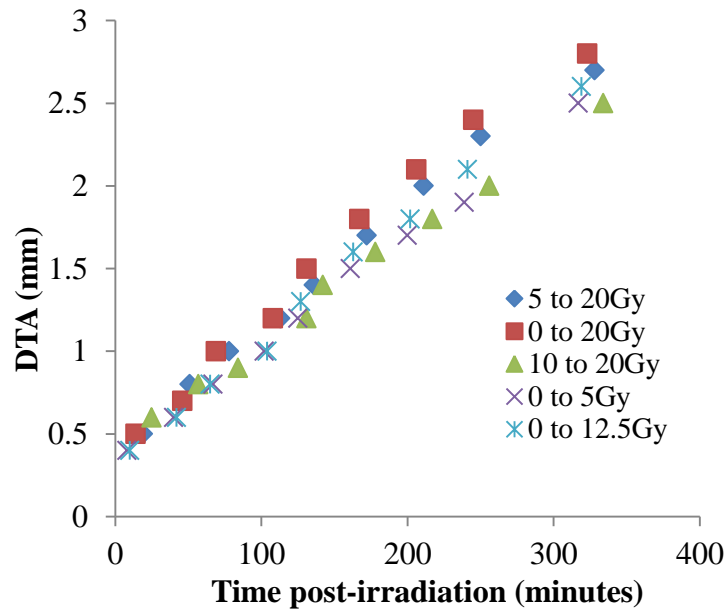
Figure 5.12: Maximum distance to agreement between measured profiles and Eclipse TPS profile versus time post irradiation. Plotted for the five different dose gradients.

The time at which DTA exceeded 1mm and 2mm is shown in Table 5.5 for each of the dose gradients. The dose gradient was quantified in terms of Gy per mm

Table 5.5 Time to exceed 1mm DTA and 2mm DTA for the various dose gradients

Irradiation details	Dose gradient within +/- 2mm of CAX (Gy mm^{-1})	Time to exceed 1mm DTA (min)	Time to exceed 2mm DTA (min)
0 to 20Gy	3.2	70	200
5 to 20Gy	2.4	80	220
0 to 12.5Gy	2.0	90	235
10 to 20Gy	1.6	90	250
0 to 5Gy	0.8	95	245

5.4 Discussion

The first experiments in this chapter focussed on the effect of gel cooling on the homogeneity of Fricke gel detectors. Other groups have shown some detector inhomogeneity for agarose based gels [89]. However, agarose must be heated to much higher temperatures than gelatine during manufacture due to a higher melting point. The same investigators evaluated other agarose types with lower melting point and a polysaccharide added, with a reduction in inhomogeneity. However, their analysis was based on the difference in dose sensitivity of small volume samples cooled rapidly in air versus slowly in the gel mixture. They did not investigate the homogeneity across large volume samples. Here, we have shown an acceptable homogeneity across unirradiated and uniformly irradiated gel detectors, requiring nothing other than some time to cool at room temperature prior to refrigeration. Once again, this is aligned with our aim to create a simple detector for use in clinical radiotherapy departments.

The volume dependence of Fricke gel detectors has not been investigated in the literature. A volume dependence might exist as smaller samples cool faster than larger ones. However, there was no volume dependence for the Fricke gel detector investigated here; T_2 values for different volume samples irradiated to the same dose agreed to within 1%. This is in contrast to a similar experiment carried out using a commercial polymer gel detector where large variation (up to 35%) in measured dose between test tube samples and larger volumes was demonstrated [40]. It has been demonstrated that it is appropriate to use small volume samples to calibrate larger volume experimental samples, which simplifies the calibration methodology.

The diffusion coefficient for ferric ions has been investigated and reported by many groups [29, 31, 32, 90, 110]. However, different conclusions have been drawn from these results. The diffusion of ferric ions has been reported to render Fricke gel dosimetry impractical due to the blurring of measured dose distribution over time following irradiation [110]. Balcom *et al* stated that 24 hours were required post irradiation for scanning therefore concluded that recovering the spatial information of the radiation dose is impractical [30]. Others concluded that gels should be scanned within an hour [22], 2 hours [29] or within 3 hours [87, 98]. Tseng *et al* concluded that for lower dose gradients $< 2 \text{Gy mm}^{-1}$ the gels could be scanned at least 2 hours post

irradiation but for higher gradients greater than 4Gy mm^{-1} spatial information is lost after only half an hour [33].

It has been suggested that the impact of diffusion is dependent on the irradiated dose gradient [86]. One report in the literature attempted to quantify the blurring versus time by comparing measured with reference dose distribution via a gamma test [87]. This was carried out for various dose gradients up to 0 to 40Gy with gamma criteria of 3% dose difference and 2mm DTA. All analysis points passed these gamma criteria apart from the 0 to 40Gy gradient scanned at 3.25 hours post-irradiation, however the reference profile was measured with a large ion chamber which itself blurred out the steep gradient used for comparison.

The aim of the diffusion experiment in this chapter was to systematically quantify the time within which gels should be scanned to maintain agreement between a measured distribution and reference distribution to within 1mm and 2mm for five steep dose gradients. These gradients were selected to be clinically relevant for high dose techniques e.g. stereotactic radiotherapy and are far greater than dose gradients achieved for conventional radiotherapy doses. These distance to agreement criteria were also selected to be clinically relevant. Our results indicate that, for the most relevant dose gradients (0 to 12.5 Gy and smaller), a 1mm DTA can be maintained if the irradiated Fricke gels are scanned within 1 hour 30 minutes. This is sufficient time to complete an MR scan of gel phantoms, however, immediate access to the MR scanner would be required. If a 2mm DTA is deemed acceptable, Fricke gels can be scanned up to 3 hours 20 minutes for even the steepest dose gradients. For subsequent experiments in this dissertation, scanning was always completed within 45 minutes of irradiation, reducing this uncertainty due to diffusion to less than 1mm.

These results were for a gelatine based Fricke gel. The composition can be modified to reduce the diffusion, for example adding a chelating agent such as xylenol orange [31]. However, this has the disadvantage of reducing the MR sensitivity as previously demonstrated.

5.5   Conclusion

Investigations into the basic properties of large volume Fricke gel detector samples were carried out. There was no evidence of any detector inhomogeneity for this detector

composition, as long as the detector samples were cooled at room temperature for a short time post manufacture. There was also no evidence of any volume dependence which means that small volume (e.g. 15ml) samples can be used to calibrate larger volume experimental samples, requiring less gel material to be manufactured. A blurring of steep dose gradients post-irradiation was seen, which agrees with previous literature. This was quantified in terms of the spatial disagreement versus time for different dose gradients.

All the basic detector characterisation measurements have now been completed, according to the plan of section 2.5. If immediate access to an MR scanner can be arranged, the Fricke gel composition used in this work offers a simple option for 3D chemical dosimetry. For our purposes, it is possible to arrange scan time immediately following irradiation. The next chapter focuses on applying this optimised Fricke gel detector to increasingly complex treatment plans.

Chapter 6. Clinical applications

6.1 Introduction

6.1.1 Aim of this chapter

The experiments of chapters 4 and 5 systematically tested the basic properties of the Fricke gel detector in very simple radiation fields. The manufacture process has been optimised, including methods for cooling, producing gel samples of up to 500ml which uniformly respond to irradiation. There was no evidence of any clinically relevant dependence of detector signal on radiation dose rate, energy, fractionation or detector volume. The inter-sample variation was shown to be adequate over a dose range of 0 to 20Gy although when converted to dose, percentage uncertainties became unacceptable for radiation doses of less than 3Gy due to a relatively low dose response. Chemical effects were evident whereby detector signal was shown to vary with time post-irradiation, initially rapidly due to reaction completion then more slowly due to ambient conditions. It was also confirmed that the ferric ions diffuse throughout the gelatine matrix following irradiation leading to a blurring of the measured dose distribution. However, adequate and well quantified dose and spatial precision was achieved if the Fricke gels are scanned at least 12 minutes but within 90 minutes of irradiation and if they are stored in the dark.

With basic characterisation measurements completed by irradiating samples with simple radiation fields and known radiation doses, the aim of the final experiments described in this chapter was to apply the Fricke gel detector to a variety of complex radiotherapy plans. Firstly, a multiple field plan was created still with reasonably simple geometry. The plan was designed with an intentional modulation within the dose distribution to evaluate how well the detector can measure moderate variations in dose. The Fricke gel detector was then used to measure two high dose per fraction stereotactic VMAT plans.

High dose radiotherapy plans were selected due to the larger dose uncertainties demonstrated in chapter 4 at doses of less than 3Gy. This ties in with an increased interest nationally in high dose stereotactic radiotherapy and locally with an aim to start delivering stereotactic treatments on Varian linacs. Therefore, the focus in this chapter was on investigating the ability of the Fricke gel-MR system to measure these treatments. This was accomplished by irradiating Fricke gel detectors with selected

treatment plans and comparing measured dose distributions in multiple planes with doses predicted by the treatment planning system.

Dose distributions were compared quantitatively using the gamma evaluation method as described in section 1.2.7. In this project, gamma maps were calculated for each pair of measured and TPS calculated dose planes for relevant dose difference and distance to agreement tolerances. Tolerances were selected based on those currently used at St. Bartholomew's Hospital for VMAT and stereotactic dosimetry as well as published recommendations.

Gamma maps with tolerance values of 3%, 2mm and 5%, 1mm were calculated reflecting gamma tolerances currently set at St. Bartholomew's Hospital for VMAT and stereotactic plans respectively. These are similar to those reported for IMRT, VMAT and stereotactic national dosimetry audits [74, 75, 128]. For example, a UK VMAT dose audit reported gamma pass rates for EBT3 GafChromic film comparison with TPS of 93% with a tolerance of 2%, 2mm. A similar UK IMRT dosimetry audit reported 95% gamma pass rate for simple IMRT plans calculated with dose difference and DTA tolerances of 3%, 3mm. These also reflect uncertainties estimated by the IAEA as being achievable in their report on uncertainty in radiotherapy [70]. In terms of the accuracy of the TPS, within a single distribution, different limits are set: 3% in high dose, low gradient regions, 10% or 2mm in high dose, high gradient regions and 4% in low dose, low gradient regions. For end-to-end testing in a geometric phantom, this report recommends limits on the deviation between calculation and measurement of 3 to 10% and spatial uncertainty of 2mm. For stereotactic treatments with very steep dose gradients, it is common to have tighter distance but larger dosimetric criteria [73].

6.1.2 Chapter overview

Firstly, the procedure for the manufacture, irradiation, calibration and scanning of Fricke gels optimised throughout the previous chapters of this thesis and used for these final experiments is summarised in section 6.2.1. A commercial software program was used for the comparison of measured and calculated dose planes in this chapter, in particular the creation of gamma maps; this is described in section 6.2.2.

Three different radiotherapy plans were evaluated and are described in section 6.2.3 to 6.2.5. The plans were selected to gradually increase complexity of delivery. The first

was a simple conformal plan designed specifically to introduce some additional complexity compared with the characterisation measurements, before moving onto complex VMAT plans. Two VMAT plans were then selected in order to introduce different clinical challenges. The first was a single brain metastasis with no directly abutting organs at risk, therefore a more straightforward clinical scenario. The final plan evaluated was a much more complicated situation involving a spine lesion, directly abutting the spinal cord with conflicting dose constraints between treating the PTV versus sparing the cord. A steep dose fall off was required to achieve these constraints, and therefore this plan represents one of the most challenging clinical situations.

For all three plans, delivered and calculated doses were compared with the gamma tolerances of 5%, 1mm and 3%, 2mm as outlined in the previous section with an aim of achieving a 95% pass rate according to common radiotherapy practice. In addition, measurements were made with other radiation detectors for comparison; using the PinPoint ionisation chamber, radiochromic film and ArcCheck diode array. Results and analysis are presented in section 6.3. A summary of the dose response of several Fricke gel batches was included in section 6.3.1. A summary of the results and analysis for the three radiotherapy plans, including gamma analysis is presented in sections 6.3.2 to 6.3.4.

6.2   Methods

6.2.1   Manufacture, irradiation and scanning

For each experiment, one batch of Fricke gels was manufactured using the optimised procedure previously described in section 3.3. One 500ml experimental sample and two 250ml calibration samples were produced. Whilst it was previously shown that smaller samples could be used for calibration, 250ml were selected for this experiment to improve the shimming for the MR scans. Shimming a larger region results in a more homogeneous magnetic field across the field of view. The Fricke gel samples were cooled at room temperature for 3 hours before being placed in the refrigerator. Irradiation was always carried out within 3 days of gel manufacture. In each case, the gel samples were removed from the refrigerator the night before irradiation and stored in an air conditioned, dark room in order to acclimatise to room temperature (22±2°C). Gels were then irradiated first thing in the morning, during a single irradiation session.

The Fricke gels were irradiated using either a Clinac 2100iX or a Varian Truebeam linac. Gel samples were positioned in the water equivalent phantom described in chapter 5 with the set up shown in Figure 6.1. Marks were carefully drawn on the bottle to indicate the top (gantry 0°) and sides (gantry 90° and 270°) in order to align the experimental sample within the phantom using the room lasers. The phantom was positioned so that the centre of the bottle was at the linac isocentre. Further details of the radiotherapy plans are given below, in sections 6.2.3 – 6.2.5. One calibration sample was irradiated with the uniform radiotherapy plan described in section 5.2.2 (either 10 or 15Gy depending on the maximum planned dose) and the other was left unirradiated.

Scanning was carried out on the MR scanner at least 15 minutes post-irradiation and for all experiments scans were completed within 45 minutes. For each experiment, the three Fricke gel samples (experimental plus two calibration samples) were positioned in the head coil and scanned simultaneously. The MR lasers were used to align the experimental phantom within the scanner. A selection of transverse, coronal and sagittal planes were acquired using the optimised CPMG sequence described in section 3.6.6.
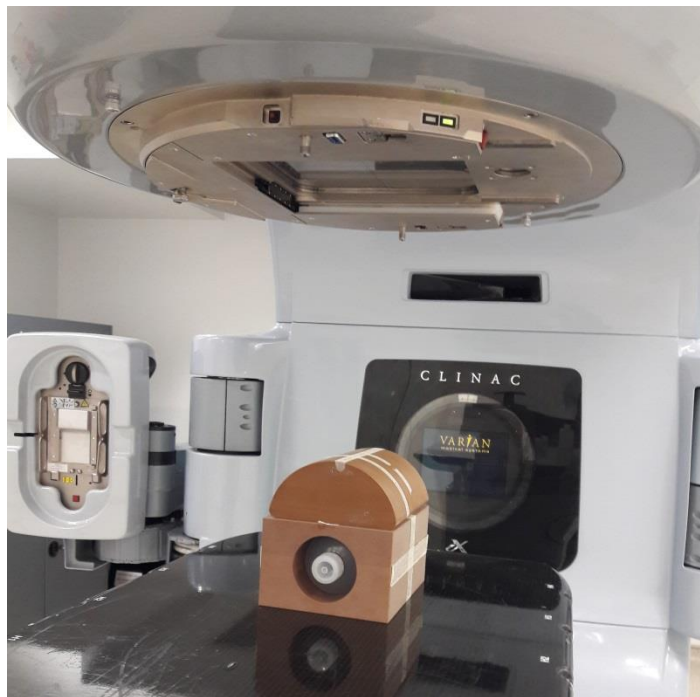
Figure 6.1: Irradiation set up for plan measurements. Dome only used for the VMAT plans, not the simple multiple field plan.

6.2.2 Analysis of dose maps

T_2 maps were first created in OsiriX using the T_2 plugin described in section 3.6. A region of interest was positioned at the centre of each of the calibration samples and the mean T_2 was noted. The dose response was plotted and the linear regression equation was used to convert the T_2 maps to dose maps. The dose maps were then exported in DICOM format.

To create the calculated dose planes for comparison, the radiotherapy plan for each experiment was applied to CT scans of the Fricke gel phantom in Eclipse treatment planning system (v11 for the simple plan, v13 for the VMAT plans). The 3D dose distribution on this phantom was calculated using the AAA photon dose algorithm. 2D dose planes corresponding to the scan planes of the irradiated Fricke gel phantom were exported as DICOM files.

Comparison between measured and TPS calculated dose planes was carried out with OmniPro I'mRT (IBA Dosimetry, Bartlett, TN, USA). This is a commercial software package already in use within the radiotherapy department for the comparison of 2D dose planes measured with the MatriXX ion chamber array and the TPS. Within OmniPro I'mRT, measured and calculated dose planes were compared using profiles and gamma evaluation as described in section 1.2.7. An example gamma map is shown in Figure 6.2.

In OmniPro I'mRT, the gamma map is plotted with a scale (also shown in Figure 6.2) such that pixels with a gamma of greater than 1 and therefore failing the gamma test are displayed in red. Pixels with a gamma of less than 1 and therefore passing are displayed in sliding scale from white to blue. The software also allows the pass rate to be calculated within a defined region of interest i.e. the percentage of measurement points within the ROI which have a gamma index of <1.
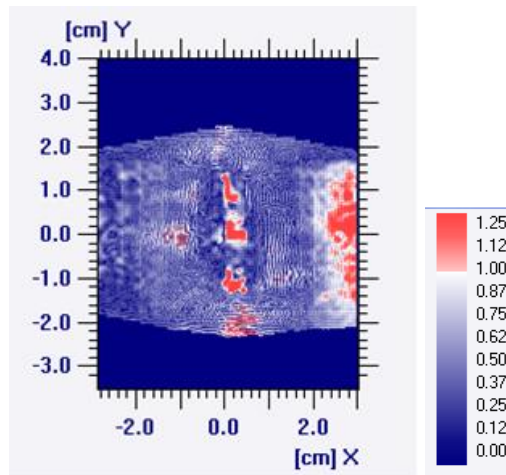
Figure 6.2: Example gamma map.

6.2.3   Simple multiple field radiotherapy plan

A simple radiotherapy plan was designed. Three open rectangular 6MV beams (i.e. no MLC shielding) were applied from anterior and lateral opposed directions. The isocentre was positioned at the centre of the phantom. Relative beam weightings and wedges were adjusted to optimise the dose distribution in terms of homogeneity. The prescription dose was set to 7Gy (100% isodose). An additional low weighted anterior field was added and MLC was introduced as in Figure 6.3. This produced an intentional dip in the horizontal dose profile through the isocentre to approximately 6Gy. The aim was to evaluate how well the Fricke gel models a moderate variation in the dose distribution. The dose distribution calculated by the treatment planning system is also shown in Figure 6.3 for the central transverse plane along with the horizontal dose profile across the centre of the Fricke sample.
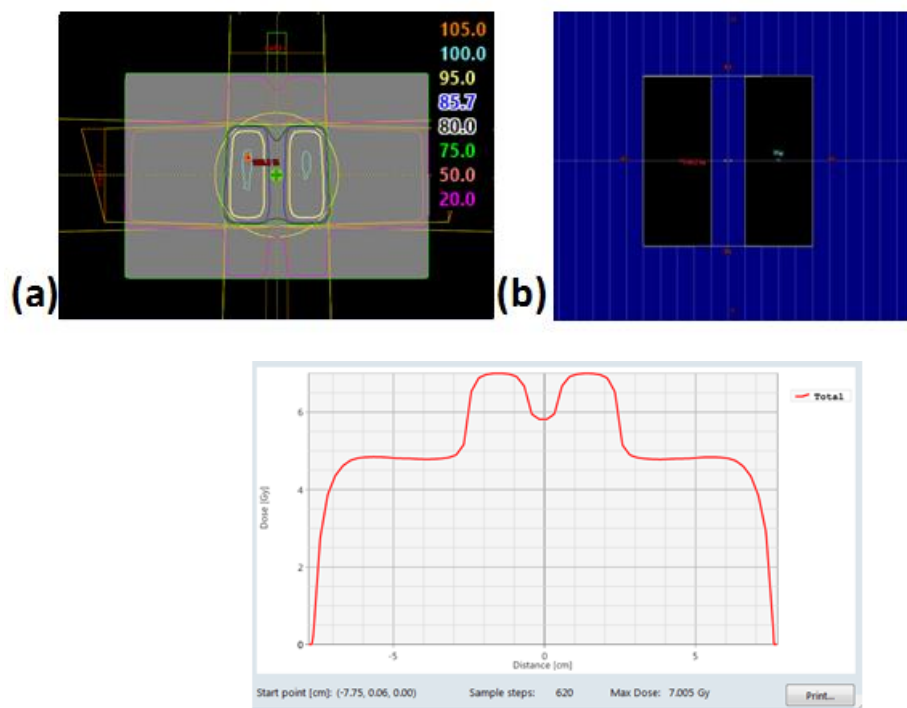
Figure 6.3: Dose distribution and field arrangement on phantom (a), MLC shape for low weighted anterior field (b) and horizontal dose profile across centre of the Fricke gel sample (c).

6.2.4 VMAT plan for a brain metastasis

A previously treated high dose VMAT plan was selected. The patient was prescribed radiotherapy for a solitary brain metastasis. The prescription dose was 30Gy in 5 fractions to the 100% isodose. Two full 360° 6MV arcs were applied, the set dose rate was 600MU min^{-1} and the collimator angles were set to 30° and 330° for the clockwise and anticlockwise arcs. Within the inverse planning module, dose constraints and relative weightings were set to fulfil planning aims; in this case only for the PTV as any relevant organs at risk were sufficiently far away. Instead dummy planning structures in the form of shells around the PTV were used to create a steep dose fall off outside the PTV. Constraints were added aiming to deliver a dose to the PTV within 95% and 107% of the prescription dose. Once optimised, the dose distribution was calculated and the plan was evaluated. This was repeated until all dosimetric requirements had been achieved. The dose distributions across central transverse and coronal planes are shown in Figure 6.4 along with a horizontal dose profile through the centre of the PTV which illustrates the steep dose gradient.

The accuracy of delivery of this plan had previously been verified using the ArcCheck diode array as described in section 1.2.6 which is an array of 1386 diode detectors arranged in a cylindrical phantom used for the VMAT patient specific QC at St. Bartholomew's Hospital. Measured ArcCheck dose distributions are compared with the TPS using dedicated software based on the gamma test method. For this plan, 94% of measured detector points passed a gamma test with tolerances of 5% and 2mm and this was deemed acceptable.

Figure 6.4: Transverse (a) and coronal (b) planes through the PTV showing the dose distribution. The horizontal dose profile across the PTV is displayed for the transverse plane (a).

The predicted dose distribution was then calculated on CT images of the Fricke gel phantom and is shown in Figure 6.5. Dose planes were exported in DICOM format for comparison with measurements. The steepest dose gradient in this plan was 1Gy mm^{-1} which means at least 1.5 hours are available to scan the detector after irradiation to maintain a spatial uncertainty to within 1mm according to the previous experiment on ferric ion diffusion.
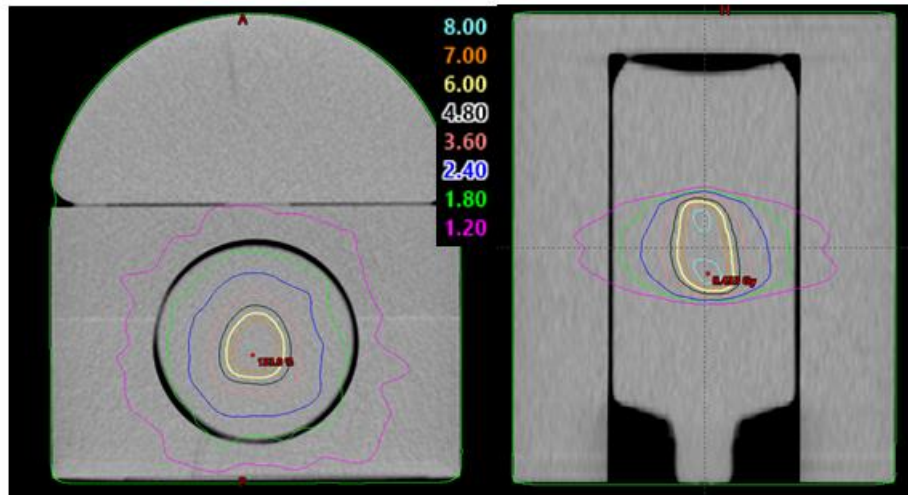
Figure 6.5: Dose distribution for the RapidArc plan re-calculated on a CT scan of the Fricke gel phantom.

6.2.5   Stereotactic VMAT SABR spine audit plan

Finally, a spinal plan used for a dosimetric audit by the national Radiotherapy Trials QA team (RTTQA) was used in the third clinical experiment. This had two benefits; firstly, the PTV is wrapped around the spinal cord therefore the additional challenge of a concave dose distribution was introduced. Secondly, this delivery was comprehensively measured by other dosimetric devices ahead of the dose audit.

The prescription dose was 27Gy/3# to the 100% isodose. Three full 360° arcs were applied (one clockwise and two counter clockwise) with collimator angles of 30°, 330° and 10°. Planning aims were set according to normal departmental protocols and SABR consortium guidelines [129], as follows. 95% of the PTV should receive at least the prescription dose and the maximum PTV dose (0.1cc) should be no more than 140% of the prescription dose (=37.8Gy). Dose limits for the spinal cord PRV (cord+2mm) were: maximum dose <22 Gy, 18Gy <0.35cc and 12Gy<1.2cc. Dose constraints and relative weightings were set in the optimiser aiming to fulfil these planning targets. Once again, the optimiser was run, followed by a full dose calculation and plan evaluation, repeating optimisation until final dose distribution met the plan aims. Figure 6.6 shows the plan and dose distribution calculated on the RTTQA audit phantom.
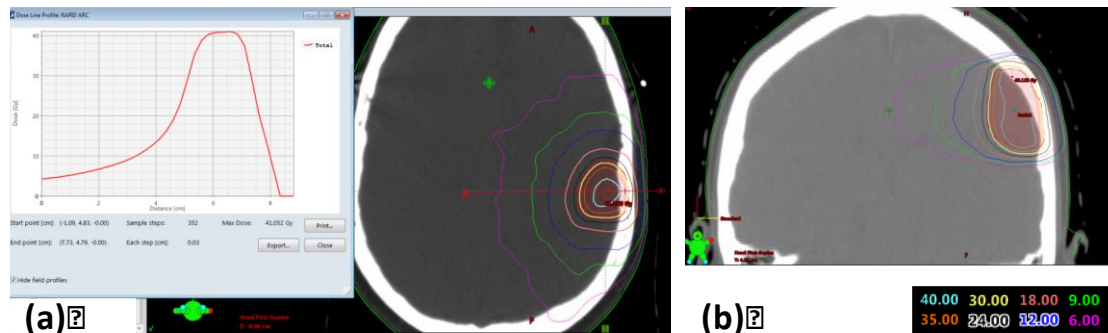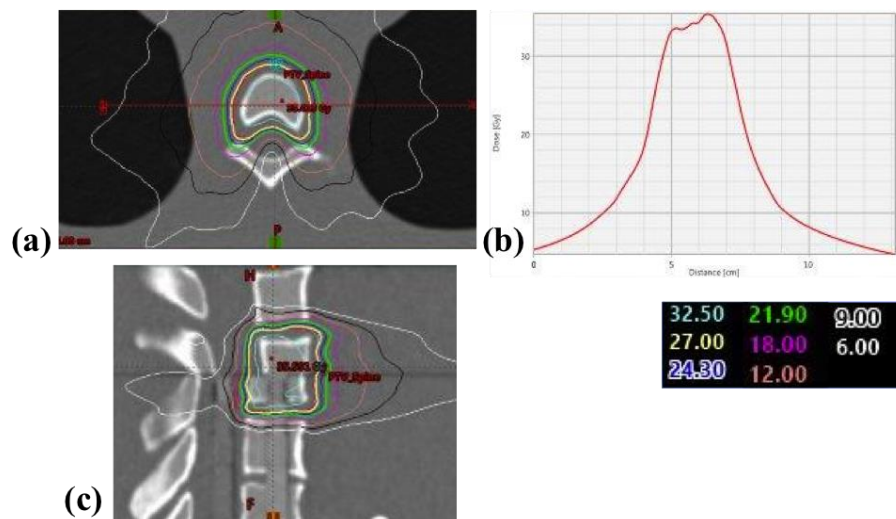
Figure 6.6: Transverse (a) and coronal (c) planes through the PTV showing the dose distribution. The dose profile through the centre of the transverse plane is shown in (b).

Prior to the RTTQA audit, measurements were carried out by radiotherapy physicists to verify the accuracy of dose distribution using existing dosimetry techniques. The dose was recalculated on a water equivalent phantom which can accommodate a $0.015cm^3$ PinPoint ionisation chamber (PTW, Freiberg, Germany) and piece of EBT3 GafChromic film (Ashland, Bridgewater, NJ, USA). A dose measurement with the PinPoint ionisation chamber was carried out at a point in the centre of the PTV. A single sagittal dose plane was measured using the radiochromic film and compared to the corresponding plane exported from the TPS using gamma analysis within SNC patient software (Sun Nuclear Corporation, Melbourne, FL). These methods are used routinely at St. Bartholomew's Hospital for the verification of the accuracy of stereotactic treatments delivered with the Cyberknife treatment machine. The PinPoint chamber measurement gave a measured dose of +3.2% when compared with the treatment planning system, which was deemed acceptable. The comparison between film distribution and TPS yielded excellent results as shown in Figure 6.7. A gamma test was carried out in relative dose mode with tolerances of 5% and 1mm and >97% of pixels passed.
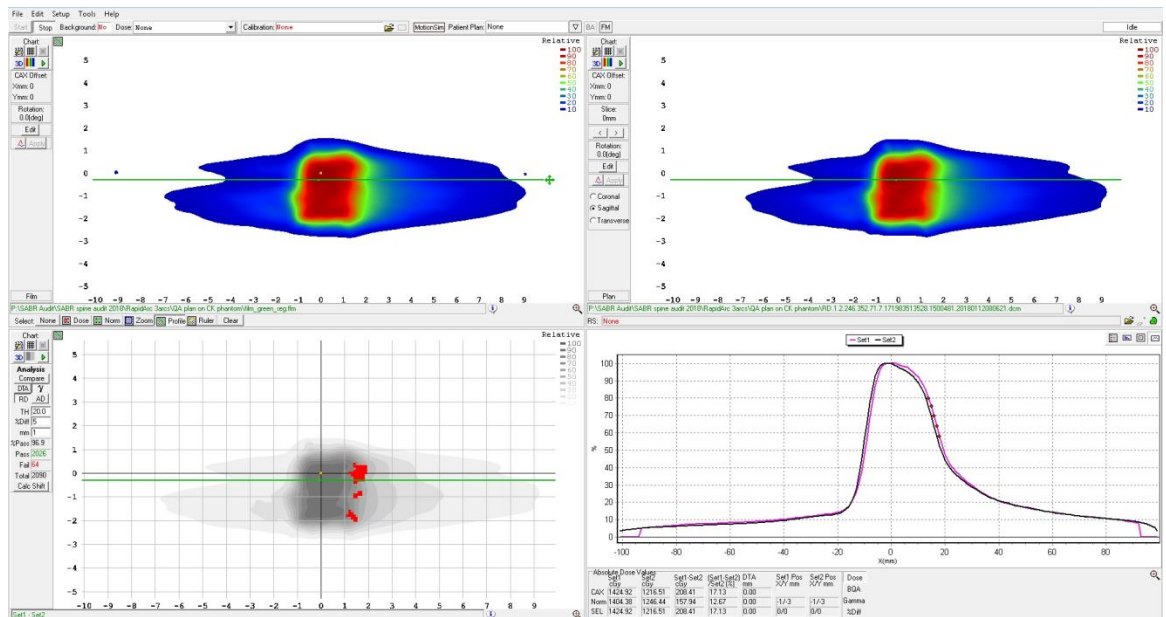
Figure 6.7: Comparison between radiochromic film plane (top left) and TPS (top right) showing excellent agreement between measurement and TPS. Gamma test results (bottom left) were carried out for 5% 1mm, relative dose mode, both normalised to point of dose maximum on film.

The dose distribution was recalculated on the CT scan of the Fricke gel phantom (Figure 6.8). This was then exported to enable comparison with the measured dose distribution. The calibration sample was irradiated to 15Gy in this instance as the maximum planned dose was 12Gy. The steepest dose gradient in this plan was again 1Gy mm^{-1} which again allows at least 1.5 hours post irradiation to scan the phantom.
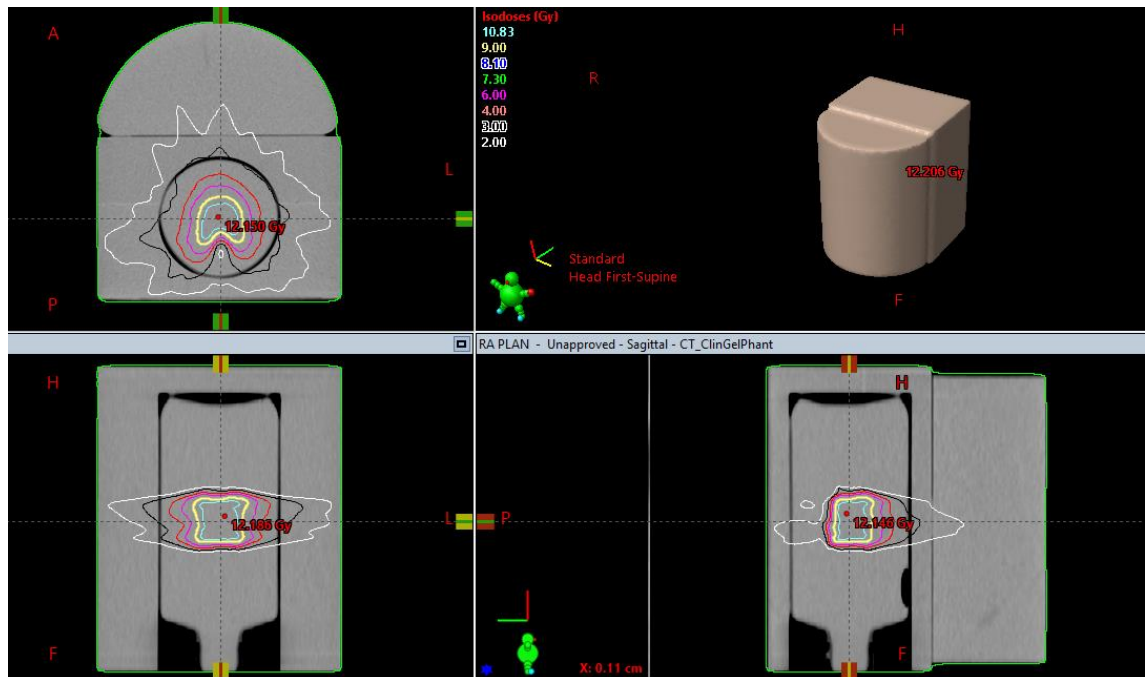
Figure 6.8: Dose distribution for the SABR spine plan calculated on a CT scan of the Fricke gel phantom.

6.3   Results

6.3.1   Calibration.

A summary of the dose response curves for five Fricke gel batches used in the homogeneity experiments described in chapter 5 and clinical plan experiments in this chapter is shown in Figure 6.9. Again, this was carried out as a check of the consistency of the detector manufacture process as dose response will be characterised for each batch and measurement session. The slope for all 5 batches was within the range 0.0631- 0.0697 s^{-1} Gy^{-1} (mean 0.0660 s^{-1} Gy^{-1}, CV 4%) and the intercepts were all within the range 1.241-1.449 s^{-1} (mean 1.342 s^{-1}, CV 7.5%). These results indicate consistency of manufacture process but again, it also highlights the need to quantify the dose response for each gel batch.
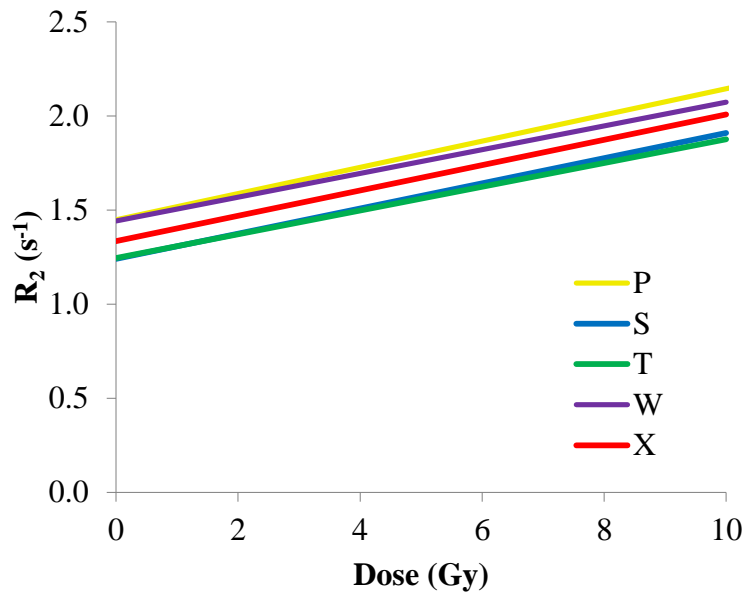
Figure 6.9: Comparison between dose response curves for different Fricke gel batches.

6.3.2 Simple multiple field radiotherapy plan

The T_2 map for the central transverse plane of the simple radiotherapy plan is shown in Figure 6.10a. The T_2 within a region of interest positioned on each of the calibration bottles was noted and used to calculate the linear regression equation which characterises the dose response. This was then applied to the T_2 map to create a dose map.

Visual inspection of the measured and calculated dose profiles indicated good agreement in the shape albeit with a small systematic dose offset of 4%. The measured dose distribution was higher than the calculated. This agrees with the PinPoint chamber dose, which was 2% high compared with TPS dose, to within measurement uncertainty. OmniPro I'mRT analysis for this plan is shown in Figure 6.10b-d with this offset applied. The measured dose distribution is shown along with the distribution calculated by the treatment planning system.
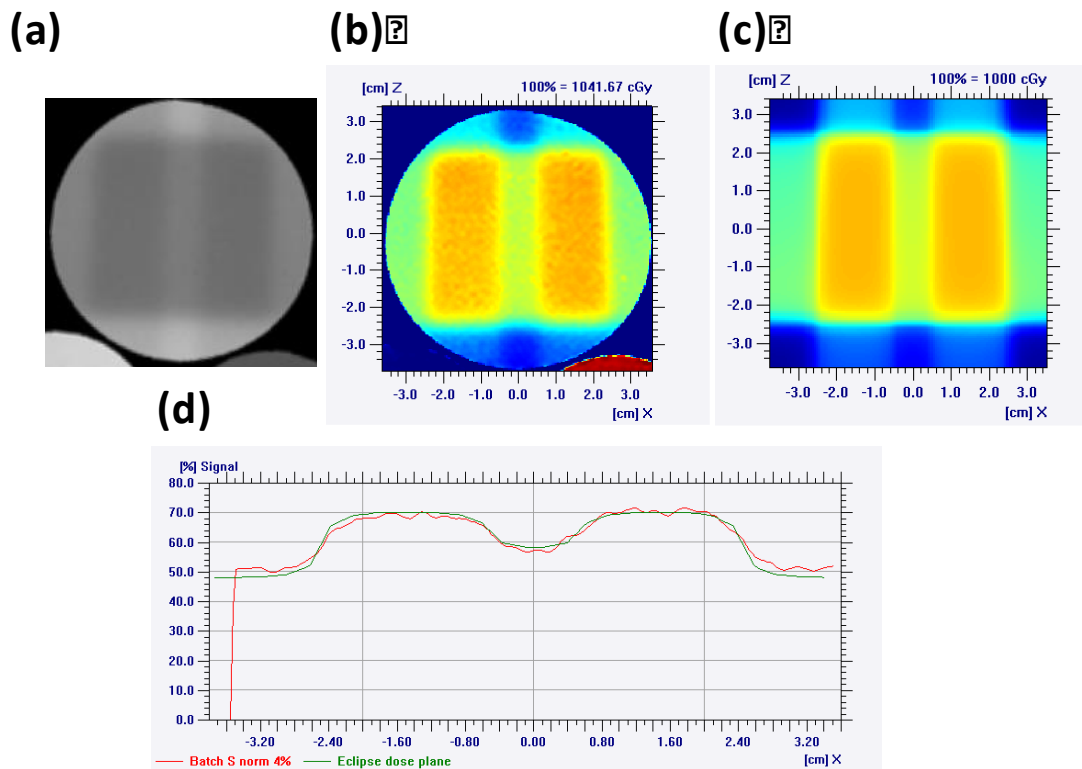
Figure 6.10: T$_2$ map of the transverse plane through the centre of the simple radiotherapy plan (a) and corresponding I'mRT software analysis; (b) measured dose plane, (c) TPS calculated dose plane and (d) example profile through measured and calculated dose plane.

Gamma maps were calculated for the selected dose difference and distance to agreement tolerances again with this offset applied. These are shown in Figure 6.11. Visually, only small regions of red on the gamma maps are seen, indicating good agreement between measured and TPS dose distributions. To quantify this in terms of percentage pass rates, a region of interest was positioned entirely within the bottle (to exclude high gamma values outside of the bottle) and the percentage of pixels passing the gamma test criteria were calculated (Table 6.1). The pass rate was greater than the set target of 95% for gamma tolerances of 3%, 2mm, and for 5%, 1mm.
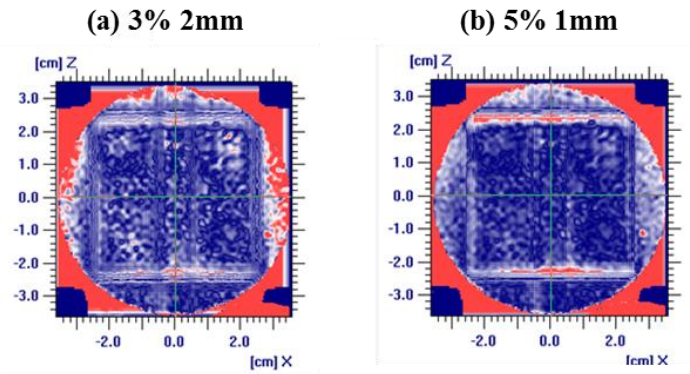
Figure 6.11: Gamma maps for different dose difference and DTA tolerances: (a) 3% 2mm and (b) 5% 1mm.

Table 6.1: Gamma test results for the multiple field plan

Gamma settings	Transverse pass rate (%)
3% 2mm	98.5
5% 1mm	96.2

6.3.3   VMAT plan for a brain metastasis

Transverse and coronal T_2 maps through the centre of the first high dose RapidArc plan are shown in Figure 6.12a. Measured and calculated dose maps for the central transverse and coronal planes are shown along with a horizontal profile plotted through the centre of each plane in Figure 6.12b-d. In this case, visual inspection between measured and calculated dose profiles indicated no systematic dose offset and therefore no re-scaling necessary. Gamma maps for the selected dose difference and DTA tolerances are shown for the central transverse plane and coronal plane in Figure 6.13. Gamma pass rates are shown in Table 6.2. More than 95% of pixels passed for both sets of tolerances for the transverse plane and the coronal plane. A region of gamma failures are seen on the coronal plane towards the edge of the Fricke gel sample, however this is away from the high dose, steep gradient region and gamma pass rates met the 95% set tolerance.

Table 6.2: Gamma test results for the stereotactic brain plan

Gamma settings	Transverse pass rate (%)	Coronal pass rate (%)
3% 2mm	99.8	96.6
5% 1mm	99.8	99.1

6.3.4 Stereotactic VMAT SABR spine audit plan

Transverse and coronal T_2 maps through the centre of the high dose SABR spine VMAT plan are shown in Figure 6.14a. The was again a small offset of 4% between measured and calculated doses, with measured dose greater than the TPS. This agreed with the PinPoint ionisation chamber dose measurement, which was +3% compared with the TPS. I'mRT software analysis is shown for the central transverse, coronal and sagittal planes (Figure 6.14b-d) with this re-normalisation applied. Visual inspection indicates good agreement between the measured and calculated dose profiles in terms of the shape especially in the steep fall of region. To quantify this, gamma maps for the selected dose difference and DTA tolerances were calculated, shown for the central transverse, coronal and sagittal planes in Figure 6.15.

The percentage of pixels passing the gamma test tolerances within a region of interest is shown in Table 6.3. Larger regions of failure are seen for this plan, although these are away from the central high dose, high gradient region. Pass percentages were still greater than 95% for the transverse plane. For the coronal and sagittal planes, pass rates were below 95%. For the 5%, 1mm tolerance typically used for stereotactic dosimetry, the pass rate in the sagittal plane was 93% but for the coronal plane was only 84%. This can be seen in the gamma maps, where large regions of gamma failures are seen laterally towards the edge of the bottle.

Table 6.3: Gamma test results for the SABR spine plan

Gamma settings	Transverse pass rate (%)	Coronal pass rate (%)	Sagittal pass rate (%)
3% 2mm	98.7	85.5	92.1
5% 1mm	98.4	84	92.9
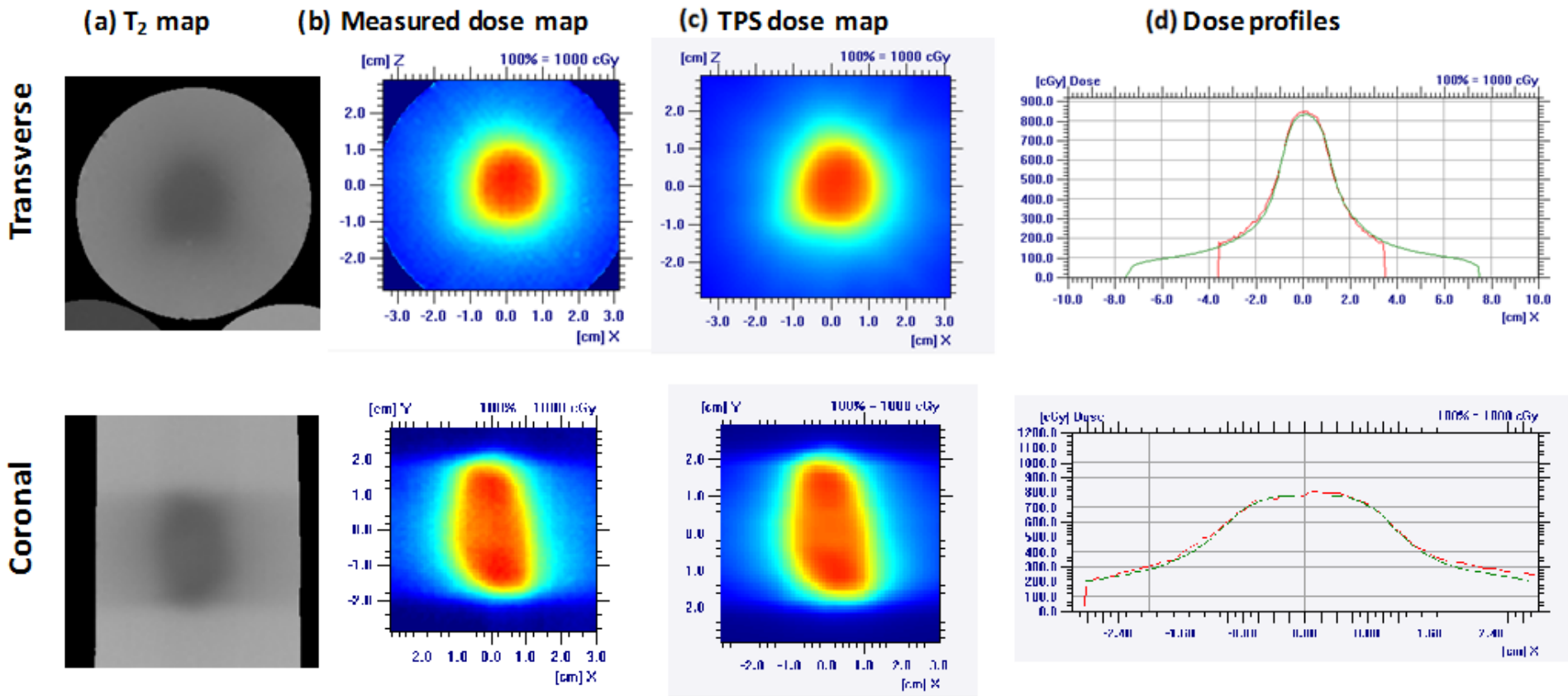
Figure 6.12: T$_2$ maps (a) and I'mRT software analysis of the brain VMAT plan for the central transverse and coronal planes. (b) measured dose map (c) TPS calculated dose map and (d) example measured (red) and calculated (green) dose profiles.
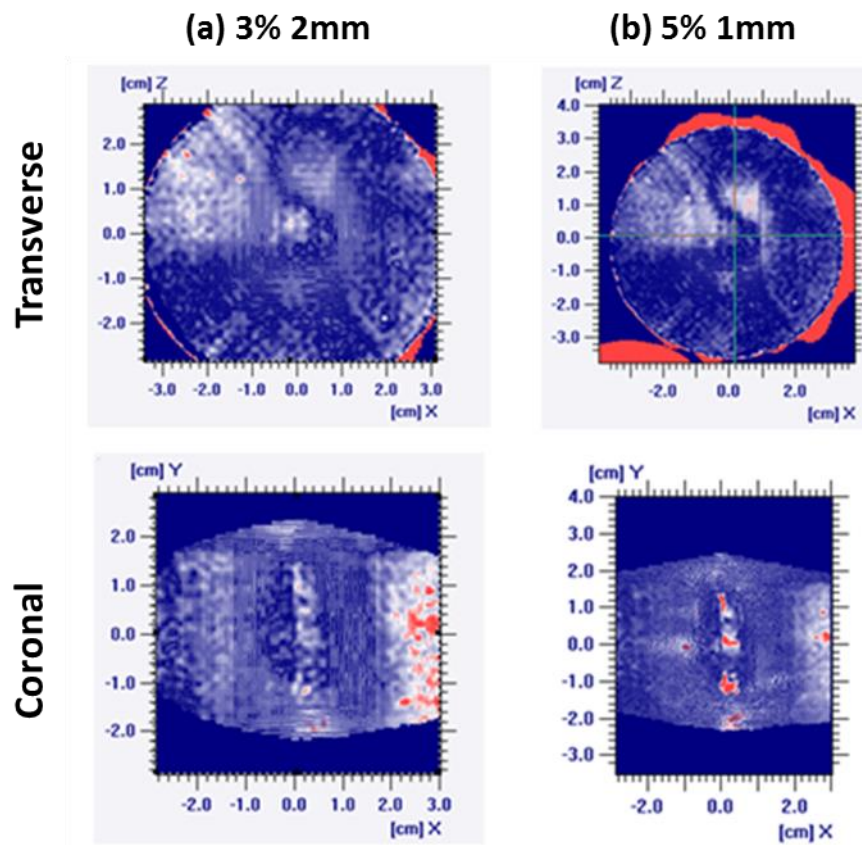
Figure 6.13: I'mRT software analysis for the central transverse and central coronal planes of the brain VMAT plan: (a) 3% 2mm and (b) 5% 1mm.
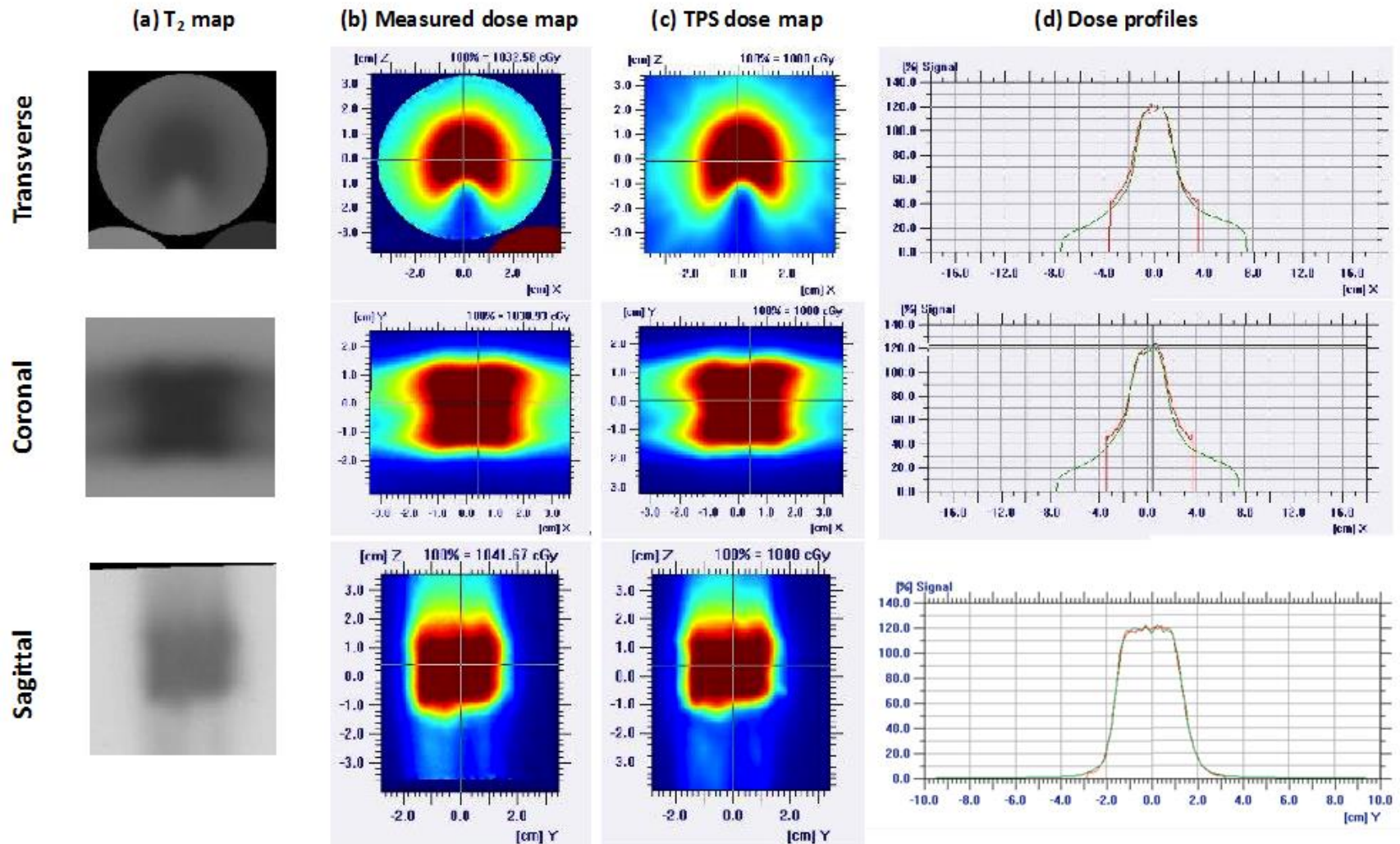
Figure 6.14: T$_2$ maps (a) and I'mRT software analysis of the SABR spine radiotherapy plan for the central transverse, coronal and sagittal planes (b) measured dose map (c) TPS calculated dose map and (d) example measured (red) and calculated (green) dose profile.
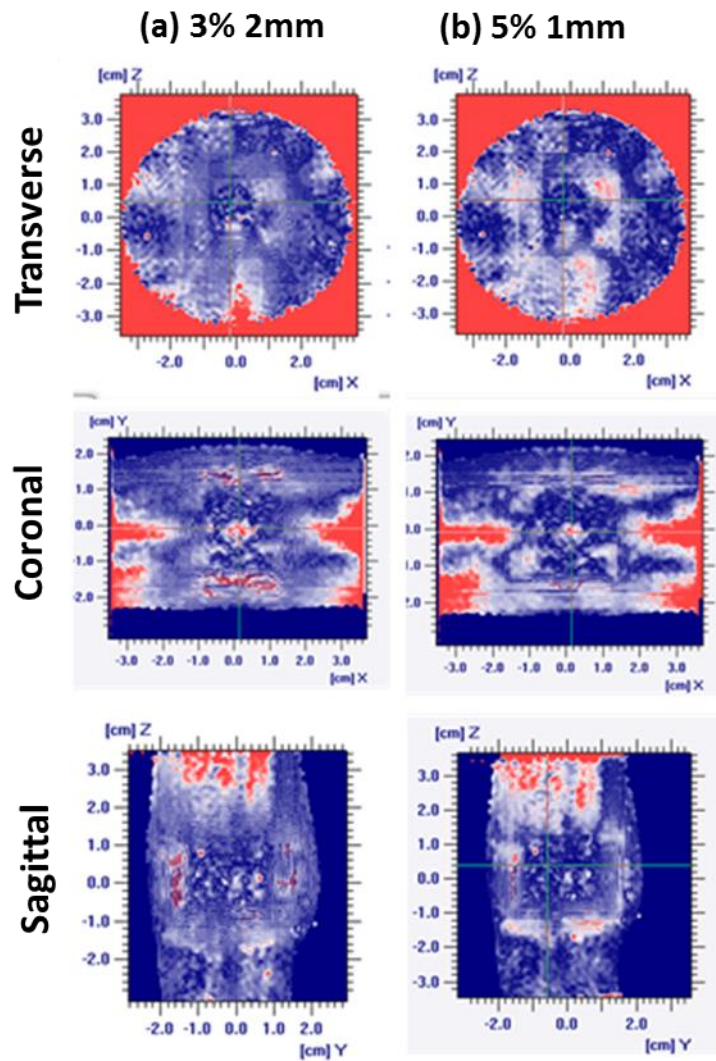
Figure 6.15: I'mRT software analysis for the SABR spine plan showing gamma test results for tolerances of (a) 3%2mm and (b) 5% 1mm.

6.4   Discussion

The focus of the final experiments described in this chapter was the irradiation of Fricke gel detectors with more complex radiotherapy plans in order to develop and assess the process by which they perform the function of a 3D commissioning measurement of VMAT dose calculation and delivery. The dosimetric characterisation of these detectors had been carried out in previous chapters in line with methods used to characterise other radiation dosimeters in the literature. The aim for a dosimetric uncertainty of less than 3% was achieved, and is similar to other 2D detectors used for VMAT dosimetry summarised in table 2.1

Fricke gel detectors were irradiated with a series of treatment plans and 2D dose maps in coronal, transverse and sagittal planes were created. These dose maps were compared against corresponding calculated dose distributions exported from the treatment planning system. In order to quantitatively compare distributions, gamma evaluation was carried out using a commercial software package, OmniPro I'mRT.

Gamma evaluation is widely used in radiotherapy for the comparison of measured and calculated IMRT and VMAT dose distributions. Tolerances are set for acceptable values of dose difference and distance to agreement. To put the results obtained in this project into context, publications describing national dosimetry audits i.e. inter-comparison between different radiotherapy centres were reviewed. In the UK, national IMRT, VMAT and SABR (Lung) dose audits have been carried out [74, 75, 84, 128].

Budgell *et al* published details of a UK wide IMRT dose audit [128]. Less complex (non head and neck) IMRT plans were reported to all achieve greater than 95% pass rates for gamma tolerances of 3%, 3mm with evaluation within the 20% isodose. More complex head and neck plans were reported to achieve greater than 95% pass rates only for tolerances of 4%, 4mm. For VMAT, another UK dose audit was carried out using a 2D PTW array and EBT3 radiochromic film. Here, the mean pass rate for H&N plans with tolerances of 2%, 2mm was 93.4% [75]. Seravalli *et al* reported on a Dutch dose audit including stereotactic treatments for which 5%, 1mm gamma tolerances were set and achieved greater than 98% pass rate, carried out using a EBT3 film and an 2D array [73].

In this investigation, gamma maps were calculated for selected gamma tolerances. 3%, 2mm was selected to represent tolerances commonly used in radiotherapy for the verification of conventional dose VMAT plans and 5%, 1mm appropriate for stereotactic radiotherapy. A typical aim adopted in the radiotherapy literature is for 95% of measured points to pass a gamma test.

For the first experiment in this chapter, a multiple field plan was created. The aim was to increase the complexity of radiation distribution beyond the previous characterisation experiments but still deliver the plan with conventional, non-modulated fields. An MLC field was added with central shielding to create an intentional dip in the dose distribution in order to investigate how well the Fricke gel measured this. The measured dose distribution for the central transverse plane was compared with the distribution predicted by the treatment planning system. Visual inspection indicated good agreement in the shape of the radiation distribution for this plan but a systematic offset in the dose of 4%. This dose agreed with the PinPoint ion chamber dose to within measurement uncertainty. If the measured dose distribution was re-normalised by 4%, then gamma test results achieved the set 95% pass rate.

The second plan evaluated was a previously treated clinical VMAT plan for a brain metastasis. This was a reasonably straightforward clinical plan with no directly abutting critical structures. The dosimetric accuracy had been verified previously with the ArcCheck diode array. Visual inspection of the dose distributions in terms of dose profiles indicated that no re-scaling was necessary for this plan. Again, the pass rate was greater than 95% for both sets of gamma tolerances and both image planes analysed. Visual inspection of the gamma maps and profiles showed a region of disagreement laterally in a reasonably low dose region (<40% of maximum dose) however this was away from the very steep dose gradient.

The third experiment used a stereotactic spine test plan that was being used for a joint SABR consortium/ RTTQA UK dose audit. This was evaluated as part of the commissioning process for a Truebeam machine not clinical yet for stereotactic radiotherapy and represented a more complex clinical scenario. The PTV directly abutted the spinal cord, therefore introducing conflicting dose constraints into the planning process. The dosimetric accuracy of this plan was evaluated using the standard departmental procedure with a PinPoint ionisation chamber and a radiochromic film for

a single sagittal plane. The PinPoint chamber measured dose was 3% greater than that predicted by the TPS and film results showed acceptable agreement in the shape of the distribution in the sagittal plane. In terms of the Fricke gel results, visual inspection of the dose distributions and dose profiles indicated good agreement in the shape of the distribution in the three measured planes. However once again a dose offset was required; the Fricke gel measured dose was higher than that predicted by the TPS by approximately 4%. This agreed with the PinPoint measured dose to within 1%.

For the transverse plane, gamma test results once again, achieved a pass rate of more than 95% for both sets of gamma tolerances. For the 5%, 1mm tolerance commonly used in stereotactic radiotherapy dosimetry, the pass rate was 93% for the sagittal plane but only 84% for the coronal plane with areas of disagreement seen laterally on the gamma map. The cause of this disagreement is unclear. It is not seen in the transverse plane which also measures the dose laterally; gamma results for this dose map were within acceptable limits. Also, it seems unlikely to be due incorrect dose calibration. A steeper dose gradient and wider dose range is present in the anterior-posterior direction but in this direction measured and calculated doses agree very well as shown by profiles for the sagittal plane in Figure 6.14.

This should be further investigated. The beam model within the treatment planning system may possibly need to be further optimised very slightly for stereotactic radiotherapy with this treatment machine, although even with these discrepancies, this dose disagreement is only seen in a low dose region, away from any steep dose gradients. In this plan, the critical structure is the spinal cord, therefore the verification of the fall-off in the dose in the anterior-posterior direction is of particular interest. The measured and delivered dose profiles showed excellent agreement in this direction, confirming the dose accuracy to the cord. According to our clinical practice, this plan would be accepted for treatment.

6.5   Conclusion

In this final set of experiments, a comparison was carried out between dose distributions measured with the optimised Fricke gel-MR system and those predicted by the treatment planning system for three radiotherapy plans. For two of the plans evaluated, a small re-normalisation was required to the measured dose distribution (4%). This dose

deviation did agree with the dose measured by the PinPoint ionisation chamber to within measurement uncertainties and is likely to be a combination of detector uncertainty and a small actual deviation in dose calculation and delivered dose. PinPoint dose measurements were within local clinically acceptable tolerances. Combining chemical dosimetry with a more precise ionisation chamber dose measurement is a common approach [7, 74].

Measured and calculated distributions were then compared quantitatively using the gamma evaluation method for a range of dose difference and DTA tolerances. Standard departmental tolerances of 3%, 2mm for VMAT and 5%, 1mm for the stereotactic plans were used. For a simple multiple field plan and a high dose VMAT plan for a brain metastasis a 95% pass rate was achieved for the standard departmental tolerances. For the spine stereotactic VMAT plan, these criteria were also achieved for the transverse plane. Gamma pass rates were less than 95% for the central sagittal and coronal planes of this plan. However, the gamma maps indicated that disagreement was mostly in regions away from the high dose region and in practice this plan would be accepted for treatment. Measured and calculated doses agreed well in steep dose gradients, critically across the junction between the PTV and the spine.

These experiments described in this chapter demonstrated the ability of the Fricke gel detector to measure complex VMAT, stereotactic dose distributions. In this study, multiple 2D planes were analysed so full 3D dosimetry has not yet been demonstrated. However, the ability to acquire multiple 2D dose maps for one detector irradiation is already an advantage over existing 2D measurement devices such as radiochromic film. For 2D films one irradiation is required per measured dose plane. The extension to 3D will be the subject of future work. For now, this device has been demonstrated to be a useful tool for future work to commission and test the accuracy of new high dose radiotherapy treatment techniques, equipment and software.

Chapter 7. Discussion

7.1   Review of project background

This project was prompted by the difficulties encountered by physicists within a clinical radiotherapy department when trying to commission and verify the accuracy of modern radiotherapy techniques. Over recent years, radiotherapy technology has evolved and now offers the ability to focus dose distributions precisely to the tumour volume in 3D. This is accomplished in various ways; with IMRT by moving MLC leaves across the beam during treatment and with VMAT by rotating the linac gantry around the patient and simultaneously varying the dose rate, gantry speed and MLC shape. These advances in technology allow radiation doses to tumour volumes to be boosted and doses to neighbouring organs at risk to be spared, however alongside this is an increased risk of errors in dose calculation and delivery. MLC shapes and leaf motions are complex and it has been shown that sub-mm errors in MLC position can cause dose errors of several percent. Since the start of this project, there has also been an increased interest in stereotactic radiotherapy whereby large (ablative) radiation doses are delivered with precise spatial accuracy to tumours over only a few treatment fractions. Typical doses in conventional radiotherapy are in the region of 2-3Gy per fraction whereas stereotactic doses may be up to 20Gy in a single fraction. Stereotactic radiosurgery describes the treatment of intracranial tumours whereas stereotactic ablative body radiotherapy describes the delivery of high dose treatments to other body sites. At St. Bartholomew's Hospital, stereotactic radiotherapy is currently delivered using a Cyberknife unit which is a linear accelerator mounted on a robotic arm. The treatment is delivered with many tens of small radiation beams directed from a wide range of non-coplanar beam angles which sum together to create the 3D dose distribution. It is proposed to start delivering stereotactic treatments using Varian Truebeam linacs which offer benefits for certain tumour sites in terms of a faster treatment delivery and pre-treatment soft tissue imaging via on board cone beam CT (CBCT). Stereotactic treatments involve very high dose gradients and therefore there are stringent requirements on spatial accuracy in particular.

It is no longer appropriate to check the accuracy of the treatment planning system for specific patient plans by hand calculation only as the dose to one point is not reflective of the whole 3D distribution. The steep dose gradients introduce additional dosimetric

challenges. It was proposed that with the introduction of IMRT and VMAT, another type of verification was required. Rather than checking each individual step in the radiotherapy process, it was proposed that the overall accuracy of calculation and delivery would be verified and this would be carried out by a measurement of delivered dose in a phantom. This measurement is compared with the dose predicted by the treatment planning system. For the commissioning of new radiotherapy technology, software and techniques, a high resolution dose measurement is recommended.

Dose measurements in radiotherapy are currently carried out using a variety of point, 2D and pseudo-3D detector arrays which offer benefits for particular applications but none of which allow a high resolution measurement of the entire 3D dose volume. The most commonly used systems are radiochromic film, the EPID and pseudo-3D arrays such as the ArcCheck and Delta 4. Radiochromic film offers a high resolution measurement but only for a single selected 2D plane. The EPID is emerging as a useful tool in terms of transit dosimetry whereby the exit dose transmitted through the patient is measured and reconstructed to predict the dose actually delivered to the patient. The EPID may also be used for pre-treatment QC of patient plans, however, this method does not provide a direct measurement of the delivered dose within the patient (or a phantom) and software tools are required to predict the dose distribution within the patient which must itself be rigorously checked. In addition, the EPID, rotates with the linac gantry and therefore will not pick up errors in gantry speed or motion. 3D detector arrays are commonly used for patient specific QC and are useful for this task as they give an immediate, fast measurement of dose. However, the devices available such as the ArcCheck and Delta4 involve large detector spacing (>0.5cm) and the detectors are not positioned throughout the entire 3D volume. None of the detectors currently available offer a high resolution measurement required for the commissioning stage of new techniques and technology.

3D chemical dosimetry was proposed as a solution to this dosimetric challenge. Chemical detectors undergo a measurable change when irradiated for example a colour change or a rise in temperature. When mixed into a solid matrix, such as gelatine or agarose, the chemicals are fixed and the 3D delivered dose distribution may be mapped. Fricke gel dosimetry was proposed in the early 1980's, based on the radiation induced oxidation of ferrous to ferric ions. This causes a change in the optical density which may be quantified using optical-CT scanners, but also a change in the R_1 and R_2

relaxation rates enabling 3D dose mapping using MRI scanners. Benefits of Fricke gel detectors include a simple chemistry, low toxicity chemicals, linear dose response and no dose rate or energy dependence. However, concerns about the post irradiation diffusion of ferric ions causing a blurring of the measured dose distribution turned the focus towards polymer gel dosimetry. Polymer gel detectors involve a monomer such as acrylamide which polymerises on irradiation forming long polymer chains. Again, this affects the optical density and R_2 relaxation rate therefore readout may be with optical CT or MRI. Polymer gel detectors involve more toxic chemicals, and require oxygen to be removed from the mixture. This was either achieved by bubbling nitrogen through the mixture (requiring a fume hood) or adding oxygen scavengers. Either way, the manufacture of these detectors is less straightforward than Fricke gel dosimetry. Alternate radiochromic detectors were proposed, such as Presage, also involved more complicated manufacture procedures and at the inception of this project were not commercially available.

Despite the potential benefits of 3D chemical dosimetry and many years of research, focussing on detector composition, manufacture methods and readout methodology, 3D chemical dosimetry is still not implemented widely in clinical radiotherapy. This was true at the start of this project and is still the case now. A recently published text book on 3D dosimetry for modern radiotherapy highlighted again the need for a 3D detector and the potential for 3D chemical dosimetry to fulfil this function but acknowledged that chemical detectors still hadn't been widely adopted beyond research groups. This has been attributed to complicated manufacture procedure in polymer gel detectors and Presage, difficult access to scanners but importantly a lack of confidence in their dosimetric performance. It is crucial to establish the dosimetric performance for any radiation detector prior to applying to them to complex dose distributions. For any detector, a systematic characterisation of detector properties such as dose rate, energy dependence, and homogeneity is required.

The aim of this project was to evaluate a 3D chemical detector for use within a clinical radiotherapy department. In the absence of commercial options, it was decided to manufacture this detector in-house, therefore Fricke gel dosimetry was selected as it is based on non-toxic chemicals and may be manufactured in a simple laboratory with basic equipment. Optical-CT and MRI have been used for the readout of Fricke gel detectors. MRI was selected for this study, again due to the availability of a clinical

MRI scanner within the hospital. It has been suggested that optical-CT could be more suitable as accessing an MRI scanner can be difficult due to clinical workload, however, access was possible within the department at St. Bartholomew's Hospital. In contrast, an optical-CT scanner would have to be purchased, or built, and commissioned specifically for chemical dosimetry. There are still only limited commercial options, the most common being a Vista cone-beam CT scanner which has reported issues with stray light. Manufacturing an optical-CT scanner within the department at St. Bartholomew's Hospital was considered beyond limits of available time and expertise.

With the detector-imaging system selected, the focus of the project was then on the systematic evaluation of detector performance before application to complex radiotherapy scenarios, which is summarised in the following sections.

7.2   Project overview

7.2.1   Chapter 2: Literature review

The first step in this project was to outline and quantify at the outset the requirements of a detector for the 3D measurement of VMAT radiotherapy techniques. This was accomplished with reference to international guidance documents [9, 10, 70]. Basic requirements were that this detector should offer a 3D measurement, and that this measurement should be a direct dose measurement in a phantom throughout the high dose region. Ideally, it would be possible to position a detector in a variety of geometric and anthropomorphic phantoms. Limits for dosimetric and spatial uncertainty of 3% and 1mm were set based on analysis of reference reports on the accuracy practically achievable in radiotherapy and the measurement uncertainty achieved in non 3D detectors. It is also acknowledged in radiotherapy that there are inherent compromises with radiation dosimetry, i.e. increasing detector resolution is done at the expense of dosimetric uncertainty [76]. The detectors currently in use in clinical radiotherapy do not meet these requirements as none offer a true 3D measurement.

A literature review was then carried out to search for existing evidence on detector performance for Fricke gel dosimetry. The entire manufacture, irradiation and readout process was analysed to identify all possible sources of measurement uncertainty. These included inter-sample variation, chemical and spatial instability, dose rate, energy and volume dependence and inhomogeneity of detector response. The literature was then

reviewed to identify papers which described any of these factors for Fricke gel detectors.

Whilst many papers investigated specific properties for particular compositions, there was a lack of systematic approach to their commissioning. There was no or very little evidence for some factors including inter-sample variation, volume dependence and detector homogeneity. Other factors were shown to depend on the detector composition and constituent chemicals, such as dose response, homogeneity, chemical and spatial stability which highlighted the importance of performing this systematic characterisation for each specific detector composition.

Chemical stability had been studied previously by several groups, albeit for optical-CT analysis, demonstrating a steep initial increase in signal due to reaction completion followed by a more gradual change due to chemical reactions caused by other effects. However, the effect of ambient light, often a cause of signal drift for chemical detectors, had not been investigated despite being a common cause of signal instability for chemical detectors. Dose response had been widely studied and shown to be dependent on chemical composition, time between manufacture, irradiation and scanning and was shown to vary for different batches of the same detector. Most authors had demonstrated a linear relationship between detector signal (optical density of relaxation rate) and dose for doses of at least 20Gy, although some had shown a deviation from linearity. Linearity is desirable as it makes calibration and the characterisation of the dose response relationship simpler.

Inhomogeneity of detector response across large volume agarose based detectors had been previously demonstrated, due to the different cooling rate following manufacture between the centre and edge of the detector. This had not been fully investigated for gelatine based detectors which are heated to lower temperatures during manufacture and therefore might be less of an issue. Finally, many groups had highlighted a post-irradiation diffusion of ferric ions causing a blurring of the measured dose distribution over time. The focus in previous work had been on quantifying the diffusion coefficient and the effect of this diffusion on measured dose distributions had not been fully quantified. Only one paper was found which had attempted to quantify diffusion for a range of dose gradients in a systematic way. Therefore, the time within which detectors

should be scanned following irradiation had been reported as between 0.5 to 3 hours or that the ferric ion diffusion rendered Fricke gel dosimetry impractical altogether.

This review was used to develop an experimental plan for this project; a systematic method of commissioning a 3D chemical detector. It was recommended that basic dosimetric characteristics including chemical stability, dose response and inter-sample variation will be evaluated first using test tube samples of Fricke gel irradiated with simple radiation fields and analysed with an NMR spectrometer. Larger volume samples analysed with an MRI scanner could then be used to explore detector homogeneity, the impact of ferric ion diffusion on clinically relevant dose gradients and volume dependence. Finally, only if results show adequate detector performance, would the detector be applied to increasingly complex radiotherapy plans.

7.2.2   Chapter 3: Gel Manufacture and MR analysis methods

The first aim of chapter 3 was to develop methods for the manufacture of Fricke gel detectors. The chemical composition was decided by reviewing the literature for existing evidence on the effect of different chemical constituents on parameters such as detector sensitivity. The focus was on simplicity, aiming to incorporate as few chemicals as possible with a low toxicity. This was accomplished and the final composition was 0.5mM ferrous ammonium sulphate, 25mM sulphuric acid, 5% gelatine and distilled water. The manufacture of approximately 1l batches of Fricke gel detectors within a simple laboratory was streamlined. The final optimised process took 2 hours plus cooling time.

Once the manufacture process had been developed, attention turned towards the readout of detectors. A bench-top NMR spectrometer was commissioned for the analysis of test tube Fricke gel samples, and a whole-body MRI scanner for the quantification of larger volume samples. It was unclear from the literature review whether T_1 or T_2 quantification was more appropriate for Fricke gel dosimetry, therefore this was to be the subject of future investigation.

For the NMR spectrometer, an inversion recovery sequence was used for T_1 quantification, and a CPMG sequence for T_2 quantification. Copper sulphate QC samples were used to evaluate and compare different pulse sequence parameters in terms of repeatability and linearity of R_1 and R_2 versus copper sulphate concentration.

Repeatability was within 0.2% for both sequences and the relationship between relaxation rates and copper sulphate concentration was linear for both sequences as expected. The measurement time for the typical relaxation times expected for Fricke gel samples was 5 minutes for T_1 compared with 1 minute for the optimised T_2 sequence.

Pulse sequences were then customised for a Philips Achieva 3T MRI scanner. Analysis software was written within OsiriX open source image analysis platform for the creation of T_1 and T_2 maps and dose maps. A Look Locker sequence was used for T_1 quantification and CPMG sequence used for T_2 quantification. Pulse sequence parameters were set to optimise the sequence in terms of maximizing SNR. Larger volume copper sulphate samples were prepared for the evaluation of sequences in terms of SNR, noise, homogeneity and repeatability. SNR was higher and image uniformity was improved for the optimised protocol for T_2 quantification when compared with the Look Locker protocol for scan times of similar duration.

7.2.3 Chapter 4: Establishing basic detector properties

The next chapter described systematic investigations into some of the basic properties of our Fricke–MR system using test tube samples analysed using an NMR spectrometer. Investigations into the chemical stability of this detector demonstrated an increase in relaxation rate immediately following irradiation due to reaction completion, in agreement with previous reports. The reaction time was shown to depend on radiation dose, but was a maximum of 12 minutes for the highest radiation dose. There followed a slower increase in relaxation rate over time, however this was reduced from 2% to 0.2% per hour by storing the detectors in the dark in between measurements.

The precision in the measured R_1 and R_2 relaxation rates was less than 0.5% for unirradiated samples and for samples irradiated to known doses of 1 to 20Gy indicating an excellent chemical consistency throughout the batch. In comparison, similar analysis for a polymer gel dosimeter reported a coefficient of variation of up to 5% over the same dose range [39]. The dose response was characterised over the dose range 0 to 20Gy. The dose response was linear, which simplifies detector calibration as only two dose levels are required to characterise the dose response relationship. A comparison between the dose response relationships of different batches showed good agreement. The dose response relationship was then used to convert relaxation rate to dose for every Fricke gel sample in order to estimate the uncertainty in the measured dose at

each dose level. At doses used in conventional radiotherapy of 0 to 3Gy, the dose uncertainty was greater than 3%. Despite the excellent measurement precision, the relatively low dose response causes dose uncertainties below 3Gy that are unacceptable in clinical radiotherapy. Uncertainties were less than 3% for doses of greater than 5Gy, suggesting that this detector is more suitable for high dose per fraction techniques.

Results were equivalent in terms of dose response and measurement precision for T_1 and T_2 quantification methods, in contrast to some previous studies indicating that either method may be used for the analysis of irradiated Fricke gel detectors. In this study T_2 quantification was selected due to the much improved SNR and image uniformity for the CPMG sequence when compared with Look Locker sequence. Finally, there was no dependence of detector response on the radiation dose rate or energy, agreeing with previous studies.

This chapter showed benefits of this Fricke gel detector of a linear dose response, no dose rate, or effect of fractionated dose delivery and negligible energy dependence. T_2 was demonstrated to be at least equivalent to T_1 quantification in contrast to some other reports in the literature which is important as it is generally simpler to obtain high SNR and uniformity for clinical T_2 sequences when compared with T_1. There was some chemical instability but this is minimised by waiting at least 12 minutes before scanning the detectors, and storing them in the dark. However, results demonstrated dose precision within 3% only for doses of greater than 3Gy.

7.2.4   Chapter 5: Larger volume suitability

Attention then turned to larger volume detectors readout using the optimised CPMG sequence using the MRI scanner. The homogeneity of detector response, detector volume and the effect of ferric ion diffusion were investigated. Previous studies had shown an unacceptable detector inhomogeneity for agarose gels due to a different cooling rate in the centre of a detector compared with the edge during manufacture. This might be expected to be less of an effect for gelatine based detectors due to lower melting point. This was investigated for unirradiated detectors and for a detector irradiated with a homogeneous 10Gy dose. Fricke gel batches with different cooling methods were compared; in water bath and cooled at room temperature for 3 hours prior to being placed in a refrigerator at 4$^{\text{o}}$C. The samples were then scanned with the CPMG sequence and a T_2 map created. The homogeneity was better than 1%, deemed

161

acceptable in terms of visual inspection of profiles plotted across the T_2 map, statistical variation in T_2 within a large region of interest and small variation in T_2 for small ROIs positioned in varying locations across the bottle.

Similarly, a volume dependence might exist as smaller samples cool faster than larger ones. This was investigated by irradiating different volume samples with the same homogeneous dose distribution. There was no volume dependence for the Fricke gel detector investigated here. This in contrast to a similar experiment carried out using a commercial polymer gel detector where large variations with volume and shape of detector were seen. This indicates that small volume samples may be used to calibrate larger volume experimental samples.

Ferric ion diffusion has been reported by many groups which causes a blurring of the measured dose distribution with time post-irradiation. The aim of the diffusion experiment in this chapter was to quantify the time within which gels should be scanned to maintain agreement between a measured distribution and reference distribution to within a specified spatial limit. This was carried out for 5 clinically relevant dose gradients of between 0.8Gy mm^{-1} to 3.2Gy mm^{-1} in their steepest section. Repeated scans were carried out for 5 hours following irradiation with a slightly modified sequence with a higher resolution in the direction of the dose gradient at the expense of the slice thickness. The maximum distance between the measured and reference TPS profile was noted at each time point. The time at which the maximum distance between measured and reference profile exceeded 1 and 2mm was quantified. These distance to agreement criteria were also selected to be relevant to spatial accuracy required for stereotactic techniques.

For the most relevant dose gradients, a 1mm DTA can be maintained if the irradiated Fricke gels are scanned within 1 hour 30 minutes. This is sufficient time to complete an MR scan of gel phantoms, however, immediate access to the MR scanner would be required. If a 2mm DTA is deemed acceptable, This Fricke gel composition can be scanned up to 3 hours 20 minutes for even the steepest dose gradients.

The composition can be modified to reduce the diffusion, for example adding xylenol orange. However, as this also reduces the dose response and immediate access to the MRI scanner can be arranged at St. Bartholomew's Hospital, it was decided to continue with the existing chemical composition for the clinical studies.

7.2.5 Chapter 6: Application to clinical plans

The focus of the final set of experiments was the irradiation of Fricke gel detectors with more complex radiotherapy plans. Fricke gel detectors were irradiated with a series of treatment plans, scanned with the optimised CPMG sequence in selected transverse, coronal and sagittal planes and 2D dose maps were created. These 2D dose maps were compared against corresponding calculated dose distributions exported from the treatment planning system. Plans had already been independently measured by existing radiation detectors such as ion chambers, radiochromic film and an ArcCheck diode detector array.

In order to quantitatively compare measured with calculated dose distributions, gamma evaluation was carried out using a commercial software package, OmniPro I'mRT. Gamma maps were calculated for two sets of gamma tolerances selected based on current VMAT and stereotactic practice at St. Bartholomew's Hospital and published recommendations. The percentage of pixels within a region of interest with a gamma of < 1 and therefore passing the gamma test was presented. A typical aim is for 95% of measured points to pass a gamma test although in practice results are a guide and analysed in terms of where failures occur for example whether they are in a low or high dose region, or near a critical structure.

Three radiotherapy plans were measured and analysed. They were selected with the aim to gradually increase plan complexity. The first was a simple, multiple field plan with some MLC shielding in one field to create a small dip in the dose distribution in order to investigate how well the Fricke gel measured this. The measured dose distribution for the central transverse plane was compared with the distribution predicted by the treatment planning system. If the measured dose distribution was re-normalised by 4%, the gamma pass rate was greater than 95% for both sets of gamma tolerances used.

The second plan evaluated was a previously treated clinical VMAT plan for a brain metastasis. In this case, no re-normalisation was required. For the central transverse and coronal planes, the gamma test pass rate was greater than 95% both sets of dose difference and DTA tolerances. A small region of disagreement was seen laterally in a low dose region (<40% of maximum dose) away from the very steep dose gradient.

The third experiment used a stereotactic spine test plan as part of the commissioning process for stereotactic treatments on a Varian Truebeam linear accelerator. This was a more complex treatment situation. A Fricke gel was irradiated and dose maps were created for the central transverse, coronal and sagittal planes. Again a small re-normalisation of 4% was required. When applied, the shape of the distribution agreed well in high dose and high dose gradient regions although again some disagreement was seen in the lateral direction in lower dose regions towards the edge of the bottle. Gamma test pass rates were greater than 95% for the transverse plane for both sets of gamma criteria. For the 5%, 1mm tolerance commonly used in stereotactic radiotherapy dosimetry, the pass rate was 93% for the sagittal plane but only 84% for the coronal plane with large areas of disagreement seen on the gamma map. This should be investigated further and perhaps indicates a slight further optimisation required in the TPS beam model for this machine and technique. However, the dose disagreement is only seen in a low dose region, away from steep dose gradients. In high dose, high gradient regions, the measured and calculated distributions agreed to within set tolerances and this plan would be accepted for treatment in clinical practice.

In terms of the re-normalisation required for two of the three plans, this is a common approach for other chemical dosimetry techniques. It is common to combine a measurement which supplies 2D or 3D spatial dose information with a higher precision measurement at a single dose point for example an ionisation chamber. This would also be reasonable solution for 3D chemical dosimetry. In all three plans, the dose measured by the Fricke gel agreed with the PinPoint measured dose to within measurement uncertainty and the PinPoint dose was clinically acceptable according to local clinical tolerances.

Gamma test results were similar to those presented in the literature for other 2D and pseudo-3D dosimetry techniques. The ability of this Fricke gel detector to carry out 3D dosimetry for complex dose distributions was demonstrated

7.3   Overall conclusions

Several reasons have been proposed for the lack of uptake of chemical dosimetry within clinical radiotherapy. Firstly, for some detectors such as polymer gel and Presage, the manufacture process requires laboratory facilities beyond those available to most

clinical radiotherapy physics departments. In terms of imaging, the recent focus has predominantly been on optical-CT scanners which would need to be purchased and commissioned specifically for gel dosimetry. Once again, it is beyond the expertise and time available for most clinical departments to develop their own scanners. Fricke gel detectors are simpler, but it was suggested that MR imaging was limited to T_1 quantification. As was shown in this project, T_1 sequences typically available on clinical scanners such as the Look Locker sequence tend to be very fast sequences for cardiac imaging with inherently poor SNR. The issue of ferric ion diffusion has written off Fricke gel dosimetry for some. Finally, a lack of evidence for dosimetric performance for chemical detectors in general has led to uncertainty regarding the reliability of these techniques.

These issues have been addressed in this project. A Fricke gel detector has been evaluated for use as a 3D dosimeter in a structured and logical way. The Fricke gel–MR system was optimised in terms of manufacture process and scan protocols. Focus was on simplicity and application within a clinical radiotherapy department. Detector manufacture was within a simple laboratory, involved non-toxic chemicals taking less than 2 hours and scanning was accomplished with clinically available MR pulse sequences. Consistency of dose response was demonstrated for different batches even with these basic facilities. T_2 quantification was demonstrated to be at least equivalent to T_1 quantification in terms of dose precision and response. A readily available clinical CPMG sequence was customised with little effort resulting in T_2 and dose maps with high SNR and excellent uniformity.

The optimised system was then subjected to commissioning measurements as if it were a commercial detector to quantify all factors which might affect its measurement accuracy. The dosimetric requirements were defined and quantified at the start. Detector characterisation was then accomplished in a systematic way, starting with basic characteristics evaluated using small volume test tube samples analysed with an NMR spectrometer before moving onto larger samples and dose mapping with a clinical MRI scanner.

A tolerance of 3% was set at the outset for the overall dosimetry uncertainty based on available evidence in reference reports and dosimetric performance achieved by 2D detectors. The experimental dosimetric results demonstrated many benefits of this

detector. The T_1 and T_2 inter-sample variation was small (CV <0.5%) indicating a uniform chemical composition. The dose response was linear to doses of at least 20Gy.There was no evidence of any dose rate, energy or volume dependence; results were all within measurement uncertainty. Detector inhomogeneity was demonstrated to be within acceptable limits (<1%) for samples of up to 500ml. If detectors were scanned at least 15 minutes following irradiation and were stored in the dark, chemical instability was minimal, and in any case for all clinical irradiations in this project experimental and calibration samples were stored together and scanned simultaneously.

The characterisation experiments highlighted two main contributions to measurement uncertainty. Firstly, despite very small variations between the T_2 of different samples, the relatively low dose response meant that when converted to dose, dose uncertainties were greater than 3% over the 0 to 3Gy dose range

For doses of greater than 3Gy, dose uncertainty was less than 3%. Therefore, for the remainder of this project, the focus was on higher dose techniques. This restriction is a limitation. However, there has been an increased interest in stereotactic radiotherapy over recent years. UK wide programmes are underway to evaluate the efficacy of stereotactic ablative body radiotherapy for a variety of treatment sites and there has been a rollout of stereotactic intracranial radiosurgery. In addition, stereotactic radiotherapy involves very steep dose gradients for which 3D dosimetry would be of particular benefit. Recent clinical trials have investigated hypofractionated radiotherapy for two of the most common cancers: breast and prostate cancer, with results recently reported for the FAST trial for breast cancer indicating that hypofractionated radiotherapy (>5Gy per fraction) should be adopted. The PACE trial is also investigating high dose per fraction (> 7Gy) treatments for prostate cancer.

The second issue highlighted, as previously reported, was the blurring of the measured dose distribution with time post-irradiation due to ferric ion diffusion throughout the gelatine matrix. This is particularly important for the higher dose stereotactic treatments which involve steep dose gradients, often close to critical normal tissues. However, this was quantified and even for dose gradients higher than seen clinically, spatial accuracy is maintained to within 1mm as long as scanning is completed within 1.5 hours. This was easily achievable for the clinical studies where imaging was within an hour of irradiation, introducing only sub-mm errors.

Calibration has not been the focus of many publications for Fricke gel dosimetry. The T_2 versus dose response must be characterised for each measurement session due to chemical instability and variation in dose response between different batches. This potentially can be cumbersome requiring multiple additional samples to be irradiated to known doses. In fact, several factors for this Fricke gel detector are beneficial in terms of simple detector calibration. A lack of volume dependence means that small samples may be used for calibration. Small inter-sample variation and a linear dose response meant that only two samples can be used to characterise the dose response.

When applied to clinical radiotherapy plans, gamma test results were compared to those presented in the literature for other detector types. For a brain plan, gamma test results achieved the set 95% pass rate. The results for a spine plan demonstrated a 4% high measured dose compared with the TPS, in agreement with the ionisation chamber measurement. When re-normalised, gamma test results again achieved the set pass rate for high dose and high gradient regions. For both plans, recommended accuracy requirements for the high dose, high gradient regions of 2-3mm DTA and 3-5% dose difference were satisfied [127].

The Fricke gel system demonstrated similar dosimetric results to other detectors used for VMAT dosimetry with the added benefit of performing a 3D measurement. This technique could now be implemented for the commissioning of new techniques and technology in our department, with some work required to streamline the imaging and analysis process which will be outlined in the next section. To increase the confidence with the Fricke gel system still further, a range of clinical plans could be measured and evaluated. With another year, I would use the Fricke gel detectors for a range of clinical plans, covering different treatment sites and scenarios before moving onto plans with known errors introduced. This would complete the structured validation of this detector.

7.4   Future work

The dosimetric performance of this Fricke gel detector has been demonstrated to be sufficient for the verification of the accuracy of complex radiotherapy plans. Further work is required however to finalise MR and analysis methods. So far, analysis has been via the creation of 2D dose planes with relatively large slice thickness in order to

improve the in-plane spatial resolution whilst maintaining SNR. These sequences were designed specifically for the characterisation experiments of this PhD where the dose did not vary greatly out of plane. However, for the measurement of clinical plans the MR methodology should be developed further in terms of 3D analysis. 3D MR sequences are available [130], and have been applied to Fricke gel dosimetry [99]. Alternatively a greater number of contiguous 2D planes could be acquired if required.

To automate the analysis, work is also required to develop the software further. Currently T_2 maps are created automatically within OsiriX, but the dose response has to be manually plotted and the code manually edited to create dose maps. The DICOM header then has to be manually edited to allow exported dose planes to be successfully imported into OmniPro I'mRT software. This could all be automated within the plugin. Optionally, the plugin could be developed to also calculate gamma maps.

Localisation so far was accomplished by manually marking up the bottle and aligning with linac lasers and MR lasers. Small adjustments were required during the analysis to fine tune the location of the measured dose map versus calculated dose map i.e. the measured map was moved where an obvious systematic shift was seen. This was again reasonable for this investigation into the dosimetric capability of the Fricke gel detector, but in the verification of clinical plans a higher spatial accuracy is required. Incorporating fiducial markers which are visible on the T_2 map would accomplish this and would further streamline the whole process.

Alternatively, a phantom could be designed to hold the detector both during radiotherapy delivery and MRI scanning which would allow localisation by registering images. This could be more patient like and manufactured using a 3D printer. The end-to-end testing of the entire radiotherapy process using anthropomorphic phantoms manufactured using 3D printers is the subject of current research [131-134]. The use of 3D chemical dosimetry within 3D printed anthropomorphic phantoms, would be a powerful dosimetric tool for the end-to-end testing of complex radiotherapy techniques.

The whole process should then be validated for a wider range of clinical plans covering a different prescription doses, treatment sites and techniques. It is possible, although not straightforward, to introduce intentional errors into VMAT plans. Proving the ability of the Fricke gel detector to correctly identify treatment errors in this way would be a worthwhile concluding investigation.

References

[1]   ICRU, "International Commission on Radiation Units and Measurements. *Prescribing, recording, and reporting photon beam therapy. ICRU Report 50.*," *ICRU,* 1993.

[2]   ICRU, "International Commission on Radiation Units and Measurements. *Prescribing, recording, and reporting photon beam therapy (Supplement to ICRU Report 50). ICRU Report 62.*," 1999.

[3]   ICRU, "International Commission on Radiation Units and Measurements. *Prescribing, Recording, and Reporting Photon-Beam Intensity Modulated Radiation Therapy (IMRT). ICRU report 83*," *J. ICRU,* vol. 10, no. 1, 2010.

[4]   S. C. Lillicrap, B. Owen, J. R. Williams, and P. C. Williams, "Code of practice for high-energy photon therapy based on the NPL absorbed dose calibration service," *Physics in Medicine and Biology,* vol. 35, no. 10, pp. 1355-1360, Oct 1990.

[5]   K. Otto, "Volumetric modulated arc therapy: IMRT in a single gantry arc," *Medical Physics,* vol. 35, no. 1, pp. 310-317, 2008.

[6]   T. LoSasso, C.-S. Chui, and C. C. Ling, "Physical and dosimetric aspects of a multileaf collimation system used in the dynamic mode for implementing intensity modulated radiotherapy.," *Medical Physics,* vol. 25, no. 10, pp. 1919-1927, 1998.

[7]   G. S. Ibbott, D. S. Followill, H. A. Molineu, J. R. Lowenstein, P. E. Alvarez, and J. E. Roll, "Challenges in credentialing institutions and participants in advanced technology multi-institutional clinical trials," *International Journal of Radiation Oncology* Biology* Physics,* vol. 71, no. 1, pp. S71-S75, 2008.

[8]   J. Van Dyk, "Quality assurance of radiation therapy planning systems: current status and remaining challenges," (in English), *International Journal of Radiation Oncology, Biology, Physics,* vol. 71, no. 1 Suppl, pp. S23-7, 2008.

[9]   M. Alber *et al.*, "Guidelines for the verification of IMRT," *ESTRO booklet,* vol. 7, 2008.

[10] D. A. Low, J. M. Moran, J. F. Dempsey, L. Dong, and M. Oldham, "Dosimetry tools and techniques for IMRT," (in English), *Medical Physics,* Article vol. 38, no. 3, pp. 1313-1338, Mar 2011.

[11] D. A. Low, W. B. Harms, S. Mutic, and J. A. Purdy, "A technique for the quantitative evaluation of dose distributions," (in English), *Medical Physics,* vol. 25, no. 5, pp. 656-61, May 1998.

[12] T. Depuydt, A. Van Esch, and D. Huyskens, "A quantitative evaluation of IMRT dose distributions: refinement and clinical assessment of the gamma evaluation.," *Radiotherapy and Oncology,* vol. 62, no. 3, pp. 309-319, 2002.

[13] C. De Wagter, "The ideal dosimeter for intensity modulated radiation therapy (IMRT): What is required?," in *Journal of Physics: Conference Series*, 2004, vol. 3, no. 1: IOP Publishing, p. 4.

[14] J. C. Gore, Y. S. Kang, and R. J. Schulz, "Measurement of radiation-dose distributions by nuclear magnetic resonance (NMR) imaging," *Physics in Medicine & Biology,* vol. 29, no. 10, pp. 1189-1197, 1984.

[15] H. Fricke and E. J. Hart, Eds. "Chemical Dosimetry," (Radiation Dosimetry. New York: Academic Press, 1966.

[16] L. E. Olsson, S. Petersson, L. Ahlgren, and S. Mattsson, "Ferrous sulphate gels for determination of absorbed dose distributions using MRI technique: basic studies," *Physics in Medicine & Biology,* vol. 34, no. 1, pp. 43-52, 1989.

[17] L. E. Olsson, A. Fransson, A. Ericsson, and S. Mattsson, "MR imaging of absorbed dose distributions for radiotherapy using ferrous sulphate gels," (in English), *Physics in Medicine & Biology,* vol. 35, no. 12, pp. 1623-31, Dec 1990.

[18] C. Duzenli, R. Sloboda, and D. Robinson, "A spin-spin relaxation rate investigation of the gelatin ferrous sulphate NMR dosimeter," (in English), *Physics in Medicine & Biology,* vol. 39, no. 10, pp. 1577-92, Oct 1994.

[19]   G. Gambarini, S. Arrigoni, M. C. Cantone, N. Molho, L. Facchielli, and A. E. Sichirollo, "Dose-response curve slope improvement and result reproducibility of ferrous-sulphate-doped gels analysed by NMR imaging," (in English), *Physics in Medicine & Biology,* vol. 39, no. 4, pp. 703-17, Apr 1994.

[20]   S. A. Johansson Back *et al.*, "Improvements in absorbed dose measurements for external radiation therapy using ferrous dosimeter gel and MR imaging (FeMRI)," (in English), *Physics in Medicine & Biology,* vol. 43, no. 2, pp. 261-76, Feb 1998.

[21]   A. Appleby and A. Leghrouz, "Imaging of radiation dose by visible color development in ferrous-agarose-xylenol orange gels," (in English), *Medical Physics,* vol. 18, no. 2, pp. 309-12, Mar-Apr 1991.

[22]   M. A. Bero, W. B. Gilboy, P. M. Glover, and J. L. Keddie, "Three-dimensional radiation dose measurements with ferrous benzoic acid xylenol orange in gelatin gel and optical absorption tomography," (in English), *Nuclear Instruments & Methods in Physics Research Section A,* Article; Proceedings Paper vol. 422, no. 1-3, pp. 617-620, Feb 1999.

[23]   M. A. Bero, W. B. Gilboy, and P. M. Glover, "An optical method for three-dimensional dosimetry," (in English), *Journal of Radiological Protection,* vol. 20, no. 3, pp. 287-94, Sep 2000.

[24]   M. A. Bero, W. B. Gilboy, and P. M. Glover, "Radiochromic gel dosemeter for three-dimensional dosimetry," (in English), *Radiation Physics and Chemistry,* Article; Proceedings Paper vol. 61, no. 3-6, pp. 433-435, Jun 2001.

[25]   K. C. Chu, K. J. Jordan, J. J. Battista, J. Van Dyk, and B. K. Rutt, "Polyvinyl alcohol-Fricke hydrogel and cryogel: two new gel dosimetry systems with low Fe3+ diffusion," (in English), *Physics in Medicine & Biology,* vol. 45, no. 4, pp. 955-69, Apr 2000.

[26]   B. Hill, S. A. J. Back, M. Lepage, J. Simpson, B. Healy, and C. Baldock, "Investigation and analysis of ferrous sulfate polyvinyl alcohol (PVA) gel dosimeter," (in English), *Physics in Medicine & Biology,* vol. 47, no. 23, pp. 4233-46, Dec 7 2002.

[27]   B. J. Healy, M. H. Zahmatkesh, K. N. Nitschke, and C. Baldock, "Effect of saccharide additives on response of ferrous-agarose-xylenol orange radiotherapy gel dosimeters," (in English), *Medical Physics,* vol. 30, no. 9, pp. 2282-91, Sep 2003.

[28]   J. B. Davies and C. Baldock, "Sensitivity and stability of the Fricke-gelatin-xylenol orange gel dosimeter," *Radiation Physics and Chemistry,* doi: 10.1016/j.radphyschem.2008.01.007 vol. 77, no. 6, pp. 690-696, 2008.

[29]   L. E. Olsson, B. A. Westrin, A. Fransson, and B. Nordell, "Diffusion of ferric ions in agarose dosimeter gels," *Physics in Medicine & Biology,* vol. 37, no. 12, pp. 2243-2252, 4 August 1992 1992.

[30]   B. J. Balcom, T. J. Lees, A. R. Sharp, N. S. Kulkarni, and G. S. Wagner, "Diffusion in Fe(II/III) radiation dosimetry gels measured by magnetic resonance imaging," (in English), *Physics in Medicine & Biology,* vol. 40, no. 10, pp. 1665-76, Oct 1995.

 [31]   W. I. Rae, C. A. Willemse, M. G. Lotter, J. S. Engelbrecht, and J. C. Swarts, "Chelator effect on ion diffusion in ferrous-sulfate-doped gelatin gel dosimeters as analyzed by MRI," (in English), *Medical Physics,* vol. 23, no. 1, pp. 15-23, Jan 1996.

[32]   T. V. Pedersen, D. R. Olsen, and A. Skretting, "Measurement of the ferric diffusion coefficient in agarose and gelatine gels by utilization of the evolution of a radiation induced edge as reflected in relaxation rate images," (in English), *Physics in Medicine & Biology,* vol. 42, no. 8, pp. 1575-85, Aug 1997.

[33]   Y. J. Tseng *et al.*, "The role of dose distribution gradient in the observed ferric ion diffusion time scale in MRI-Fricke-infused gel dosimetry," (in English), *Magnetic Resonance Imaging,* vol. 20, no. 6, pp. 495-502, Jul 2002.

[34]   M. J. Maryanski, J. C. Gore, R. P. Kennan, and R. J. Schulz, "NMR relaxation enhancement in gels polymerized and cross-linked by ionizing radiation: a new approach to 3D dosimetry by MRI," (in English), *Magnetic Resonance Imaging,* vol. 11, no. 2, pp. 253-8, 1993.

[35]   M. J. Maryanski *et al.*, "Magnetic resonance imaging of radiation dose distributions using a polymer-gel dosimeter," (in English), *Physics in Medicine & Biology,* vol. 39, no. 9, pp. 1437-55, Sep 1994.

[36]   M. Oldham, J. H. Siewerdsen, S. Kumar, J. Wong, and D. A. Jaffray, "Optical-CT gel-dosimetry I: basic investigations," (in English), *Medical Physics,* vol. 30, no. 4, pp. 623-34, Apr 2003.

[37]   E. Pappas *et al.*, "A new polymer gel for magnetic resonance imaging (MRI) radiation dosimetry," (in English), *Physics in Medicine & Biology,* vol. 44, no. 10, pp. 2677-84, Oct 1999.

[38]   P. M. Fong, D. C. Keil, M. D. Does, and J. C. Gore, "Polymer gels for magnetic resonance imaging of radiation dose distributions at normal room atmosphere," (in English), *Physics in Medicine & Biology,* vol. 46, no. 12, pp. 3105-13, Dec 2001.

[39]   N. D. MacDougall, M. E. Miquel, D. J. Wilson, S. F. Keevil, and M. A. Smith, "Evaluation of the dosimetric performance of BANG3 polymer gel," (in English), *Physics in Medicine & Biology,* vol. 50, no. 8, pp. 1717-26, Apr 21 2005.

[40]   N. D. MacDougall, M. E. Miquel, and S. F. Keevil, "Effects of phantom volume and shape on the accuracy of MRI BANG gel dosimetry using BANG3," (in English), *British Journal of Radiology,* vol. 81, no. 961, pp. 46-50, Jan 2008.

[41]   A. Karlsson, H. Gustavsson, S. Mansson, K. B. McAuley, and S. A. J. Back, "Dose integration characteristics in normoxic polymer gel dosimetry investigated using sequential beam irradiation," (in English), *Physics in Medicine & Biology,* vol. 52, no. 15, pp. 4697-706, Aug 7 2007.

[42]   Y. De Deene, "Polymer Gel Dosimetry," in *Clinical 3D Dosimetry in Modern Radiation Therapy*, B. Mijneer, Ed. (Imaging in Medical Diagnosis and Therapy, A. Karellas and B. Thomadsen, Eds. Boca Raton, FL: Taylor & Francis Group, 2017.

[43]   J. Adamovics and M. J. Maryanski, "Characterisation of PRESAGE: A new 3-D radiochromic solid polymer dosemeter for ionising radiation," (in English), *Radiation Protection Dosimetry,* vol. 120, no. 1-4, pp. 107-12, 2006.

[44]   P. Guo, J. Adamovics, and M. Oldham, "A practical three-dimensional dosimetry system for radiation therapy," (in English), *Medical Physics,* vol. 33, no. 10, pp. 3962-72, Oct 2006.

[45]   P. Y. Guo, J. A. Adamovics, and M. Oldham, "Characterization of a new radiochromic three-dimensional dosimeter," (in English), *Medical Physics,* vol. 33, no. 5, pp. 1338-45, May 2006.

[46]   H. S. Sakhalkar, J. Adamovics, G. Ibbott, and M. Oldham, "A comprehensive evaluation of the PRESAGE/optical-CT 3D dosimetry system," (in English), *Med Phys,* vol. 36, no. 1, pp. 71-82, Jan 2009.

[47]   C. Clift, A. Thomas, J. Adamovics, Z. Chang, I. Das, and M. Oldham, "Toward acquiring comprehensive radiosurgery field commissioning data using the PRESAGE/optical-CT 3D dosimetry system," (in English), *Physics in Medicine & Biology,* vol. 55, no. 5, pp. 1279-93, Mar 7 2010.

[48]   S. L. Brady, W. E. Brown, C. G. Clift, S. Yoo, and M. Oldham, "Investigation into the feasibility of using PRESAGE (TM)/optical-CT dosimetry for the verification of gating treatments," (in English), *Physics in Medicine and Biology,* Article vol. 55, no. 8, pp. 2187-2201, Apr 2010.

[49]   M. Hilts, C. Audet, C. Duzenli, and A. Jirasek, "Polymer gel dosimetry using x-ray computed tomography: a feasibility study," (in English), *Physics in Medicine & Biology,* vol. 45, no. 9, pp. 2559-71, Sep 2000.

[50]   J. V. Trapp, S. A. Back, M. Lepage, G. Michael, and C. Baldock, "An experimental study of the dose response of polymer gel dosimeters imaged with x-ray computed tomography," (in English), *Physics in Medicine & Biology,* vol. 46, no. 11, pp. 2939-51, Nov 2001.

[51]   M. L. Mather, A. K. Whittaker, and C. Baldock, "Ultrasound evaluation of polymer gel dosimeters," (in English), *Physics in Medicine & Biology,* vol. 47, no. 9, pp. 1449-58, May 7 2002.

[52]   G. Gambarini, D. Monti, M. L. Fumagalli, C. Birattari, and P. Salvadori, "Phantom dosimeters examined by NMR analysis: a promising technique for 3-D determinations of absorbed dose," (in English), *Applied Radiation & Isotopes,* vol. 48, no. 10-12, pp. 1477-84, Oct-Dec 1997.

[53]   Y. De Deene *et al.*, "Validation of MR-based polymer gel dosimetry as a preclinical three-dimensional verification tool in conformal radiotherapy," (in English), *Magnetic Resonance in Medicine,* vol. 43, no. 1, pp. 116-25, Jan 2000.

[54]   C. Baldock *et al.*, "Dose resolution in radiotherapy polymer gel dosimetry: effect of echo spacing in MRI pulse sequence.[Erratum appears in Phys Med Biol 2001 May;46(5):1591]," (in English), *Physics in Medicine & Biology,* vol. 46, no. 2, pp. 449-60, Feb 2001.

[55]   T. Olding, O. Holmes, and L. J. Schreiner, "Cone beam optical computed tomography for gel dosimetry I: scanner characterization," (in English), *Physics in Medicine and Biology,* Article vol. 55, no. 10, pp. 2819-2840, May 2010.

[56]   S. J. Doran, K. K. Koerkamp, M. A. Bero, P. Jenneson, E. J. Morton, and W. B. Gilboy, "A CCD-based optical CT scanner for high-resolution 3D imaging of radiation dose distributions: equipment specifications, optical simulations and preliminary results," (in English), *Physics in Medicine and Biology,* Article vol. 46, no. 12, pp. 3191-3213, Dec 2001.

[57]   S. Babic, A. McNiven, J. Battista, and K. Jordan, "Three-dimensional dosimetry of small megavoltage radiation fields using radiochromic gels and optical CT scanning," (in English), *Physics in Medicine & Biology,* vol. 54, no. 8, pp. 2463-81, Apr 21 2009.

[58]   B. Mijneer, B. Mijneer, Ed. *Clinical 3D Dosimetry in Modern Radiation Therapy* (Imaging in Medical Diagnosis and Therapy). Boca Raton, FL: Taylor & Francis Group, 2017.

[59]   S. J. Doran and N. Krstajić, "The history and principles of optical computed tomography for scanning 3-D radiation dosimeters," *Journal of Physics: Conference Series,* vol. 56, no. 1, p. 45, 2006.

[60]   C. Hurley, A. Venning, and C. Baldock, "A study of a normoxic polymer gel dosimeter comprising methacrylic acid, gelatin and tetrakis (hydroxymethyl) phosphonium chloride (MAGAT)," (in English), *Applied Radiation & Isotopes,* vol. 63, no. 4, pp. 443-56, Oct 2005.

[61]   A. R. Farajollahi, D. E. Bonnett, A. J. Ratcliffe, R. J. Aukett, and J. A. Mills, "An investigation into the use of polymer gel dosimetry in low dose rate brachytherapy," (in English), *British Journal of Radiology,* vol. 72, no. 863, pp. 1085-92, Nov 1999.

[62]   A. E. Papadakis, T. G. Maris, F. Zacharopoulou, E. Pappas, G. Zacharakis, and J. Damilakis, "An evaluation of the dosimetric performance characteristics of N-vinylpyrrolidone-based polymer gels," (in English), *Physics in Medicine & Biology,* vol. 52, no. 16, pp. 5069-83, Aug 21 2007.

[63]   C. Baldock, P. Murry, and T. Kron, "Uncertainty analysis in polymer gel dosimetry," (in English), *Physics in Medicine & Biology,* vol. 44, no. 11, pp. N243-6, Nov 1999.

[64]   M. Oldham, M. McJury, I. B. Baustert, S. Webb, and M. O. Leach, "Improving calibration accuracy in gel dosimetry," (in English), *Physics in Medicine & Biology,* vol. 43, no. 10, pp. 2709-20, Oct 1998.

[65]   M. Oldham, "Innovation and the future of advanced dosimetry: 2D to 5D," *Journal of Physics: Conference Series,* vol. 847, 2017.

[66]   A. Niroomand-Rad *et al.*, "Radiochromic film dosimetry: recommendations of AAPM Radiation Therapy Committee Task Group 55. American Association of Physicists in Medicine," (in English), *Medical Physics,* vol. 25, no. 11, pp. 2093-115, Nov 1998.

[67]   National Institute of Science and Technology. *Uncertainty of Measurement Results* [Online]. 1998. Available: http://physics.nist.gov/cuu/Uncertainty/international1.html.

[68]   F. H. Attix, *Introduction to Radiological Physics and Radiation Dosimetry*. New York: Wiley-Interscience, 1986.

[69]   J. Van Dyk, Ed. "Modern Technology of Radiation Oncology." Madison: Medical Physics Publishing, 2013, pp. 361-415.

[70]   International Atomic Energy Agency, *Accuracy Requirements and Uncertainties in Radiotherapy* (IAEA Human Health Series, no. 31). Vienna: INTERNATIONAL ATOMIC ENERGY AGENCY, 2016.

[71]   D. Thwaites, "Accuracy required and achievable in radiotherapy dosimetry: have modern technology and techniques changed our views?," *Journal of Physics Conference Series,* vol. 444, 2013.

[72]   S. Ahmed, B. Nelms, J. Kozelka, G. Zhang, E. Moros, and V. Feygelman, "Validation of an improved helical diode array and dose reconstruction software using TG-244 datasets and stringent dose comparison criteria," *Journal of applied clinical medical physics,* vol. 17, no. 6, pp. 163-178, 2016.

[73]   E. Seravalli *et al.*, "OC-0545: Results of a national audit of IMRT and VMAT patient QA," *Radiotherapy and Oncology,* vol. 119, pp. S259-S260, 2016.

[74]   C. H. Clark *et al.*, "Dosimetry audit for a multi-centre IMRT head and neck trial," *Radiotherapy and Oncology,* vol. 93, no. 1, pp. 102-108, 2009.

[75]   C. H. Clark *et al.*, "A multi-institutional dosimetry audit of rotational intensity-modulated radiotherapy," *Radiotherapy and Oncology,* vol. 113, no. 2, pp. 272-278, 2014.

[76]   M. Oldham, J. H. Siewerdsen, A. Shetty, and D. A. Jaffray, "High resolution gel-dosimetry by optical-CT and MR scanning," (in English), *Medical Physics,* vol. 28, no. 7, pp. 1436-45, Jul 2001.

[77]   C. Martens, C. De Wagter, and W. De Neve, "The value of the PinPoint ion chamber for characterization of small field segments used in intensity-modulated radiotherapy," *Physics in Medicine & Biology,* vol. 45, no. 9, p. 2519, 2000.

[78] D. Fraser, W. Parker, and J. Seuntjens, "Characterization of cylindrical ionization chambers for patient specific IMRT QA," *Journal of applied clinical medical physics,* vol. 10, no. 4, pp. 241-251, 2009.

[79] S. Devic, N. Tomic, C. G. Soares, and E. B. Podgorsak, "Optimizing the dynamic range extension of a radiochromic film dosimetry system," (in English), *Medical Physics,* vol. 36, no. 2, pp. 429-37, Feb 2009.

[80] S. Devic, N. Tomic, and D. Lewis, "Reference radiochromic film dosimetry: review of technical aspects," *Physica Medica,* vol. 32, no. 4, pp. 541-556, 2016.

[81] E. Y. León-Marroquín *et al.*, "Spectral analysis of the EBT3 radiochromic film irradiated with 6 MV x-ray radiation," *Radiation Measurements,* vol. 89, pp. 82-88, 2016.

[82] P. B. Greer, P. Vial, L. Oliver, and C. Baldock, "Experimental investigation of the response of an amorphous silicon EPID to intensity modulated radiotherapy beams," *Medical physics,* vol. 34, no. 11, pp. 4389-4398, 2007.

[83] B. McCurdy and P. Greer, "Dosimetric properties of an amorphous-silicon EPID used in continuous acquisition mode for application to dynamic and arc IMRT," *Medical physics,* vol. 36, no. 7, pp. 3028-3039, 2009.

[84] G. Distefano *et al.*, "A national dosimetry audit for stereotactic ablative radiotherapy in lung," *Radiotherapy and Oncology,* vol. 122, no. 3, pp. 406-410, 2017.

[85] A. Appleby, E. A. Christman, and A. Leghrouz, "Imaging of spatial radiation dose distribution in agarose gels using magnetic resonance," (in English), *Medical Physics,* vol. 14, no. 3, pp. 382-4, May-Jun 1987.

[86] W. C. Chu and J. Wang, "Exploring the concentration gradient dependency of the ferric ion diffusion effect in MRI-Fricke-infused gel dosimetry," (in English), *Physics in Medicine & Biology,* vol. 45, no. 12, pp. L63-4, Dec 2000.

[87] S. Saur, T. Strickert, E. Wasboe, and J. Frengen, "Fricke gel as a tool for dose distribution verification: optimization and characterization," (in English), *Physics in Medicine & Biology,* vol. 50, no. 22, pp. 5251-61, Nov 21 2005.

[88]   S. Noda *et al.*, "Clinical application of the Fricke-glucomannan gel dosimeter for high-dose-rate (192)Ir brachytherapy," (in English), *Physics in Medicine & Biology,* vol. 53, no. 14, pp. 3985-93, Jul 21 2008.

[89]   L. E. Olsson, A. Appleby, and J. Sommer, "A new dosimeter based on ferrous sulfate-solution and agarose-gel," (in English), *Applied Radiation and Isotopes,* Article vol. 42, no. 11, pp. 1081-1086, 1991.

[90]   R. J. Schulz, A. F. deGuzman, D. B. Nguyen, and J. C. Gore, "Dose-response curves for Fricke-infused agarose gels as obtained by nuclear magnetic resonance," (in English), *Physics in Medicine & Biology,* vol. 35, no. 12, pp. 1611-22, Dec 1990.

[91]   A. Appleby, A. Leghrouz, and E. A. Christman, "Radiation chemical and magnetic resonance studies of aqueous agarose gels containing ferrous ions," *International Journal of Radiation Applications and Instrumentation. Part C. Radiation Physics and Chemistry,* vol. 32, no. 2, pp. 241-244, 1988.

[92]   R. G. Kelly, K. J. Jordan, and J. J. Battista, "Optical CT reconstruction of 3D dose distributions using the ferrous-benzoic-xylenol (FBX) gel dosimeter," (in English), *Medical Physics,* vol. 25, no. 9, pp. 1741-50, Sep 1998.

[93]   S. A. Back, J. Medin, P. Magnusson, P. Olsson, E. Grusell, and L. E. Olsson, "Ferrous sulphate gel dosimetry and MRI for proton beam dose measurements," (in English), *Physics in Medicine & Biology,* vol. 44, no. 8, pp. 1983-96, Aug 1999.

[94]   G. Bartesaghi, J. Burian, G. Gambarini, M. Marek, A. Negri, and L. Viererbl, "Evaluation of all dose components in the LVR-15 reactor epithermal neutron beam using Fricke gel dosimeter layers," (in English), *Applied Radiation & Isotopes,* vol. 67, no. 7-8 Suppl, pp. S199-201, Jul 2009.

[95]   M. Carrara, C. Fallai, G. Gambarini, and A. Negri, "Fricke gel-layer dosimetry in high dose-rate brachytherapy," (in English), *Applied Radiation & Isotopes,* vol. 68, no. 4-5, pp. 722-5, Apr-May 2010.

[96]   C. S. G. Calcina, L. N. de Oliveira, C. E. de Almeida, and A. de Almeida, "Dosimetric parameters for small field sizes using Fricke xylenol gel, thermoluminescent and film dosimeters, and an ionization chamber," (in English), *Physics in Medicine & Biology,* vol. 52, no. 5, pp. 1431-9, Mar 7 2007.

[97]   L. N. de Oliveira, A. de Almeida, and L. V. Caldas, "Measuring output factors and beam profiles formed by multileaf collimators using Fricke gel dosimeter," *Physica Medica: European Journal of Medical Physics,* vol. 30, no. 7, pp. 854-857, 2014.

[98]   H. J. Cervantes, C. C. Cavinato, L. L. Campos, and S. R. Rabbani, "Gamma Knife® 3-D Dose Distribution Mapping by Magnetic Resonance Imaging," *Applied Magnetic Resonance,* vol. 39, no. 4, pp. 357-364, 2010.

[99]   N. Y. Cho, S. C. Huang, W. Y. Chung, W. Y. Guo, and W. C. Chu, "Isotropic three-dimensional MRI-Fricke-infused gel dosimetry," *Medical physics,* vol. 40, no. 5, 2013.

[100]   W. C. Chu, W. Y. Guo, M. C. Wu, W. Y. Chung, and D. H. Pan, "The radiation induced magnetic resonance image intensity change provides a more efficient three-dimensional dose measurement in MRI-Fricke-agarose gel dosimetry," (in English), *Medical Physics,* vol. 25, no. 12, pp. 2326-32, Dec 1998.

[101]   T. Kron, "Dose measuring tools," in *The Modern Technology of Radiation Oncology*, J. Van Dyk, Ed. Madison, WI: Medical Physics Publishing, 1999, pp. 753-821.

[102]   N. D. MacDougall, W. G. Pitchford, and M. A. Smith, "A systematic review of the precision and accuracy of dose measurements in photon radiotherapy using polymer and Fricke MRI gel dosimetry," (in English), *Physics in Medicine & Biology,* vol. 47, no. 20, pp. R107-21, Oct 21 2002.

[103]   M. Bero and M. Zahili, "Radiochromic gel dosimeter (FXG) chemical yield determination for dose measurements standardization," in *Journal of Physics: Conference Series*, 2009, vol. 164, no. 1: IOP Publishing, p. 012011.

[104] M. M. Eyadeh, T. J. Farrell, and K. R. Diamond, "Evaluation of a ferrous benzoic xylenol orange transparent PVA cryogel radiochromic dosimeter," *Physics in Medicine & Biology,* vol. 59, no. 7, p. 1773, 2014.

[105] J. D. Hazle, L. Hefner, C. E. Nyerick, L. Wilson, and A. L. Boyer, "Dose-response characteristics of a ferrous-sulphate-doped gelatin system for determining radiation absorbed dose distributions by magnetic resonance imaging (Fe MRI)," (in English), *Physics in Medicine & Biology,* vol. 36, no. 8, pp. 1117-25, Aug 1991.

[106] A. M. F. Caldeira, A. M. Neto, A. C. Bento, M. L. Baesso, M. A. Silva, and A. de Almeida, "Behavior of oxidation in the radiochromic gel dosimeter through photoacoustic technique measurements," (in English), *Applied Radiation & Isotopes,* vol. 65, no. 5, pp. 605-9, May 2007.

[107] G. M. Liosi *et al.*, "Study of Fricke-gel dosimeter calibration for attaining precise measurements of the absorbed dose," in *Advancements in Nuclear Instrumentation Measurement Methods and their Applications (ANIMMA), 2015 4th International Conference on*, 2015: IEEE, pp. 1-5.

[108] T. Kron, D. Jonas, and J. M. Pope, "Fast T1 imaging of dual gel samples for diffusion measurements in NMR dosimetry gels," (in English), *Magnetic Resonance Imaging,* vol. 15, no. 2, pp. 211-21, 1997.

[109] L. N. de Oliveira, R. L. Zimmerman, M. V. Moreira, D. Ila, and A. de Almeida, "Determination of diffusion coefficient in Fricke Xylenol gel dosimeter after electron beam bombardment," *Surface and Coatings Technology,* vol. 203, no. 17–18, pp. 2367-2369, 2009.

[110] C. Baldock, P. J. Harris, A. R. Piercy, and B. Healy, "Experimental determination of the diffusion coefficient in two-dimensions in ferrous sulphate gels using the finite element method," (in English), *Australasian Physical & Engineering Sciences in Medicine,* vol. 24, no. 1, pp. 19-30, Mar 2001.

[111] T. Kron, P. Metcalfe, and J. M. Pope, "Investigation of the tissue equivalence of gels used for NMR dosimetry," (in English), *Physics in Medicine and Biology,* Article vol. 38, no. 1, pp. 139-150, Jan 1993.

[112]   P. Keall and C. Baldock, "A theoretical study of the radiological properties and water equivalence of Fricke and polymer gels used for radiation dosimetry," (in English), *Australasian Physical & Engineering Sciences in Medicine,* vol. 22, no. 3, pp. 85-91, Sep 1999.

[113]   S. A. Johansson *et al.*, "Dosimeter gel and MR imaging for verification of calculated dose distributions in clinical radiation therapy," (in English), *Acta Oncologica,* vol. 36, no. 3, pp. 283-90, 1997.

[114]   S. A. Back, P. Magnusson, L. E. Olsson, A. Montelius, A. Fransson, and S. Mattsson, "Verification of single beam treatment planning using a ferrous dosimeter gel and MRI (FeMRI)," (in English), *Acta Oncologica,* vol. 37, no. 6, pp. 561-6, 1998.

[115]   A. Rosset, L. Spadola, and O. Ratib, "OsiriX: An Open-Source Software for Navigating in Multidimensional DICOM Images," *Journal of Digital Imaging,* vol. 17, no. 3, pp. 205-216, 2004.

[116]   D. W. McRobbie, E. A. Moore, and M. J. Graves, *MRI from Picture to Proton*. Cambridge university press, 2017.

[117]   E. M. Haacke, Brown, R., . and et al., *Magnetic resonance imaging: physical principles and sequence design*. New York: John Wiley & Sons, 1999.

[118]   A. P. Crawley and R. M. Henkelman, "A comparison of one-shot and recovery methods in T1 imaging," (in English), *Magnetic Resonance in Medicine,* vol. 7, no. 1, pp. 23-34, May 1988.

[119]   D. C. Look and D. R. Locker, "Nuclear spin-lattice relaxation measurements by tone-burst modulation," *Physical Review Letters,* vol. 20, no. 18, p. 987, 1968.

[120]   A. J. Freeman, P. A. Gowland, and P. Mansfield, "Optimization of the ultrafast Look-Locker echo-planar imaging T1 mapping sequence," (in English), *Magnetic Resonance Imaging,* vol. 16, no. 7, pp. 765-72, Sep 1998.

[121]   D. R. Messroghli, A. Radjenovic, S. Kozerke, D. M. Higgins, M. U. Sivananthan, and J. P. Ridgway, "Modified Look-Locker inversion recovery (MOLLI) for high-resolution T1 mapping of the heart," (in English), *Magnetic Resonance in Medicine,* vol. 52, no. 1, pp. 141-6, Jul 2004.

[122]   H. Y. Carr and E. M. Purcell, "Effects of diffusion on free precession in nuclear magnetic resonance experiments," *Physical review,* vol. 94, no. 3, p. 630, 1954.

[123]   S. Meiboom and D. Gill, "Modified spin-echo method for measuring nuclear relaxation times," *Review of scientific instruments,* vol. 29, no. 8, pp. 688-691, 1958.

[124]   AAPM, "Acceptance testing and quality assurance procedures for magnetic resonance imaging facilities, AAPM report no. 100," 2010.

[125]   D. C. Look and D. R. Locker, "Time saving in measurement of NMR and EPR relaxation times," *Review of scientific instruments,* vol. 41, no. 2, pp. 250-251, 1970.

[126]   M. Marrale *et al.*, "Correlation between ferrous ammonium sulfate concentration, sensitivity and stability of Fricke gel dosimeters exposed to clinical X-ray beams," *Nuclear Instruments and Methods in Physics Research Section B: Beam Interactions with Materials and Atoms,* vol. 335, pp. 54-60, 9/15/ 2014.

[127]   J. Palta, S. Kim, J. Li, and C. Liu, "Tolerance limits and action levels for planning and delivery of IMRT," *Medical Physics,* vol. 30, no. 6, p. 1395, 2003.

[128]   G. Budgell, J. Berresford, M. Trainer, E. Bradshaw, P. Sharpe, and P. Williams, "A national dosimetric audit of IMRT," *Radiotherapy and Oncology,* vol. 99, no. 2, pp. 246-252, 2011.

[129]   Action radiotherapy. (2014). < *http://actionradiotherapy.org/wp-content/uploads/2014/03/UK-SABR-* Consortium-Guidelines.pdf >.

[130]   J. P. Mugler, "Optimized three-dimensional fast-spin-echo MRI," *Journal of Magnetic Resonance Imaging,* vol. 39, no. 4, pp. 745-767, 2014.

[131]   J. W. Yea *et al.*, "Feasibility of a 3D-printed anthropomorphic patient-specific head phantom for patient-specific quality assurance of intensity-modulated radiotherapy," *PloS one,* vol. 12, no. 7, p. e0181560, 2017.

[132]   T. Kamomae *et al.*, "Three-dimensional printer-generated patient-specific phantom for artificial in vivo dosimetry in radiotherapy quality assurance," *Physica Medica: European Journal of Medical Physics,* vol. 44, pp. 205-211, 2017.

[133]   R. R. Gallas, N. Hünemohr, A. Runz, N. I. Niebuhr, O. Jäkel, and S. Greilich, "An anthropomorphic multimodality (CT/MRI) head phantom prototype for end-to-end tests in ion radiotherapy," *Zeitschrift fuer Medizinische Physik,* vol. 25, no. 4, pp. 391-399, 2015.

[134]   M. Hillbrand *et al.*, "PO-0809: A 3D polymer gel dosimeter coupled to a patient-specific anthropomorphic phantom for proton therapy," *Radiotherapy and Oncology,* vol. 123, pp. S432-S433, 2017.

Appendix A.   Code for T_1 and T_2 quantification

To illustrate the work carried out to develop T_1 and T_2 quantification plugins, this appendix introduces selected excerpts from the code written. The plugins were written in objective-c for use within OsiriX as described in section 3.6.4 of the main report.

The user interface for OsiriX is shown in Figure A.1. The top pane displays the list of image series acquired during a measurement session. Bottom left are all images from one image series, in this case the images at different TE for a T_2 scan. Bottom right is a larger display of the selected image, in this case the first echo from this T_2 scan.
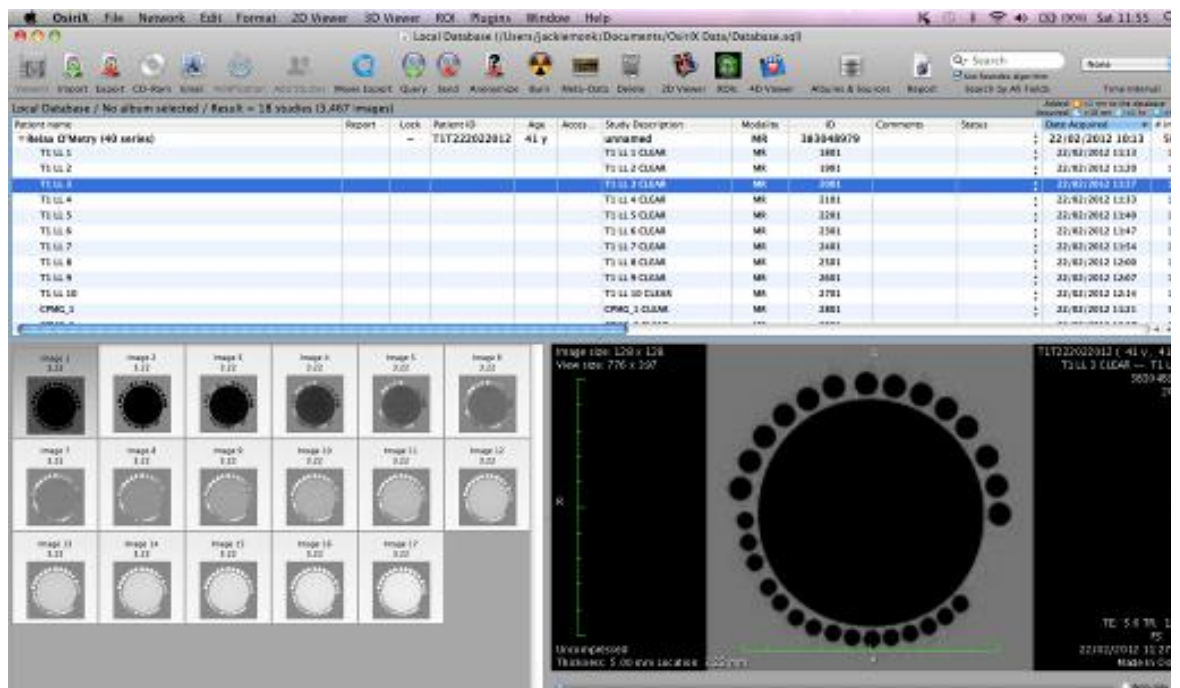

Figure A.1: screen shot of the main user interface for OsiriX.

A.1 T_1 quantification

The following excerpt of code:

(1) defines a function, f, which describes the recovery in longitudinal magnetisation for the Look Locker pulse sequence according to the equation of the form

$$y = A - B \exp(-t / T1_{eff})$$

as described in the main report, section 3.6.5

(2) defines starting points for the parameters A, B and $T1_{eff}$ of 3000, 6000 and 500 respectively.

(3) calls a routine lmcurve_fit. This runs the Levenberg-Marquardt optimisation to find optimum values of A, B and $T1_{eff}$ which best fit the actual recovery curve.

(4) returns the value for T_{1eff}.

This is carried out for every pixel. The code then continues to display the T_{1eff} for each pixel: the T_1 map.

```objc
@implementation ControllerT1Fit

/*define the function equation A - B * exp [ -t/T1eff]*/

double f( double t, const double *p )

{
    return p[0] - p[1] * exp(-t/p[2]);
}


/*this defines the parameters required as inputs into the LM optimiser*/
/*these are n_par, par[], m_dat, t, y, f*/
/*the value for t1 is returned back to controller.m*/

double computeLevenbergMarquardt(int pixList, float ttemp[], float ytemp[], double *t1)

{
  /* parameter vector */

  int n_par = 3; // number of parameters in model function f
  double par[3] = { 3000, 6000, 500 }; // array containing starting values for A, B and T1eff

      int m_dat = pixList; // number of data pairs

      double t[100];                          //array containing x-values (time)
      double y[100];                          //array containing y-values (signal)

      /*convert time and signal array elements from floats to doubles*/

      int i;
      for( i = 0; i < pixList; i++)
      {
         t[i] = (double) ttemp[i] * 1000;
         y[i] = (double) ytemp[i];
      }

    /* auxiliary parameters */

  lm_status_struct status;
  lm_control_struct control = lm_control_double;
  control.printflags = 3; // monitor status (+1) and parameters (+2)

    /* perform the fit */

  lmcurve_fit( n_par, par, m_dat, t, y, f, &control, &status );
  *t1 = par[2];               //T1 effective
  return *t1;
}
```

A.2 T$_2$ quantification

The T$_2$ for each pixel in the image is calculated from the data of M$_{XY}$ versus echo time (t) according to the equation:

$$M_{XY}(t) = M_0 e^{-t/T_2}$$

M$_{XY}$ is the residual transverse magnetisation (signal) at echo time, t. By plotting log(M$_{XY}$) versus echo time, t, the T$_2$ may be calculated according to   T$_2$ = -1 / slope

The following excerpt of code:

(1) for each pixel, calculates log(M$_{XY}$) for every T$_2$ echo image.

(2) sets the T$_2$ of the background pixels (outside of the phantom) to zero

(3) for each pixel, plots log(signal) versus echo time, performs a linear regression and returns the slope and the intercept.

(4) calculates T$_2$ = - 1 / slope

The code then goes on to display the T$_2$ map and allow analysis of the data.

```
for( x = 0; x < [firstPix pwidth]; x++)
        {
        for( y = 0; y < [firstPix pheight]; y++)
            {
            if( curROI == nil || [firstPix isInROI: curROI :NSMakePoint( x,  y)])

                    {
                    float logvalues[ 1000];
                    float values[ 1000];
                    long pos = x + y*[firstPix pwidth];

                    for( i = 0; i < [teSequence count]; i++)

                        {
                        logvalues[ i] = log( [[teSequence objectAtIndex: i] fImage] [ pos] -
background);

                        values[i] = [[teSequence objectAtIndex:i] fImage] [pos];
                        }

                    if(values[0] <100)

                            {
                            dstImage[x+y*[firstPix pwidth]] = 0;
                            }

                    else
                            {
        [self computeLinearRegression: [teSequence count] :TEValues :logvalues :&intercept :&slope];

        dstImage[ x + y*[firstPix pwidth]] = 1 / -slope;

    ….
                            }
                    }
                }
    }
```

1.

2.

3.

4.